NASA CR-66605

IITRI Project No. G6012

CHARACTERIZATION OF CERAMIC MATERIALS FOR MICROELECTRONIC APPLICATIONS

National Aeronautics
and Space Administration
Langley Research Center
Hampton, Virginia 23365

NASA CR-66605

IIT RESEARCH INSTITUTE
10 West 35th Street
Chicago, Illinois 60616

Contract No. NAS1-6919
IITRI Project No. G6012

CHARACTERIZATION OF CERAMIC MATERIALS FOR MICROELECTRONIC APPLICATIONS

Prepared by

A. J. Mountvala

Prepared for

National Aeronautics and Space Administration
Langley Research Center
Hampton, Virginia 23365

March 4, 1968

CHARACTERIZATION OF CERAMIC MATERIALS FOR MICROELECTRONIC APPLICATIONS

Abstract

A major factor to be considered in the characterization of ceramics is the significant differences between the electronic properties of single-crystal and polycrystalline materials, due to the presence of grain boundaries in the latter. The grain-boundary phase possesses a defect structure and usually has electrical properties different from those of the bulk phase. Therefore, in the characterization of $BaTiO_3$ ceramics, major emphasis has been placed in correlating the bulk properties with the surface or grain-boundary properties, taking into consideration the effects of grain size variation and deviations from stoichiometry.

CONTENTS

Section		Page
I.	SUMMARY	1
II.	INTRODUCTION	4
III.	THE CONCEPTS OF CHARACTERIZING POLYCRYSTALLINE MATERIALS	7
	A. General Discussion	7
	B. Characterization of Barium Titanate	12
IV.	THEORETICAL ANALYSIS OF THE ELECTRONIC CHARACTERISTICS OF SURFACES AND GRAIN BOUNDARIES IN $BaTiO_3$ CERAMICS	16
	A. Introduction	16
	B. Surface Barrier-Layer Model for $BaTiO_3$ Particles	19
	C. Two-Phase Model for Grains and Boundaries in $BaTiO_3$	23
	D. The Electronic "Character" of Grain Boundaries	33
V.	EXPERIMENTAL WORK	39
	A. Introduction	39
	B. Characterization of Starting Materials	39
	C. Preparation of Samples	47
	D. Characterization of Surface Defects in $BaTiO_3$ Powders	48
	1. Introduction	48
	2. Experimental Procedure	50
	3. Results and Discussion	52
	a. Stoichiometric Effects on Dielectric Loss Due to Water Vapor on $BaTiO_3$ Particulates	52
	b. Effects of Gaseous Environments on Dielectric Properties of $BaTiO_3$	59
	E. Dielectric Properties of $BaTiO_3$ at Infrared and Optical Frequencies	66
	1. Introduction	66
	2. Experimental Procedure	68
	3. Theoretical Concepts	69
	4. Results and Discussion	70
	a. Electron Micrograph Analysis	70
	b. Spectral Reflectance	78
	c. Absolute Reflectance	88

CONTENTS (Cont'd)

Section		Page
	F. Use of Electron Beam Scanning (EBS) Technique for Direct Measurement of Dielectric Properties of Grains and Grain Boundaries	95
	1. Introduction	95
	2. Experimental Procedure	95
	3. Results and Discussion	97
VI.	CONCLUSIONS	99
VII.	PERSONNEL	101
	REFERENCES	102
	DISTRIBUTION LIST	104

ILLUSTRATIONS

Figure		Page
1	Research Effort in the Field of Ionic Compounds	8
2	Intrarelationships Between First-Order Properties of Ceramic Materials by the "Mechanistic" Method	11
3	Correlation Approach to Characterization of Barium Titanate	14
4	Barrier Layer Model for $BaTiO_3$ Particle	20
5	Effective Dielectric Constant of $BaTiO_3$ Ceramic as a Function of Grain Size	26
6	Potential Distribution at the Grain Boundary	28
7	Particle Size Distribution of $BaTiO_3$ Powder Material C	43
8	Particle Size Distribution for $BaTiO_3$ Material C, for 0.5μ Intervals	44
9	Scanning Electron Micrograph of $BaTiO_3$ Powder "C"	45
10	Scanning Electron Micrograph of $BaTiO_3$ Powder "H"	46
11	Effect of P_{H_2O} On AC Conductivity of Specimen H-1p	53
12	Effect of P_{H_2O} On AC Conductivity of Specimen H-2s	54
13	Effect of P_{H_2O} On AC Conductivity of Specimen C-1p	55
14	Effect of P_{H_2O} On Dielectric Constant K' of Specimen H-1p	57
15	Effect of P_{H_2O} On Dielectric Constant K' of Specimen C-1p	58
16	Effect of Stoichiometry on Dielectric Loss Due to Water Vapor on $BaTiO_3$ Powders (Measured at 1 kHz)	60
17	Effect of Gaseous Atmospheres on Frequency Dispersion of Dielectric Constant for Sample F3 (Sintered 1350°C)	62
18a	Effect of Gaseous Atmospheres on Frequency Dispersion of D for Sample F3 (Sintered 1350°C)	63

ILLUSTRATIONS (Cont'd)

Figure		Page
18b	Frequency Dispersion of D for Sample F3 (Sintered 1350°C)	64
19	Effect of Gaseous Atmospheres on Frequency Dispersion of Resistivity for Sample F3 (Sintered 1350°C)	65
20	Electron Micrograph of $BaTiO_3$ "C" Sintered at 1240°C (X15500)	71
21	Electron Micrograph of $BaTiO_3$ "C" Sintered at 1260°C (X15500)	72
22	Electron Micrograph of $BaTiO_3$ "C" Sintered at 1280°C (X15500)	73
23	Electron Micrograph of $BaTiO_3$ "C" Sintered at 1300°C (X15500)	74
24	Electron Micrograph of $BaTiO_3$ "C" Sintered at 1320°C (X15500)	75
25	Electron Micrograph of $BaTiO_3$ "C" Sintered at 1340°C (X15500)	76
26	Electron Micrograph of $BaTiO_3$ "C" Sintered at 1360°C (X15500)	77
27	Reflectance Spectra of $BaTiO_3$ "C" Sintered at Different Temperatures	81
28	Real Part of Dielectric Constant of $BaTiO_3$ "C" vs Frequency for Different Sintering Temperatures	82
29	Imaginary Part of Dielectric Constant of $BaTiO_3$ "C" vs Frequency for Different Sintering Temperatures	83
30	Corrected Infrared Dielectric Constant of $BaTiO_3$ "C" vs Frequency for Different Sintering Temperatures	85
31	Reflection Spectra of $BaTiO_3$ "G" Sintered at Different Temperatures	86
32	Reflection Spectra of $BaTiO_3$ "C" Sintered at Different Temperatures	87

ILLUSTRATIONS (Cont'd)

Figure		Page
33	Corrected Infrared Dielectric Constant of $BaTiO_3$ "G" vs Frequency for Different Sintering Temperatures	89
34	Absolute Reflectivity of $BaTiO_3$ "C" Sintered at Different Temperatures	90
35	Absolute Reflectivity of $BaTiO_3$ "C" Sintered at Different Temperatures	91
36	Absolute Reflectivity of $BaTiO_3$ "G" Sintered at Different Temperatures	93
37	Absolute Reflectivity of $BaTiO_3$ "G" Sintered at Different Temperatures	94
38	Schematic Diagram of the Electron Beam Scanning System	96

TABLES

Table		Page
I	Measured Dielectric Constant vs Grain Size for $BaTiO_3$ Ceramic[12]	24
II	Analysis of $BaTiO_3$ Powder "C"	41
III	Chemical Analyses of $BaTiO_3$ Powders "F," "H," and "G"	42
IV	Physical and Compositional Characteristics of $BaTiO_3$ Test Specimens	51
V	Microstructural Characteristics of Sintered $BaTiO_3$ "C" Test Specimens	79
VI	Physical Characteristics of Sintered $BaTiO_3$ "G" Test Specimens	80

CHARACTERIZATION OF CERAMIC MATERIALS FOR MICROELECTRONIC APPLICATIONS

I. SUMMARY

The major emphasis in this investigation has been on the characterization of $BaTiO_3$ ceramics for microelectronic applications. A phenomenological approach has been used in correlating bulk and boundary phase properties.

In going from a single-crystal state to a polycrystalline form, a number of interacting factors--some dominant, others less so--are involved. These factors include microstresses, internal fields due to uncompensated charges at the surfaces and boundaries, and the defect boundary layer itself. Although some of the anomalous properties in $BaTiO_3$ ceramics have been satisfactorily explained, the role of surfaces in submicron-sized powders, and in particular of grain boundaries in $BaTiO_3$, has not been thoroughly understood. The importance of surfaces and grain boundaries in controlling the electrical and mechanical properties is well recognized in other material systems. Knowledge of their role in determining the electronic nature of an electroceramic material such as $BaTiO_3$ is essential to characterization.

A model for the origin of a defect layer on $BaTiO_3$ powders was formulated to explain a high-resistivity surface layer. The essential features of the proposed model are that cation vacancies created by the process of cationic migration to the surface represent acceptor states which may trap electrons from energy levels above the trap state. The number of electrons available for conduction would be drastically reduced by this means, and the resistivity of the depletion layer would rise probably by several orders of magnitude.

A theoretical analysis on the basis of a modified Bruggemann equation was also developed to quantitatively show the relationship between the dielectric constants of the bulk and grain boundary phases as a function of grain sizes. It should

be pointed out that this model is certainly oversimplified in view of the actual complexities and interactions between adjacent grains. The purpose of such a model, however, is to permit deductions on orders of magnitudes of such quantities as the dielectric constant of the grain boundary phase, hitherto, an unknown quantity. However, the simplified two-phase, Bruggemann-type approach does satisfactorily fit the experimental data on the effect of grain size on the dielectric constant of sintered $BaTiO_3$ ceramics.

The major experimental work to date has been to study the change in the dielectric behavior of barium titanate during the controlled conversion of compacted high-purity powders to increasingly densified and bonded bodies.

The results obtained on the effects of water vapor on the dielectric properties of $BaTiO_3$ are significant not only to the overall question of characterization but also to the processing and performance of microcapacitors. Our experimental results indicate that the surfaces of barium titanate powders can be characterized by evaluating the changes in the dielectric loss phenomena. Small changes in the stoichiometry of the material (BaO/TiO_2 ratio) can be correlated with a marked change in the ac conductivity (at 1 kHz) as a function of the partial pressure of water.

The characterization of $BaTiO_3$ ceramics has been attempted in terms of an equivalent circuit, with the bulk of the grains, surfaces and grain boundaries being represented by their respective capacitance and resistance. This approach towards characterization has yielded useful information. It also simplifies the interpretation of the dielectric properties of a ceramic for device applications.

The equivalent circuit approach has been carried out, primarily by evaluating the dielectric properties over a range of frequencies. This is essential in order to understand and differentiate the many complex interactions that contribute to the total permittivity in $BaTiO_3$ ceramics.

The dielectric properties of ceramic $BaTiO_3$ at infrared and optical frequencies ($\sim 10^{11}$ to 10^{14} Hz) have been evaluated. Measurements at these frequencies indicate primarily the contribution of the electronic polarizability to the total permittivity. These experiments have been carried out as a function of grain size, to differentiate the grain boundary contribution from that of the grain. The results indicate that in this frequency range, the dielectric constant decreases slightly with a decrease in grain size. The results also suggest that the grain size dependence of the dielectric constant in $BaTiO_3$ may not be entirely ferroelectric in origin, and that a contribution nonferroelectric in origin exists. This lends further support to the approach suggested in the theoretical analysis of the electronic characteristics of grain boundaries in $BaTiO_3$ ceramics, presented in this report.

The results show that $BaTiO_3$ ceramics can, indeed, be effectively characterized for microelectronic applications. It has been demonstrated that, by evaluation of selected dielectric properties, information can be obtained to characterize the material in terms of an equivalent circuit, which represents bulk grain, boundary phases, and surface phenomena such as adsorbed layer effects.

II. INTRODUCTION

In order to improve the reliability and functionality of ceramic materials for microelectronic applications it is essential to study and understand the "application-property-character" interrelationship. This, in turn, will indicate the methods and approaches for the most effective characterization.

However, technical ceramics, unlike a number of other areas which have developed into sound scientific groupings, is still somewhat empirical. The ceramist could say that it is so because nature has made ceramic materials particularly hard to understand and inordinately complex for simple theory; and while the physicist often works with high-purity single crystals, the ceramist must work with multicrystalline, polyphase materials, and must select for high purity and stoichiometry. The fact that ceramic materials cannot be prepared, as yet, with the high degree of purity of elemental materials does not preclude their scientific development. We shall see that there are other significant parameters such as stoichiometry and grain boundary-to-grain phase distributions that play a critical role in the understanding of ceramic materials.

The current program is aimed specifically at a meaningful characterization of barium titanate ceramics, which have significant applications in microelectronics. The research done at IITRI[1] has demonstrated that selected electrical measurements can be applied to yield meaningful information about the boundary and bulk properties of a ceramic, such as barium titanate. The electrical measurements are not only pertinent to the end use of $BaTiO_3$ ceramics in microelectronics, but simplify the interpretation of the electronic properties of a ceramic for device design and microelectronic applications.

The complex nature of ceramic materials makes characterization more difficult, but not impossible. Preferably, we would like to characterize ceramic materials that are free of all trace impurities. But unlike elemental semiconductor type

materials (such as silicon) the purification of ceramics presents some problems.

Because of the need for preparing high-purity materials, a number of relatively novel methods have been devised, such as plasma arc with induction coupling and the decomposition of organo-metallics. These methods do consistently produce fine particle powders of ceramic materials, but not necessarily of a higher purity than some of the other techniques. In fact, quite often small particle size refractory oxides have been obtained at the expense of stoichiometry. Even the removal of trace impurities by thermal and/or chemical techniques quite often causes problems in stoichiometry. Although impurities play an important role in the properties of ceramic materials, stoichiometry, in some instances, is much more significant. The role of impurities can be evaluated by "finger-printing" the extent of the trace impurities and their effects on the dielectric behavior of $BaTiO_3$.

Major emphasis has been placed on both stoichiometry and purity, in selecting the materials to be investigated in this program. The purity level of these ceramics is an order of magnitude superior to what is commercially available for $BaTiO_3$ ceramics. Therefore, although it is not possible, at this stage, to work with $BaTiO_3$ ceramics comparable to the "ultra-high purity" silicon materials, the very significant improvements in purity, and the fact that $BaTiO_3$ powders of controlled stoichiometry were attained in this study, justifies their use and makes the interpretation possible.

In attempting to characterize $BaTiO_3$ ceramics for microelectronic applications we have attempted to answer the following questions:

1. What are the properties of the surface defect layer of a powder particle, and how do they change with particle size, temperature, and oxygen partial pressure?

2. What are the electrical properties of the boundary phase in polycrystalline ceramics and their relationship to grain size and pressure?

3. What is the correlation between the properties of the defect surface layer of the powder particles and the properties of the boundary phase in the ceramic?

III. THE CONCEPTS OF CHARACTERIZING POLYCRYSTALLINE MATERIALS

A. General Discussion

The research effort that has been expended in the study of ionic compounds is illustrated in Fig. 1. This chart indicates not only the particular areas that have been investigated, but also indicates, qualitatively, the amount of work carried out in a particular field.

The alkali halides have been studied for a long time, theoretically as well as experimentally. Single crystals of these compounds are easily obtained and, more important, one may assume that the bonding between the ions in the alkali halides is nearly 100% ionic. The Pauli principle, then, forbids appreciable electronic overlap, and a theoretical treatment on the basis of a Slater determinant formed from Bloch functions can be applied. Single crystals of the high-melting oxides, in sizes and of a chemical purity as required for physical property measurements, became available only recently. Furthermore, the oxides constitute a special class of ionic compounds insofar as they exhibit a considerable amount of covalent bonding in addition to the ionic bond. In alumina, the covalent contribution amounts to about 40% of the total bond between cations and anions. The sharing of electrons in addition to electron exchange is difficult to approach theoretically.

The surface and volume properties of single-crystal oxides have been given much attention. Relatively little work has been done on the high-temperature charge and heat transport in single crystals of high purity. The high-temperature heat transport mechanism in ionic crystals predicted by Peierls in 1931 has not been verified experimentally in the intervening years to date, although it is of importance for the evaluation of electron phonon interactions at high temperatures. Little attempt

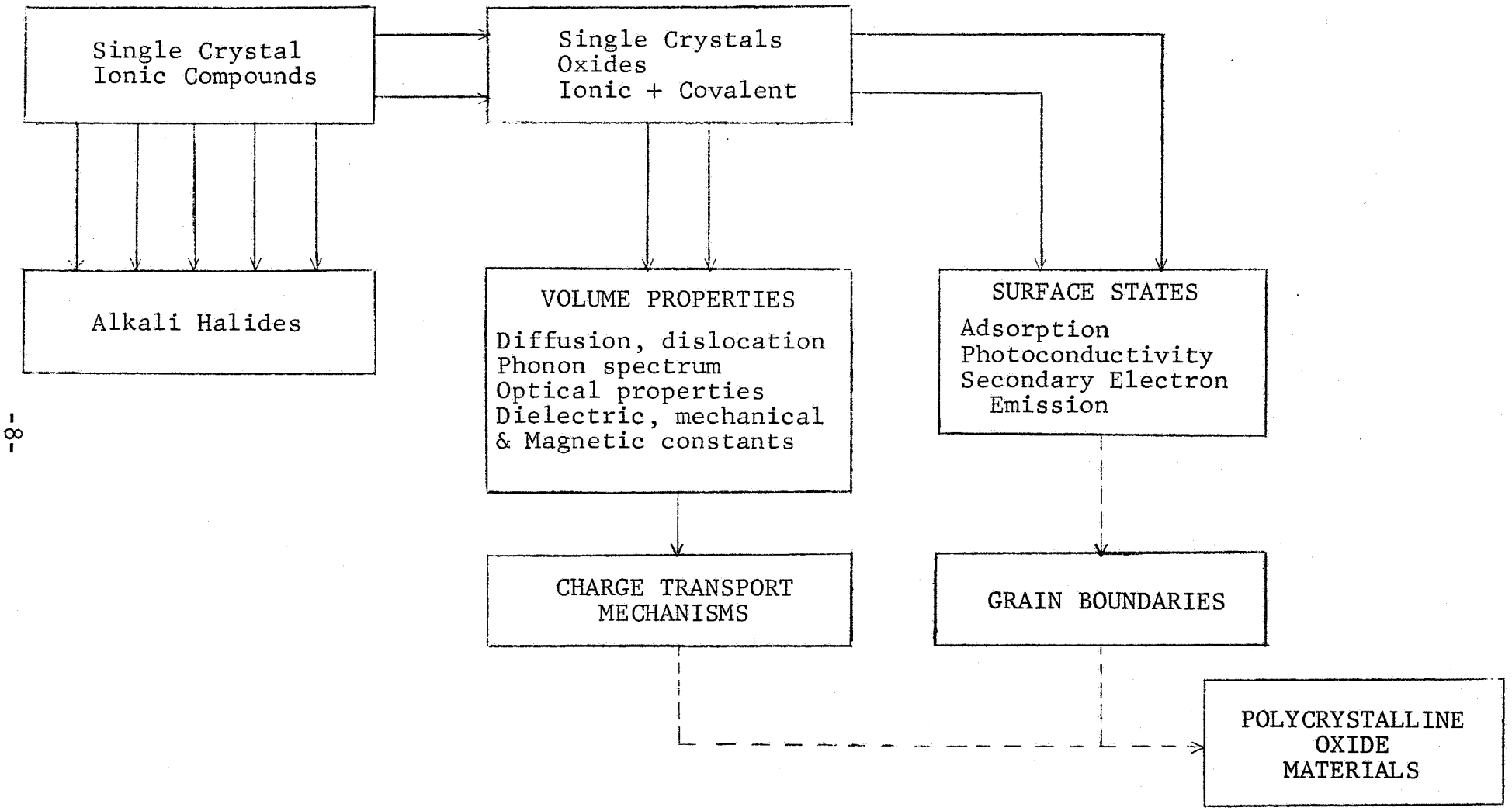

Fig. 1 - RESEARCH EFFORT IN THE FIELD OF IONIC COMPOUNDS

The number of arrows is a rough indication of the extent of research in the particular field, broken lines indicate very little work.

has been made, on the other hand, to correlate surface studies on single crystal oxides with grain-boundary effects in polycrystalline materials.

Many methods have been tried to characterize ceramic materials and, for the most part, they have not been successful in achieving this goal. They have succeeded in many cases in the identification of ceramics and have also advanced the understanding of mechanisms such as fracture, strength improvement, and corrosion resistance. Undoubtedly, some of the difficulty has been due to the orientation of the "characterizer." The nondestructive testing groups have worked with ceramics, but they are method rather than materials oriented. Materials experts have looked at individual mechanisms and appear to have overlooked their totality.

The question then arises as to what methods can be used for characterization. The two methods which should be used simultaneously can be identified as "direct" and "mechanistic." Although these two methods differ in approach, they are interrelated in devising a complete characterization of a ceramic for a particular application. The end-application for which a ceramic has to be characterized is critical in the selection of those properties or parameters which will best characterize it.

The characterization of ceramic materials by the "direct" method alone merely enables us to identify certain physical, chemical, thermal, and electrical properties of a specimen and, to some extent, relate them to the processing parameters. Undoubtedly, this approach is essential for determining the reproducibility of one piece of ceramic hardware compared to another for a particular forming or processing cycle. However, when this approach of characterization is utilized alone, it does not permit us to generically characterize a ceramic within certain predetermined "selectivity limits" (such as is possible with a silicon crystal of specified doping limit and orientation) and thereby evaluate its suitability for a specific application. Our present inability

to do this with ceramic materials is largely due to a lack of knowledge of the relationships between the inherent properties of the material and its functional characteristics.

In the second method the mechanistic property or properties that are most suitable for characterizing a ceramic material should be of first-order importance; by this we mean that they should be predominantly (if not entirely) a function of the pertinent microstructural and atomistic aspects that one wants to characterize for a particular application and should not be masked by other effects. This is essential if we are to systematically define and devise property evaluations to correlate the relationships that can effectively characterize a ceramic material.

The intrarelationships which exist between certain significant atomic and microstructural aspects and "first-order" properties in ceramic materials, and which merit further investigation, are shown in Fig. 2.

Let us consider grain size. The characterization of grain size by the direct approach is what the definition of the method implies--a direct assessment of the grain size. This can be carried out by microscopic techniques. But no matter how sophisticated and refined a measuring technique may be, it cannot characterize the volumetric or bulk effects of the grain size. In addition, there are secondary effects of potential interfacial barriers, dispersed phases, etc., all of which must be considered. Therefore, a direct evaluation of the grain size has to be carried out along with an associative approach. This second or mechanistic approach, in the case of the grain size, can take into consideration any one of the first-order properties shown in Fig. 2.

Interfacial barriers, which are responsible for a number of variations in the electrical properties of ceramics, can also be characterized by a number of "first-order" properties, as shown in Fig. 2. Stoichiometry effects with related "first-order" properties have also been shown in the same figure.

GRAIN SIZE

Piezoelectrics, titanates →	k_p (piezoelectric response)
Ferroelectrics, titanates →	TC of Dielectric constant
Most ceramics →	I-E characteristics
Capacitor materials, titanates →	TC of electrical resistivity

INTERFACIAL "ELECTRONIC" BARRIERS

Most ceramics →	I-E characteristics
Oxides, titanates →	Dielectric constant (at high and low freq)
Oxides, titanates →	Capacitance (at high and low freq)
Most ceramics →	Open circuit emf
Carbides, borides, silicides →	Work function
Oxides, carbides →	TC of electrical resistivity

STOICHIOMETRIC EFFECTS (cation/anion ratio; oxygen content)

Most ceramics →	Open circuit emf
Oxides, titanates, carbides →	TC of electrical resistivity
Most ceramics →	Electrical resistivity
Carbides, borides, silicides →	Work function
Carbides →	Hardness
Carbides →	Magnetic susceptibility
Titanates →	Dielectric constant
Titanates, semiconducting oxides →	Color centers

Fig. 2 - INTRARELATIONSHIPS BETWEEN FIRST-ORDER PROPERTIES OF CERAMIC MATERIALS BY THE "MECHANISTIC" METHOD

B. Characterization of Barium Titanate

Although this study is concerned with the characterization of $BaTiO_3$ ceramics, it is part of a broader effort to contribute to the closing of the gap between the two centers of interest, indicated in Fig. 1: the field of single crystal ionic compounds, which is of high scientific but limited technical interest, and the field of polycrystalline sintered oxides, which seems to attract lesser scientific attention but is of the highest technical interest.

In the case of barium titanate, the properties of interest are dielectric constant, dielectric loss, saturation polarization, coercive field, conductivity, breakdown field, switching time, piezoelectric coupling, Curie temperature, and the temperature coefficients of these properties. The task of characterizing $BaTiO_3$ ceramics consists, then, in finding the correlations between these properties and certain features of polycrystalline materials such as grain size, porosity, impurities, and internal stresses. The issue has been further complicated by the following experimental observations:

1. $BaTiO_3$ ceramics of comparable grain size and porosity, impurity, and stress-levels do not necessarily have identical dielectric properties.

2. Partially as a consequence of (1), there is little known about the change in dielectric behavior of $BaTiO_3$ ceramics with a change in the four parameters, grain size, porosity, impurity content, and internal stress. Only a few empirically established trends are known, and these do not allow prediction of the properties of $BaTiO_3$ ceramics with the degree of reliability and precision needed for microelectronic applications of this material.

It is necessary, therefore, to depart from the conventional way of characterizing polycrystalline $BaTiO_3$ in terms of

grain size, porosity, impurity level, and stress, and to study in detail the effect of other parameters. This approach is illustrated in Fig. 3.

The obvious effect of grain size variation on the dielectric properties of $BaTiO_3$ ceramics concerns the corresponding change in the amount of grain boundary phase present. Still another effect may arise from a dependence of the properties of the boundary phase on grain size. Such a dependence is to be expected for a powder particle small enough that its surface free energy becomes an appreciable part of its total energy. Under these circumstances, domain wall formation and surface conductivity will be particle size dependent.

On the other hand, the grain size effect on the dielectric constant of sintered $BaTiO_3$ does not necessarily result from an intrinsic property of the bulk grains. Finer particles usually yield higher densities in sintering. Higher densities, in turn, may cause a larger compressive strain in the material upon cooling through the cubic-tetragonal transformation temperature. Several investigators have found an increasing amount of cubic phase in sintered $BaTiO_3$ with decreasing grain size. The increase in dielectric constant of sintered $BaTiO_3$ with decreasing grain size could then be explained by the increasing amount of cubic phase present--that is, by the increase in internal strain rather than by a direct grain size effect.

A discussion of the effects of deviation from stoichiometry on the electrical properties of barium titanate should distinguish between several types of nonstoichiometry which may affect these properties in different ways: chemical impurities, cationic doping, oxygen deficiency, and TiO_2 excess or deficiency. The situation is complicated by the fact that the concentration of different types of deviation from stoichiometry in the bulk of the grain and along grain boundaries may vary in a different manner. Thus, grain size and stoichiometry effects cannot be considered to be independent of each other, and it is sometimes

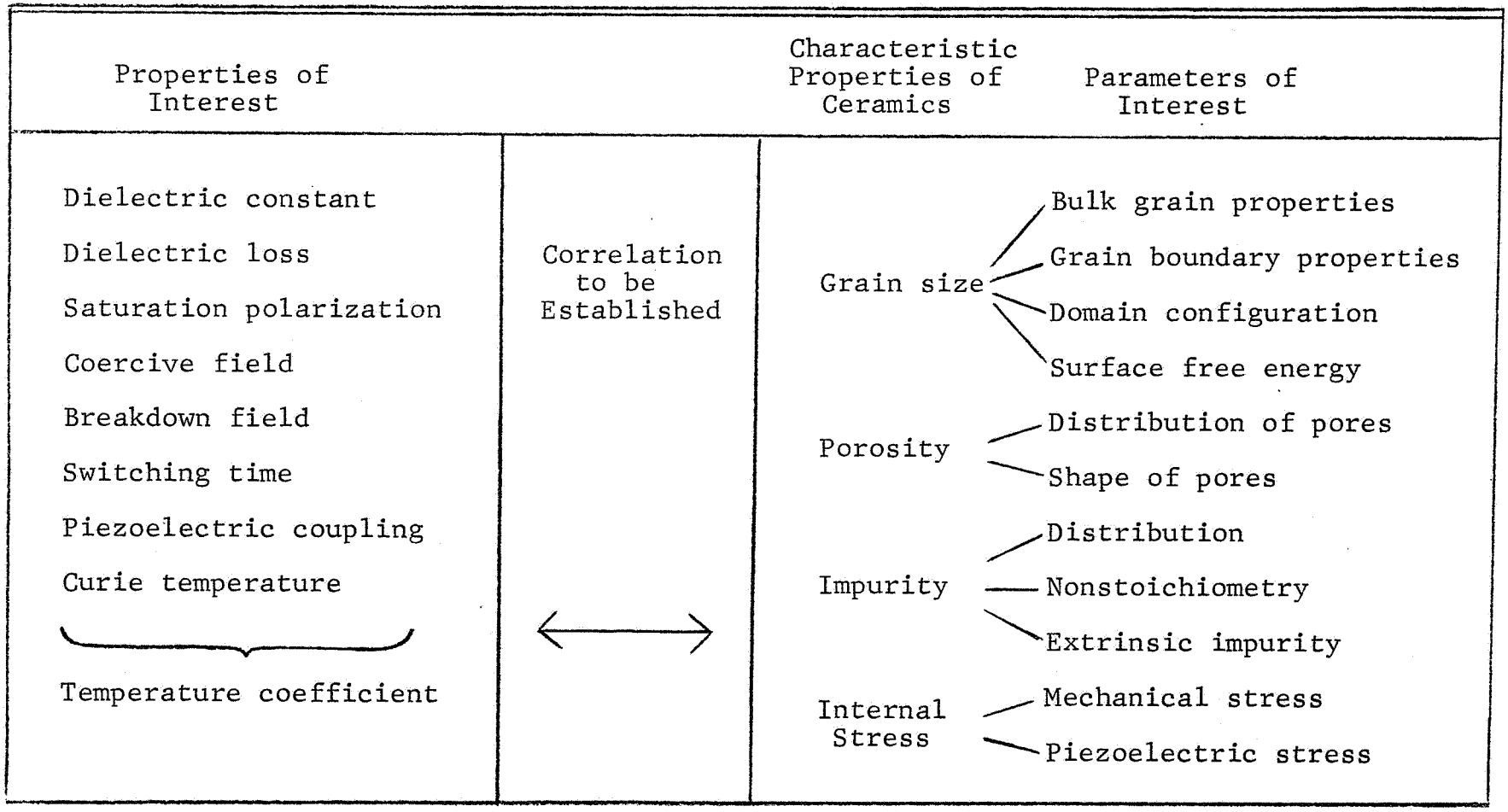

Fig. 3 - CORRELATION APPROACH TO CHARACTERIZATION OF BARIUM TITANATE

difficult to evaluate the importance of studies of stoichiometry effects if they neglect information on grain sizes.

IV. THEORETICAL ANALYSIS OF THE ELECTRONIC CHARACTERISTICS OF SURFACES AND GRAIN BOUNDARIES IN $BaTiO_3$ CERAMICS

A. Introduction

In going from a single-crystal state to a polycrystalline form, a number of interacting factors are involved. These include microstresses, internal fields due to uncompensated charges at the surfaces and boundaries, and the defect boundary layer itself. While some of the anomalous properties in $BaTiO_3$ ceramics have been satisfactorily explained by consideration of the interaction of the internal field and stress,[2] the role of surfaces in submicron sized powders, and in particular of grain boundaries in $BaTiO_3$, has not been thoroughly understood. That surfaces and grain boundaries are important in controlling the electrical and mechanical properties in ceramics is well recognized in other material systems, such as aluminum oxide[3] and magnesium oxide.[4]

The electrical characteristics of surfaces, grain boundaries, and bulk material can be represented by an equivalent circuit. In the case of $BaTiO_3$, the circuit consists of a capacitance and parallel resistance representing each of the components.

In considering a single crystal or a particle we have to consider the properties of the surface layer and the bulk. Therefore, a simple equivalent circuit would consist of a capacitance and parallel resistance representing the bulk of the particle in series with a capacitance and parallel resistance representing the surface layer. As the particles are compacted and sintered into a ceramic material, the "free" surface layer of the particles is converted into the boundary between the grains. However, it would be erroneous to assume that the characteristics of grain boundaries are identical to those determined for the free surface layer on particles or single crystals of a material. The surface properties of the sintered material should also be considered as a third component in an equivalent circuit such as:

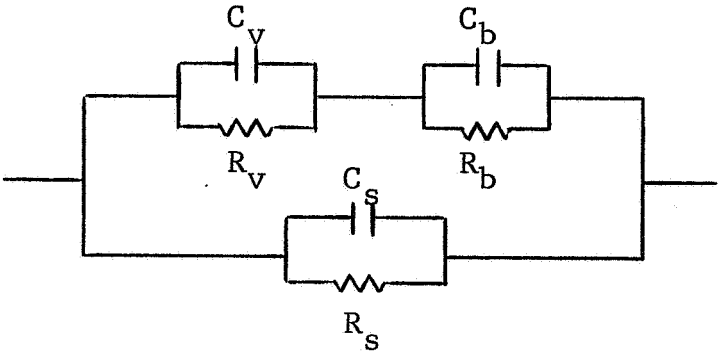

where subscripts "v," "b," and "s" represent the capacitance (C) and resistance (R) of the grain, grain boundary, and the surface of the ceramic, respectively.

Further, the surface characteristics in a sintered material may only be significant under certain conditions and may be predominated by the properties of the grain boundaries. Certainly, the microstructure of the material and, in particular, the properties of the powder or particles from which the sintered material is prepared will influence these factors. It may be more appropriate to represent the equivalent circuit of polycrystalline $BaTiO_3$ as follows:

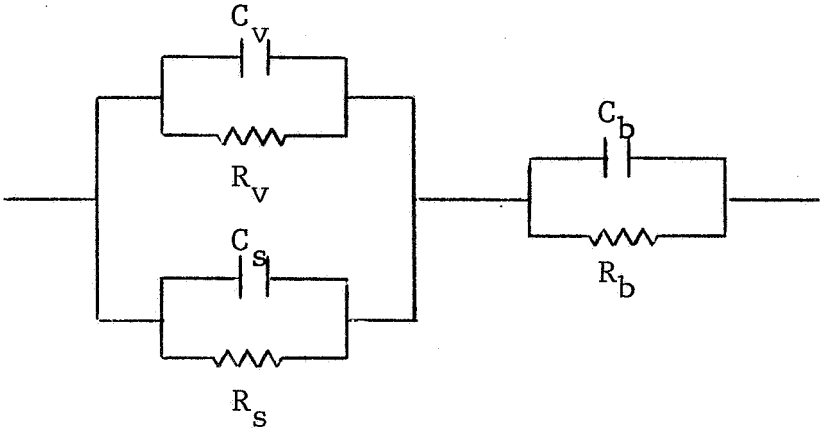

Therefore, a meaningful characterization of $BaTiO_3$ ceramics requires that the properties of the surface layer and grain-boundary phases be determined as a function of grain size, stoichiometry, and any other pertinent microstructural and atomistic parameters. An attempt has been made to theoretically interpret the nature of the defect surface layer on $BaTiO_3$ particles,

and the possible dependence of the dielectric behavior of the grain-boundary phase on grain size and stoichiometry, in polycrystalline $BaTiO_3$, in terms of the overall bulk properties.

Such a theoretical approach is essential to the overall question of characterization and complements the experimental work carried out on this program.

B. Surface Barrier-Layer Model For $BaTiO_3$ Particles

The presence of surface layers which alter the properties of $BaTiO_3$ fine particles have been postulated by Kanzig,[5,6] Chynoweth,[7] and other investigators. Electron diffraction results of Kanzig and co-workers[5] indicated that the deviations from the normal ferroelectric behavior, in very small $BaTiO_3$ particles, were mainly due to a difference between the bulk of the particles and a surface layer of about 100 A thickness. It has been further postulated[6] that this surface layer may be considered an "ionic Schottky exhaustion layer." The presence of surface layers has also been cited to explain the thickness dependence of switching parameters and other pyroelectric effects in $BaTiO_3$ single crystals. However, these surface layers on single crystals may well be of different types.

This section describes a barrier-layer model for the surface of $BaTiO_3$ particles, which mechanistically explains their experimental dielectric properties.

A model for a high resistivity boundary layer has been proposed by us to explain the experimental evidence[8] for a high resistivity surface layer on $BaTiO_3$ particles. This has been schematically shown in Fig. 4. A barium titanate particle has very probably a layer of adsorbed oxygen around its outer surface, the strength of the oxygen bond depending on the energy levels of the available states. Since the oxygen atoms or molecules accept electrons from the particle to form the bond, they represent a negative surface charge. The thickness of the surface depletion layer is considered to be of the order of 10^{-5}cm, typical for a Schottky-type barrier. The electric field across the depletion layer is on the order of 10^5 V/cm, for an assumed barrier height of 1 eV. This high electric field can induce cationic migration to the surface, especially since the titanium ion is quite mobile in the $BaTiO_3$ structure. It is assumed that the titanium would combine on the surface with oxygen, forming an extremely thin

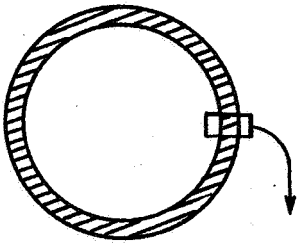

FORMATION OF SURFACE DEFECT LAYER

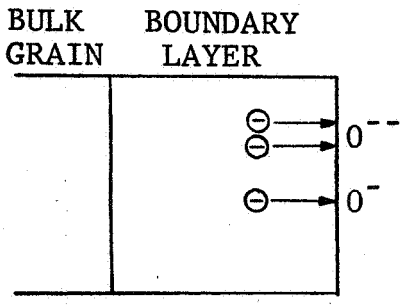

1. Chemically and Physically Adsorbed Oxygen Removes Electrons From Crystal, Creates Negative Surface Charge. Assumption: Surface States Below Fermi Level

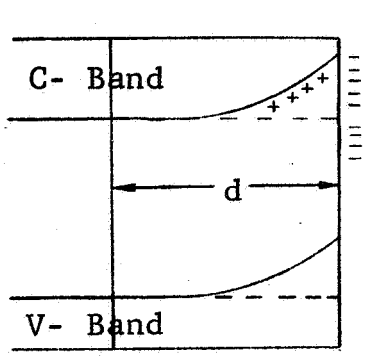

2. Electronic Energy Band Shift Due to Negative Surface Charge. Magnitude of the Effect:

Barrier Layer Thickness	d	$\cong 10^{-5}$ cm
Density of States		$\cong 10^{17}/cm^3$
Negative Surface Charges		$\cong 10^{13}/cm^2$
Barrier Height	E_B	$\cong$ 1eV
El. Field Across Barrier Layer	F_d	$\cong 10^5$ V/cm

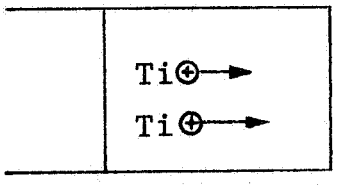

3. Field Induced Cationic Diffusion to Surface. Formation of TiO_x on Surface Extending Lattice

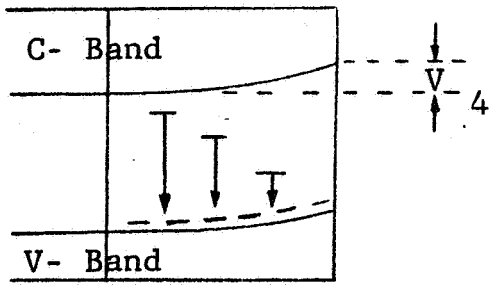

4. Equilibrium Situation, $V < E_B$. Holes in Valence Band Create Acceptor States Which Trap Electrons From Higher States, Increasing Barrier Layer Resistivity.

Fig. 4 - BARRIER LAYER MODEL FOR $BaTiO_3$ PARTICLE

layer of "TiO_x", undetectable by x-ray techniques. The neutralization of the adsorbed oxygen by the formation of an oxide of titanium reduces the negative surface charge and thus the electric field. The field-induced cationic migration to the surface comes to a standstill after a certain portion of movable cations have migrated to the surface.

The essential feature of the proposed model is that the cation vacancies created by the process of cationic migration to the surface represent acceptor states which trap electrons from energy levels above the trap state. The number of electrons available for conduction are drastically reduced by this means, and the resistivity of the depletion layer rises.

Such a cationic diffusion-barrier model can also explain the particle size dependence of the dielectric constant of unsintered, pressed $BaTiO_3$. The dielectric constant (at 1 kHz) of unsintered pressed barium titanate as a function of particle size has been experimentally determined,[9] and found to decrease continuously from a value of about 360 to approximately 65 with decreasing particle size (from 149 to 1-5μ). This behavior is opposite to that of sintered $BaTiO_3$ where the dielectric constant increases with decreasing grain size, up to 1μ.[10,11]

The dielectric constant of a barium titanate particle with a depletion layer as described in Fig. 4, can be expressed by the following relationship:

$$\epsilon = \frac{2\pi N_t^2 q^2}{\Phi N_d} \qquad (1)$$

where ϵ = permittivity
N_t = number of electrons trapped per cm^2 of surface
N_d = donor concentration
Φ = barrier height
q = electronic charge

Now, with decreasing particle size, the free energy of the particle increases and the bonding of adsorbed oxygen becomes

stronger. This implies that the energy levels at the surface decrease in height from the valence band and more negative charge would accumulate in the surface layer. The increased negative charge would enhance cationic diffusion to the surface in a very narrow region, as proposed in our model. The resulting effect would be an increase in the donor concentration (N_d) in the space charge region, perhaps by orders of magnitude. An increase in N_d, assuming constancy of other parameters in Eq. 1 would decrease the permittivity (ϵ). The barrier layer model, therefore, offers a model towards qualitatively explaining the experimentally observed dependency of the dielectric constant on particle size in unsintered, pressed $BaTiO_3$.

C. Two-Phase Model for Grains and Boundaries in $BaTiO_3$

The functional characteristics of ceramic materials are strongly influenced by the properties of grain boundaries. Therefore, in order to characterize these materials for electronic applications, it is necessary to understand the electronic behavior and structure of the grain-boundary region.

A theoretical analysis on the basis of a modified Bruggemann equation has been carried out to show semiquantitatively the relationship between the dielectric constants of the bulk and grain-boundary phases as a function of grain size. The dielectric constant of the grains was assumed to be constant, while that of the grain boundary changes from a high value for large grains to a smaller value for small grains. On the basis of this hypothesis, the effective dielectric constant (K_m) of a dense $BaTiO_3$ ceramic would then pass through a maximum, increasing first with decreasing grain-size, but then decreasing with decreasing grain-size below a certain size (probably in the submicron range).

It should be pointed out that this simplified model is certainly untenable if one considers the actual complexities and interactions between adjacent grains. The model, however, does permit deductions on orders of magnitude of such quantities as the dielectric constant of the boundary phase, hitherto an unknown quantity. However, the simplified Bruggemann type approach does satisfactorily explain certain experimental data on the effect of grain size on the dielectric constant of sintered $BaTiO_3$ ceramics.

Experimental results are available which indeed support this theoretical model. Table I summarizes the experimental data obtained on ultrafine-grained $BaTiO_3$, super-pressed at moderate temperatures at USAECOM.[12] The results indicate that the dielectric constant, measured at 10^3 Hz, reached a maximum value of about 5500 corresponding with a microstructure in which the average grain size was about 1μ. Specimens with an average grain size of less than 1μ showed reduced dielectric constant values. The

Table I

MEASURED DIELECTRIC CONSTANT VS GRAIN SIZE FOR $BaTiO_3$ CERAMIC[12]

Average Grain Size, μ	Measured Dielectric Constant (at 1 kHz)
3	3200
2	4400
1	5500
0.7	3600
~0.2	2800

results shown in Table I correspond to samples of nearly identical density, close to the theoretical value. This is the first experimental confirmation of our hypothesis on the relationship between the dielectric constants of the bulk and the grain boundary. On the basis of these experimental results, the characteristics of the grain-boundary phase and its effects on the dielectric properties of $BaTiO_3$ ceramics have been further pursued.

Quantitative correlation between USAECOM's experimental data and our results, calculated from the modified Bruggemann equation, yeilds a definite trend line. Figure 5 shows the change in the effective dielectric constant (K_m) of a $BaTiO_3$ ceramic mixture with decreasing grain size, as a function of the parameter "a." The parameter "a" is the ratio of the dielectric constants of grain boundary (K_b) and the bulk (K_v). With the introduction of the parameter, $a = K_b/K_v$, the modified Bruggemann equation is:

$$\left[\frac{1}{1-a}\right]\left[1-\frac{K_m}{K_v}\right] = \left[1-V\right]\left[\frac{K_m}{aK_v}\right]^{1/2} \qquad (2)$$

The volume fraction in Fig. 5 has been translated into grain size, assuming a grain layer thickness of 10^{-5} cm (0.1μ). This assumption and the further assumption that the thickness of the boundary layer does not depend on grain size appears reasonable on the basis of previous data in the literature. The value of dielectric constant of the bulk or the grain, K_v, is assumed to be 1000 and independent of the grain size. The dielectric properties considered are representative of values at frequencies of around 10^3 Hz.

By substituting the values of the experimentally determined effective dielectric constants (K_m) for various grain sizes (see Table I) in Eq. 2 (modified Bruggemann equation) the values of the parameter "a" have been determined. The values of the parameter "a" corresponding to the measured dielectric constant (K_m) have been shown in Fig. 5. The results indicate that the value of "a" changes from about 39 to 30 to 16 to 7 to 2.8 for average grain sizes corresponding to 3, 2, 1, 0.7 and 0.2μ.

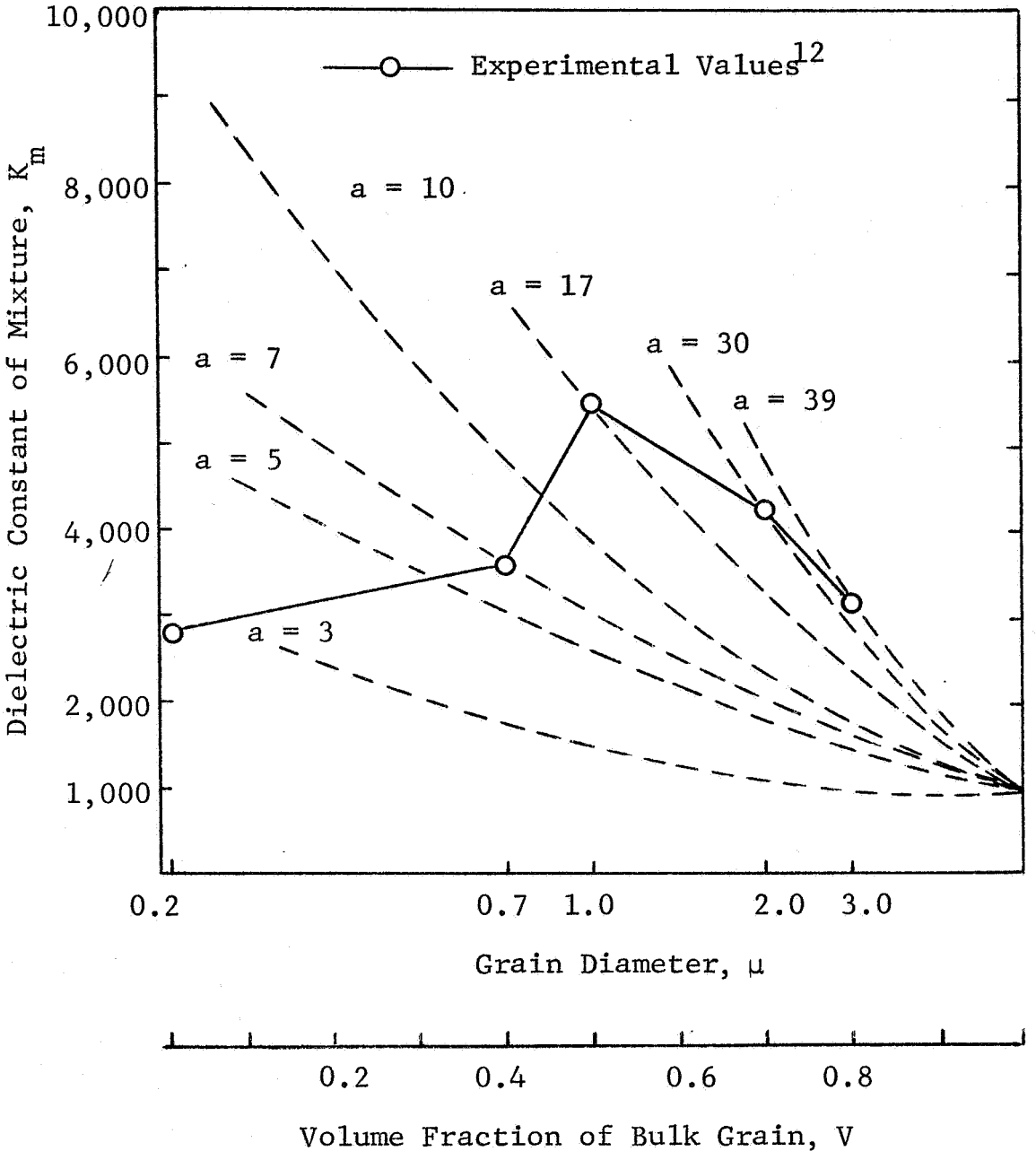

Fig. 5 - EFFECTIVE DIELECTRIC CONSTANT OF $BaTiO_3$ CERAMIC AS A FUNCTION OF GRAIN SIZE

WHERE: GRAIN LAYER THICKNESS = 0.1μ = CONSTANT
$K_b = aK_v$ AND $K_v = 1000$

Since $K_v = 10^3$, and $a = K_b/K_v$, we can calculate the dielectric constants of the grain boundary (K_b) as a function of grain size. The results indicate the following:

Average Grain Size, μ	Calc. K_b
3	3.9×10^4
2	3.0×10^4
1	1.6×10^4
0.7	7.0×10^3
0.2	2.8×10^3

In the following paragraphs, a boundary barrier layer model has been proposed and calculations on the conduction across the grain boundary carried out. It is shown that the values of the grain-boundary dielectric constant (K_b) obtained from a combination of USAECOM's experimental results and our modified Bruggemann equation are compatible with the calculated K_b values from the barrier layer model.

The shape of the potential barrier around the grain boundary is determined by the nature of the barrier states connected with the grain boundary. Although the exact nature of such grain-boundary barrier states in $BaTiO_3$ is not known, it is possible to hypothesize the characteristics of the barrier on the basis of observed experimental data on $BaTiO_3$.

By formulating such a boundary model and applying the theory of current flow across grain boundaries, an analysis of the relationship between barrier states and the dielectric properties of the boundary has been carried out.

The potential distribution in the boundary region of a polycrystalline material such as $BaTiO_3$ is shown in Fig. 6. The grain boundary is $x = 0$. The barrier height (Φ) is measured from the bottom of the conduction band at the negatively-based side of the boundary. The extent of the barrier region is from $x = -\ell_1$ to $x = +\ell_2$. The region between $x = -x_1$ to $+x_2$, in the barrier is where the hole density is equal to the donor concentration, N_d.

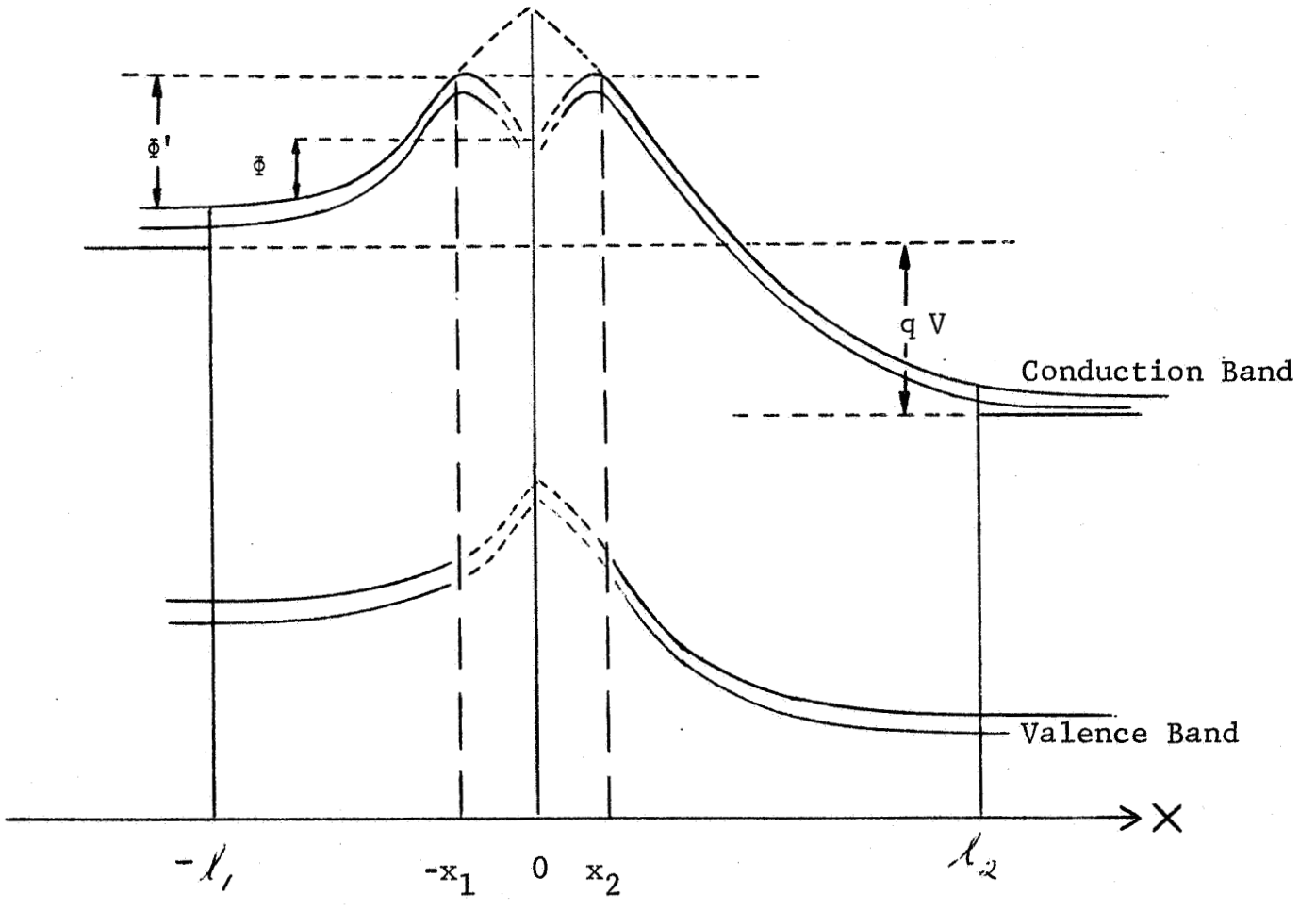

Fig. 6 - POTENTIAL DISTRIBUTION AT THE GRAIN BOUNDARY

The potential at this point is Φ', which is also measured from the bottom of the conduction band at the negatively-based side of the boundary.

Now the capacitance of the grain boundary will depend on the height of the potential barrier, Φ, only if Φ is smaller than the value of $\Phi' = 2kT \ln (N_d/n_i)$, in eV, where N_d is the number of uncompensated donors per cm^3 in the boundary region and n_i is the intrinsic carrier density. For higher barrier potentials (i.e., $\Phi > \Phi'$), the grain boundary capacitance is, in good approximation, a function of the bulk properties only.

The characteristics of the proposed grain-boundary barrier layer for $BaTiO_3$ ceramics are as follows:

Barrier layer thickness, $\ell = 2 \times 10^{-5}$ cm
Uncompensated donor concentration, $N_d = 10^{17}/cm^3$
Intrinsic carrier density, $n_i = 4 \times 10^{-1}/cm^3$
Trapped negative charges at the boundary interface, $N_t = 10^{13}/cm^2$ (The value of N_t is dependent on the grain diameter, especially in the micron-submicron range.)
Barrier height, $\Phi = 1$ eV
Electrical field across barrier layer, $F_\ell \approx 10^5$ V/cm
For $\ell = 2 \times 10^{-5}$ cm, V = 2 volts

On the basis of the above model, at T = 298°K the value of $\Phi' = 2kT \ln (N_d/n_i)$ is equal to 2.11 eV. Since $\Phi = 1$ eV, $\Phi < \Phi'$, and the dielectric properties of the grain boundary will be different from that of the bulk. This further supports the earlier hypothesis, that the dielectric constant of the grain boundary is significantly different from that of the grain in $BaTiO_3$ ceramics. Also, as $\Phi' > \Phi$, the electron potential distribution in the conduction band (Fig. 6) tends to have two maxima in the barrier region.

In considering the conduction mechanism across grain boundaries of undoped barium titanate ceramics, which can be considered as n-type materials, a semiconductor approach has been

taken. The role of the grain boundary has been considered to be primarily related to the trapping of carriers (in this case, electrons). This is valid in view of the high degree of disorder that prevails in the boundary region. For instance, the grain-boundary region can be described by an array of dislocations, which have been shown to trap electrons in other materials. The short-range order in the grain boundary, as compared to the crystallinity in the region of the grains, can also be responsible for trapping the carriers.

If the number of electrons trapped per cm^2 of the grain-boundary surface is N_t, the barrier height is Φ, N_d is the donor concentration, and q represents the electronic charge, the dielectric constant of the boundary region (K_b) can be given by:

$$K_b = \frac{2\pi N_t^2 \, q^2}{\Phi N_d \, (8.68 \times 10^{-14})} \qquad (3)$$

On the basis of our proposed boundary barrier layer model:

$$N_t = 10^{13}/cm^2$$

$$\Phi = 1 \text{ eV} = 1.6 \times 10^{-19} \text{ joules}$$

$$N_d = 10^{17}/cm^3$$

$$K_b = \frac{2\pi(10^{13})^2 \, (1.6 \times 10^{-19})^2}{(1.6 \times 10^{-19})(10^{17})(8.86 \times 10^{-14})}$$

$$K_b = 1.13 \times 10^4$$

This value of the dielectric constant of the grain boundary phase is in close approximation to the calculated value of 1.6×10^4 (from the Bruggemann equation) for an average grain size of 1μ.

The decrease in the dielectric constant of the grain-boundary phase with decreasing grain size, especially in the submicron range, could be due to a decrease in the number of trapped electrons per cm^2 of the boundary surface. If we assume that when the grain size decreases to say 0.2μ, the number of trapped electrons

per cm^2 (N_t) is reduced to 5×10^{12}, Eq. 3 gives a value of $K_b = 2.8 \times 10^3$. This value is identical to the value of K_b calculated from our earlier Bruggemann equation, using the experimental data obtained at USAECOM for $BaTiO_3$ grains of 0.2μ.

However, it is not possible as yet to define the precise mechanism responsible for decrease in the grain boundary dielectric constant with grain sizes below 1μ, in the frequency range considered. A number of mechanisms, all somewhat speculative at this stage, could be considered. The role of dislocations at grain boundaries and their interaction with free carriers is one possibility. A better understanding of the atomistic nature of the grain boundary is needed. What does an interface between grains imply? Some of these unknowns will be considered in greater depth in Section IV-D.

The exact values for the grain-boundary dielectric constant, as obtained by our calculations, do not necessarily imply that all $BaTiO_3$ ceramics have boundaries with identical K_b values. The atmosphere during preparation, the degree of stoichiometry in the material, and the presence of other titanates could certainly alter the values of Φ and N_d in Eq. 3. This would then change the value of K_b. However, the overall relationship between K_v and K_b would remain essentially unaltered. The grain-boundary phase in $BaTiO_3$ would have a dielectric constant that is grain size dependent and changes from a high value for large grains to a smaller value with decreasing grain size in the audiofrequency range. This is especially true for grain sizes from 5μ down to the submicron range.

A simple equivalent circuit, for $BaTiO_3$ ceramics on the basis of the above calculations and results would be:

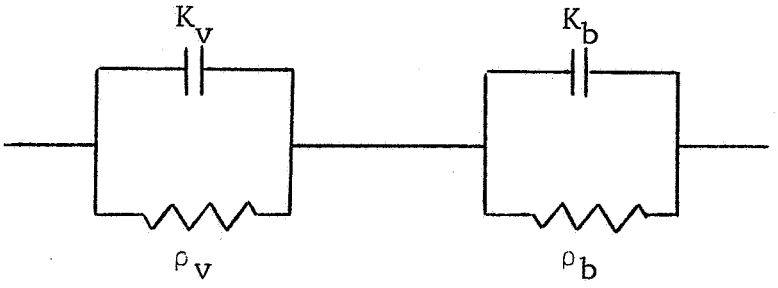

where

$K_v = 10^3$ (for all grain sizes)

$K_b = 3.9 \times 10^4$ (grain size = 3μ)

$= 3.0 \times 10^4$ (grain size = 2μ)

$= 1.6 \times 10^4$ (grain size = 1μ)

$= 7.0 \times 10^3$ (grain size = 0.7μ)

$\doteq 2.8 \times 10^3$ (grain size = 0.2μ)

$\rho_v \approx 10^9$ ohm-cm

ρ_b is probably $> \rho_v$

The calculations shown above must be considered within the limits of the assumptions in the potential distribution at the boundary. However, they do indicate that the two-phase mixture model provides a useful approach in characterizing the dielectric properties of the grain (or bulk) and grain-boundary regions.

D. The Electronic "Character" of Grain Boundaries

In studying the role of grain boundaries in the electronic properties of $BaTiO_3$ ceramics, we should attempt to recognize those salient features of a boundary region which could significantly alter or affect the electronic processes in the material.

The grain boundary (g.b.) region in ceramic materials can be considered in a number of different ways. Grain boundaries have often been referred to as "amorphous" in nature. A better way of characterization would be by defining the g.b. region as having "short-range order" or a high degree of disorder.

The grain-boundary region consists of an array of dislocations. In addition, in presently available polycrystalline materials, the impurities, vacancies, and adsorbed gases further contribute to the imperfections of the grain boundaries. Dislocations can have pronounced effects on the electrical properties of electronic materials. Associated with dislocations are energy states lying in the energy gap. The majority of the work on the electrical effects of dislocations has been done on semiconductor materials such as Ge, Si, and InSb. The observations of Gallagher[13] and Pearson et al[14] on lightly deformed Ge show that the dislocation energy levels are acceptor types; that is, the introduction of dislocations results in a decrease in the number of conduction electrons. The dislocations also scatter electrons and so reduce the mobility. Another effect associated with dislocations in Ge and Si is the formation of an atmosphere of impurity atoms along the dislocation line. This further enhances the recombination by providing localized impurity trapping levels.

Although the majority of the theoretical and experimental work pertaining to the electrical properties of dislocations has been on broad-band semiconductor materials, some evidence is available on the effects of dislocations on oxide-type materials. Chang[15] has observed that during "transient" creep of Al_2O_3, the electrical resistivity decreases. This has been attributed to the

creation of new dislocations carrying charges opposite in sign to that of the free carriers in the bulk of the material. The observed increase in electrical resistivity during "steady state" creep has been attributed to the creation of carrier-trapping point defects in the wake of moving dislocations. Recent experimental data on polycrystalline Al_2O_3 in our own laboratories[16] also indicates that charged dislocations at grain boundaries can act as traps for electrons.

Therefore, it is most probable that in $BaTiO_3$ ceramics the presence of an array of dislocations in the g.b. region acts as a barrier to electronic transport. The dislocation interaction of the g.b. region would be further dependent on the size of the adjoining grains, and would therefore exert a different "trapping" effect for large and small grain-sizes.

Attempts to explain the grain-size dependence of the dielectric properties of $BaTiO_3$, due to the active interaction of stress fields between the grains--as done by Buessem, Cross, and Goswami[2]--can be translated in terms of the electrical effects of the dislocations generated by these stresses. Therefore, consideration of the electronic properties of $BaTiO_3$ ceramics due to the interaction of dislocations with electronic transport processes does not preclude the stress interaction effects. In fact, it extends the "defect layer" concepts previously applied to other electronic ceramic materials. While the active interaction-stress approach has been successful in explaining the increase in the dielectric constant with decreasing grain sizes (down to 1μ), it cannot explain the recent results of Brandmayr et al[17] that with a further decrease in grain size (below 1μ), the dielectric constant begins falling off again. This is not explainable from the standpoint of Buessem, Cross, and Goswami's phenomenological theory[2] and their evaluation that the critical diameter of 90° domains is 1μ, because in that case the stresses in a single domain particle should not depend on its absolute size.

However, by considering the role of the grain boundary in terms of electrical (rather than mechanical) interaction of dislocations (and other defects) with the carriers, it may be possible to explain the dependency of the dielectric properties on grain size in a more coherent way.

In addition to dislocations in the g.b. region of $BaTiO_3$ ceramics, impurity ions, vacancies and adsorbed gases can all interact and contribute towards the creation and interaction of charge carriers in the material. All these imperfections must be considered as traps at grain boundaries, forming potential barriers through which electrons, taking part in the conduction process, have to tunnel.

It is not yet clear how the g.b. region acquires electrical characteristics different from that of the bulk or the mechanism whereby it is responsible for creating barriers for electron transport between adjacent grains. However, several possibilities do exist.

For instance, if dislocations accept electrons, the g.b. charges up negatively and presents a barrier to current flow in n-type materials; if they donate electrons, the g.b. charges up positively and presents a barrier to current flow in p-type materials. Electrical conductivity measurements by Rupprecht et al[18] on single-crystal $SrTiO_3$ unambiguously indicate that this material is an n-type semiconductor, with a mobility of the order of 10 cm^2 $volt^{-1}$ sec^{-1}. Results by Heywang[19] on $BaTiO_3$ also tend to indicate that $BaTiO_3$, like $SrTiO_3$, is an n-type material. Therefore, in $BaTiO_3$ ceramics, the array of dislocations in the g.b. region would present a barrier to current flow, and the g.b. would have a higher resistivity than the bulk.

The depletion of oxygen vacancies from the g.b. region under an electrical field could also lead to a high-resistivity region.

Deviations from stoichiometry in $BaTiO_3$ further complicate the situation. If the deviation from stoichiometry, for instance, resulted in more anion (oxygen) vacancies rather than cation vacancies and if dislocations are regarded as a source of vacancies, then they would acquire, in equilibrium, more negatively charged jogs than positive. The dislocation line would then become negative with respect to the bulk and would be surrounded by a positive space charge of anion vacancies.

The negative charge of a g.b. can come from the donors in $BaTiO_3$, whose electrons are captured by boundary states. As a result, grain boundary charges leave ionized donors behind.

It should be remembered that oxygen vacancies, along with Ti^{+3} groups, can be formed easily during the high-temperature preparation of $BaTiO_3$ ceramics. The oxygen vacancies are closely bound to the Ti^{+3} groups and cannot participate in any low-temperature conduction process. However, they can experience a torque which leads to a direct dielectric polarization and a direct dielectric absorption current.

Although it is not possible at this time to define the predominant mechanism that characterizes the grain-boundary region, it seems certain that this region is electronically different from the adjoining grains. The manner in which this defect region interacts with the bulk charge transport processes would depend on the dimensions of the adjoining grains. The thickness of the g.b. region may be of the order of 0.1 to 1.0μ, typical for a Schottky-type barrier or space-charge dominated region. For $BaTiO_3$ ceramics, with grain size less than 1μ, the effective properties would then be significantly altered by the characteristics of the g.b. region, and would be different from those of comparatively larger grain sizes ($\geq 1\mu$). Undoubtedly, much remains to be done to unambiguously characterize the properties of the g.b. region.

In considering electronic processes in a low-conductivity material such as barium titanate, we are cognizant of the fact that conventional band theory cannot be rigorously applied. Charge transport in materials having mobilities of the order of less than 1 cm^2 $volt^{-1}$ sec^{-1} have been described in terms of an electron (or polaron) hopping between localized sites. At low temperature, the polaron tunnels through the crystal in a narrow band, the bandwidth and mobility decreasing rapidly with increasing temperature, until the mean free path becomes equal to the lattice spacings. The band model, then, is not applicable, and the polaron jumps randomly from ion to ion by means of a phonon-activated process.

To date, however, few aspects of this theory have been experimentally tested. At present, the only unequivocal example of hopping transport in a crystalline solid is provided by orthorhombic sulfur. Recent results[20] have led to the rejection of the hopping model for NiO and other 3d oxides, and raises doubts on its validity for other materials such as ferrites, titanates, etc. It is not certain as yet which type of narrow band model is appropriate. The presence of grain boundaries in sintered ceramic materials such as $BaTiO_3$ could produce misleading effects in interpreting the conduction process in terms of a possible hopping model. The introduction of disorder, especially in the boundary regions, leads to localized states. The low mobilities observed in some oxides may be due to shallow trapping. It is possible that disorder can introduce "tails" on the energy states which extend into the forbidden gap and corresponds to localized states. Thus, hopping conduction could predominate at low temperatures ($T < 298°K$), and some kind of band conduction at higher temperatures.

Furthermore, in mixed oxide materials such as $BaTiO_3$, deviations from stoichiometry, vacancies and other defects result in additional energy levels in the band gap. This further complicates the band structure, and narrow bands may exist in addition to the valence bands. This results in lower activation

energies for conduction than in single oxides (Al_2O_3), because the excitation energy is less than the full gap width, and the narrow band limits the charge density thus reducing the mobility.

Undoubtedly, in working with materials such as Al_2O_3 but less so with TiO_2 and $BaTiO_3$, the limits of the band model are approached. However, it should be pointed out that in spite of a partial breakdown of band theory in insulating materials, band theory has proved remarkably successful in explaining a wide range of electronic properties of ceramic oxides.

V. EXPERIMENTAL WORK

A. Introduction

The experimental work described in this section encompasses the following interrelated areas: the characterization of defect surface layers, especially in micron and submicron sized $BaTiO_3$ powders; the role of grain boundaries in the electronic behavior of sintered $BaTiO_3$ ceramics as a function of grain size and stoichiometry; and exploratory work on a new electron beam scanning technique to directly evaluate the dielectric characteristics of boundaries and interfaces.

B. Characterization of Starting Materials

In obtaining $BaTiO_3$ powders from various sources, major emphasis was placed on the stoichiometry and purity levels of the material. A number of the materials used in this program are in the developmental stage and not necessarily available commercially. Although the purity level of these powders is not similar to what has been achieved with elemental semiconductor materials, such as silicon, it is an order of magnitude superior to what is used for commercial $BaTiO_3$ capacitors. Efforts are being continued to obtain sample powders of higher and better purity. The fact that the extent of purity has been "finger-printed" for all our starting materials enables us to determine the possible effects of various impurities.

As pointed out in the preceding discussions, stoichiometry is an important factor in $BaTiO_3$ ceramics. The ratio of BaO/TiO_2 and the presence of other titanates of barium, must also be taken into consideration. To this extent, we have been able to obtain $BaTiO_3$ powders of exact stoichiometry.

Therefore, although the concept of "ultra high purity" as defined for silicon has not yet been achieved for $BaTiO_3$, the very significant improvements in the purity and stoichiometry of the $BaTiO_3$ material to be investigated on this program justifies their use and makes the interpretation meaningful.

The barium titanate powders used in this investigation were obtained from the National Lead Co. Tables II and III list data on these powders, provided by the manufacturers. Material "C" is a high purity $BaTiO_3$, prepared by the Titanium Pigment Division. The $BaTiO_3$ powders shown in Table III were obtained from the TAM Division. Material "F" is TAM C. P. $BaTiO_3$ which has had a low thermal treatment (700°C). Material "H" is an experimental stoichiometric powder which has a BaO/TiO_2 ratio corresponding to unity. Material "G" is TAM $BaTiO_3$ capacitor grade material and was included for comparison purposes, only.

The particle size distribution of material "C" has been determined by a Kaye Centrifugal Disc Photosedimentometer developed at IITRI. In this process, powder suspensions are passed through the photosedimentometer in which the attenuation of light passing through the settling particles is measured and recorded on a strip chart. The chart data are programmed into a computer for final analysis. Figure 7 shows the particle size distribution for this material. This distribution at 0.5μ intervals is shown in Fig. 8.

Figures 9 and 10 show scanning electron micrographs of $BaTiO_3$ powders "C" and "H" which were used in the dielectric characterization of surface defects in particulate systems described in following sections.

Table II

ANALYSIS OF $BaTiO_3$ POWDER "C"
(Provided by National Lead Co., Titanium Pigment Division)

Chemical Analysis			
BaO	65.9 wt%		
TiO_2	34.5 wt%		
Spectrographic Analysis			
SiO_2	0.0008%	Mg	<0.0001%
Fe_2O_3	<0.001%	Cu	<0.0001%
Al_2O_3	0.0005%	Pb	<0.0001%
Sb_2O_3	<0.005%	Mn	<0.00001%
SnO_2	<0.0005%	Cr	<0.00005%

Table III

CHEMICAL ANALYSES OF $BaTiO_3$ POWDERS "F," "H," AND "G"
(Provided by National Lead Co., TAM Division)

	$BaTiO_3$ "F"	$BaTiO_3$ "H"	$BaTiO_3$ "G"
Chemical			
BaO + SrO	64.81 wt%	65.79 wt%	64.70 wt%
TiO_2	34.00	34.21	33.60
Al_2O_3	---	---	0.37
SO_3	---	---	0.21
SiO_2	---	---	0.27
P_2O_5	---	---	0.06
CO_2	0.90	0.05	0.86
Spectrographic			
SrO	0.02		0.49
ZrO_2	0.01		0.03
Fe_2O_3	---		0.005
Al_2O_3	0.005		---
SiO_2	0.02		---
MgO	---		0.03
CaO	---		0.10
Na_2O	0.01		0.10
Particle Size			
Fisher No.	0.55	1.10	1.52

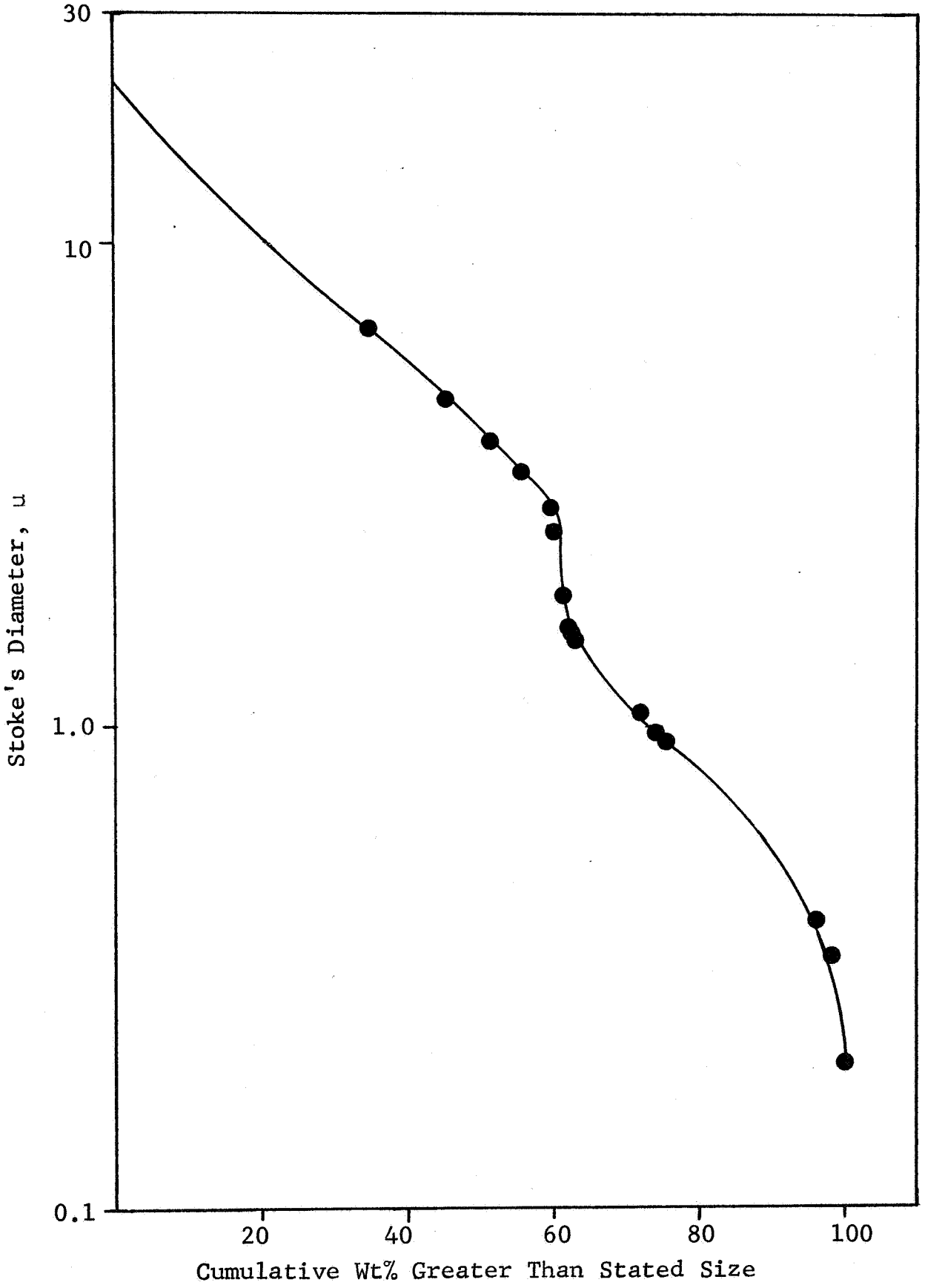

Fig. 7 - PARTICLE SIZE DISTRIBUTION OF $BaTiO_3$ POWDER - MATERIAL C

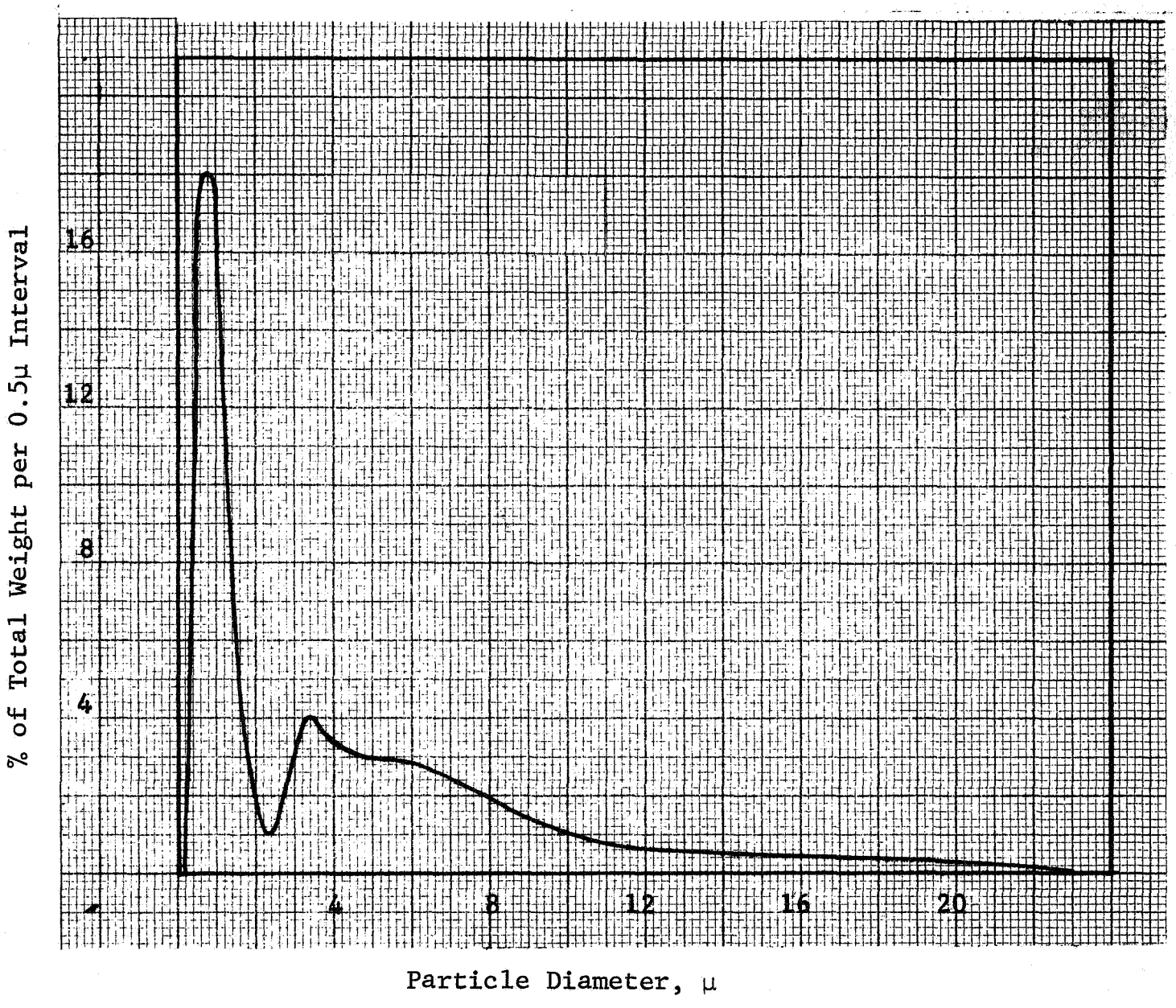

Fig. 8 - PARTICLE SIZE DISTRIBUTION FOR $BaTiO_3$ MATERIAL C, FOR 0.5μ INTERVALS

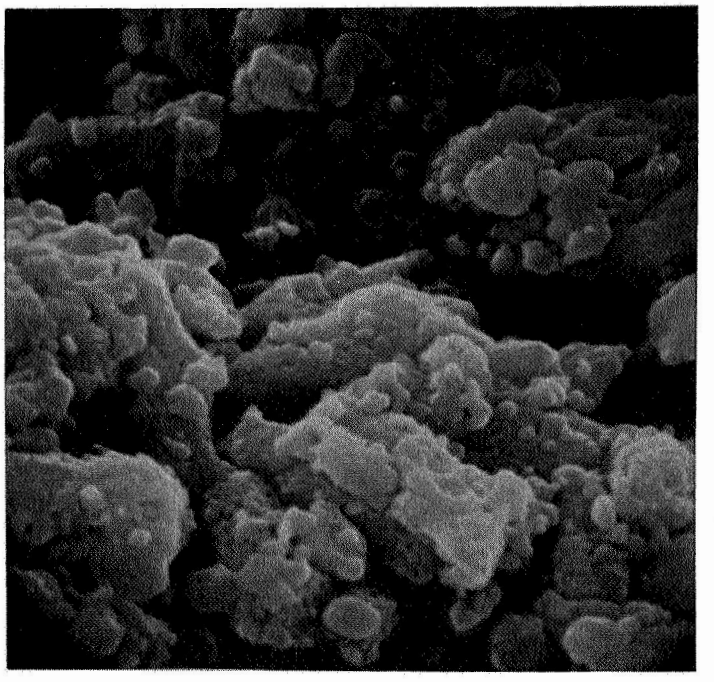

Fig. 9 - SCANNING ELECTRON MICROGRAPH OF $BaTiO_3$ POWDER "C" (X6000)

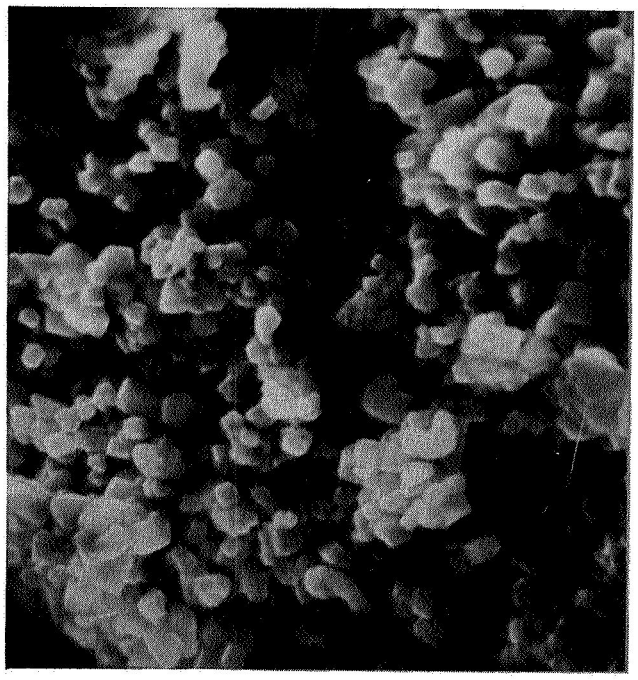

Fig. 10 - SCANNING ELECTRON MICROGRAPH OF $BaTiO_3$ POWDER "H" (X10000)

C. Preparation of Samples

The steps in preparation of the samples were as follows:

a) Addition of organic binder to the as-recieved powder. The binder chosen was 1.5% cellulose acetate plus 6% dibutyl phthalate in acetone.

b) Cold pressing of discs--5.4 cm (2 1/8 in.) diameter by 1-3 mm thick--in steel dies at 10,000 psi.

c) Burning out of the organic binder--650°C for about 1/2 hr.

d) Sintering of the samples at various temperatures. The heating rate was ~250°C/hr. The sintering atmosphere was air with oxygen fed in at a low rate.

e) Application of electrodes: a number of different electrode materials, such as gold, platinum, and silver, applied by vapor deposition and in the form of a paint, have been used.

Cold-compaction characteristics of the selected starting materials have been determined and discussed in an earlier IITRI report.[1] An evaluation of the optimum compaction and firing procedures was obtained and applied to the test specimens chosen for this investigation.

D. Characterization of Surface Defects in $BaTiO_3$ Powders

1. Introduction

The characteristics of the surface defect layer of powders play a significant role in determining the properties of the sintered ceramic. Surface phenomena strongly affect particle size distribution and shape, its rheology in the forming operations, degasification during green body compaction, and finally the sintering mechanism itself. All these factors are interrelated to the microstructure of the final ceramic, and hence affect its properties. With micron and submicron sized powders, because of the increased surface-to-volume ratio, the effects due to adsorbed gases and surface charges can alter the electronic behavior of the fired ceramic.

Generally speaking, the surface of a solid material is in an unusual crystallographic state due to valence requirements. In nonreducible oxides such as SiO_2 and Al_2O_3, the requirements of lowest energy lead to a surface ordinarily consisting of oxide ions rather than less polarizable metal ions. Further, to satisfy chemical valences, many of the dibalent surface oxide ions have univalent hydrogen attached to them.

Water vapor plays a significant role in determining surface phenomena of ceramic powders. The interaction of H_2O with oxide surfaces depends to some extent on the nature of the chemical bonding of the material. For instance, with silica and alumina the valence of the cation and the lattice structure of the oxide suggest the possibility of surface hydroxyl groups, for satisfying the valence requirements at the surface. In the case of a ceramic material with an ionic lattice, such as MgO, the above-mentioned condition does not arise. This results in the adsorbed water being in the form of hydroxyl ions rather than uncharged hydroxyl groups which form covalent bonds with the lattice. Recent work done by Anderson et al[21] tends to

indicate that at temperatures exceeding 250°C chemisorption of H_2O takes place. A simple model for water chemisorbed on MgO consists of a hydroxyl group adsorbed on a surface Mg^{+2} ion and the remaining hydrogen forming a second hydroxyl group with an adjacent O^{2-} ion. Studies on the adsorption of water on BeO powders[22] indicate that, even at 25°C, water is physically as well as chemically adsorbed. Further, chemisorbed water in the form of hydroxyl groups greatly increases the number of defects at or near the surface of BeO.

The possible role of the proton in the degradation process of titanates has been suggested by a number of investigators.[1,23] The proposed degradation mechanisms entailed proton generation at the anode and migration towards the cathode, or generation of anion vacancies. In either case, the electronic conductivity of the degrading titanate can be ascribed to the "hopping" of the 3d electrons of the Ti^{+3} ions. It is also possible that field-induced changes in electron distribution could be responsible for the degradation process.

However, not enough is understood about the effects of water vapor on micron and submicron sized $BaTiO_3$ powders. What are the nature of the defects, as dehydration proceeds? Does the high energy surface strain condition on $BaTiO_3$ powders, due to extensive dehydration, affect the polarization processes in a material that is both ferroelectric and piezoelectric? From an electronic point of view, dehydration can be considered analogous to charging a condenser, as the "dry surface" is assumed to have a more pronounced "double-layer" characteristic than the surface covered with hydroxyl ions. What is the precise electronic structure of this outer defect layer? All these are unanswered questions that are pertinent to the characterization of $BaTiO_3$ powders.

An investigation on the effects of various gaseous environments on the dielectric characteristics of $BaTiO_3$ powders and sintered specimens has been carried out. Particular emphasis has been placed on the creation and interaction of surface defects

on micron and submicron sized powders due to water vapor. The results indicate that the surface of barium titanate powders can be characterized by evaluating the changes in ac conductivity due to controlled partial pressure of water. Further, it may be possible to monitor very small deviations in stoichiometry (BaO/TiO_2 ratio) from a significant change in ac conductivity ($\Delta\sigma$) as a function of P_{H_2O}.

2. Experimental Procedure

Dielectric measurements were carried out on cold-compacted (unsintered) and sintered $BaTiO_3$ specimens, under controlled gaseous environments. The test specimens were prepared by cold-pressing and conventional sintering process from three types of starting materials, referred to as "C", "F", and "H". The chemical analysis of these $BaTiO_3$ powders has been shown in Tables II and III (see Section VB).

The dielectric measurements were carried out in situ under controlled gaseous environments in a modified vacuum system. Prior to the introduction of a specific atmosphere, the specimen in the bell-jar system was subjected to a vacuum of about 10^{-6} torr. The specimen was evaluated in air, vacuum ($\sim 10^{-6}$ torr), and under positive pressures of oxygen and nitrogen. The partial pressure of water vapor, P_{H_2O}, was controlled by passing high-purity argon gas over drying columns of Drierite ($CaSO_4$), then Anhydrone ($Mg(ClO_4)_2$) to control P_{H_2O} at 7×10^{-6} atm, and over 85.70 and 45% strength H_2SO_4 solutions to obtain P_{H_2O} values of 7×10^{-5} atm, 1.0×10^{-3} atm, and 1.5×10^{-2} atm, respectively. The argon gas was bubbled through distilled water to control P_{H_2O} at 3×10^{-2} atm.

The effects of water vapor were evaluated on two different types of $BaTiO_3$ powders, having comparable particle size but differing BaO/TiO_2 ratios. The two types of powders identified as "C" and "H" are high-purity materials not available on a commercial basis. The compositional characteristics of the test specimens are shown in Table IV. Specimen No. H-1p was

Table IV

PHYSICAL AND COMPOSITIONAL CHARACTERISTICS
OF $BaTiO_3$ TEST SPECIMENS

Specimen No.	#Initial Average Particle Size, u	BaO/TiO_2	Density, % Theoretical
H-1p (cold-compacted)	0.75	1.001	54
H-2s (sintered)	--	1.001*	95
C-1p (cold-compacted)	0.8	0.995	52

*Value obtained on starting material.
#Determined at IITRI by Kaye Centrifugal Disc Photosedimentometer.

cold-compacted from material H, and had a density 54% of theoretical. The agglomerated particles should, by and large, have surface characteristics corresponding to the initial powder particulates. Specimen H-2s was sintered to a density 95% of theoretical, also prepared from the same material H. Characterization of dielectric loss phenomenon on these two specimens should indicate some correlation between the nature of the defect surface layer of the powder particles and the boundary phase in the ceramic.

Specimen No. C-1p was cold-compacted from material C, and had a density 52% of theoretical. The original particle size of material C was similar to that of material H. However, their BaO/TiO_2 ratios are different: 1.001 for specimen H-1p and 0.995 for specimen C-1p. Whether the rate-controlling species due to the effects of water vapor are influenced by the stoichiometry of the material should be revealed by comparing the data on the two specimens.

The samples were evaluated, simultaneously, at various P_{H_2O} values, ranging from 7×10^{-6} to 10^{-1} atm. To obtain equilibration, the specimens were exposed to each of the controlled atmospheres for about 70 hr prior to obtaining the electrical measurements.

All dielectric measurements were performed with a General Radio type 1615-A capacitance bridge. The capacitance and dissipation factors were measured between frequencies of 20 to 10^5 Hz. From these data the values of dielectric constant (K'), dissipation factor (D), and ac conductivity (σ_{ac}) were calculated.

3. Results and Discussion

a. Stoichiometric Effects on Dielectric Loss Due to Water Vapor on $BaTiO_3$ Particulates

The effects of the water partial pressure on the ac conductivity (σ_{ac}) of specimens H-1p, H-2s, and C-1p are shown in Figs. 11, 12, and 13, respectively. The results indicate that

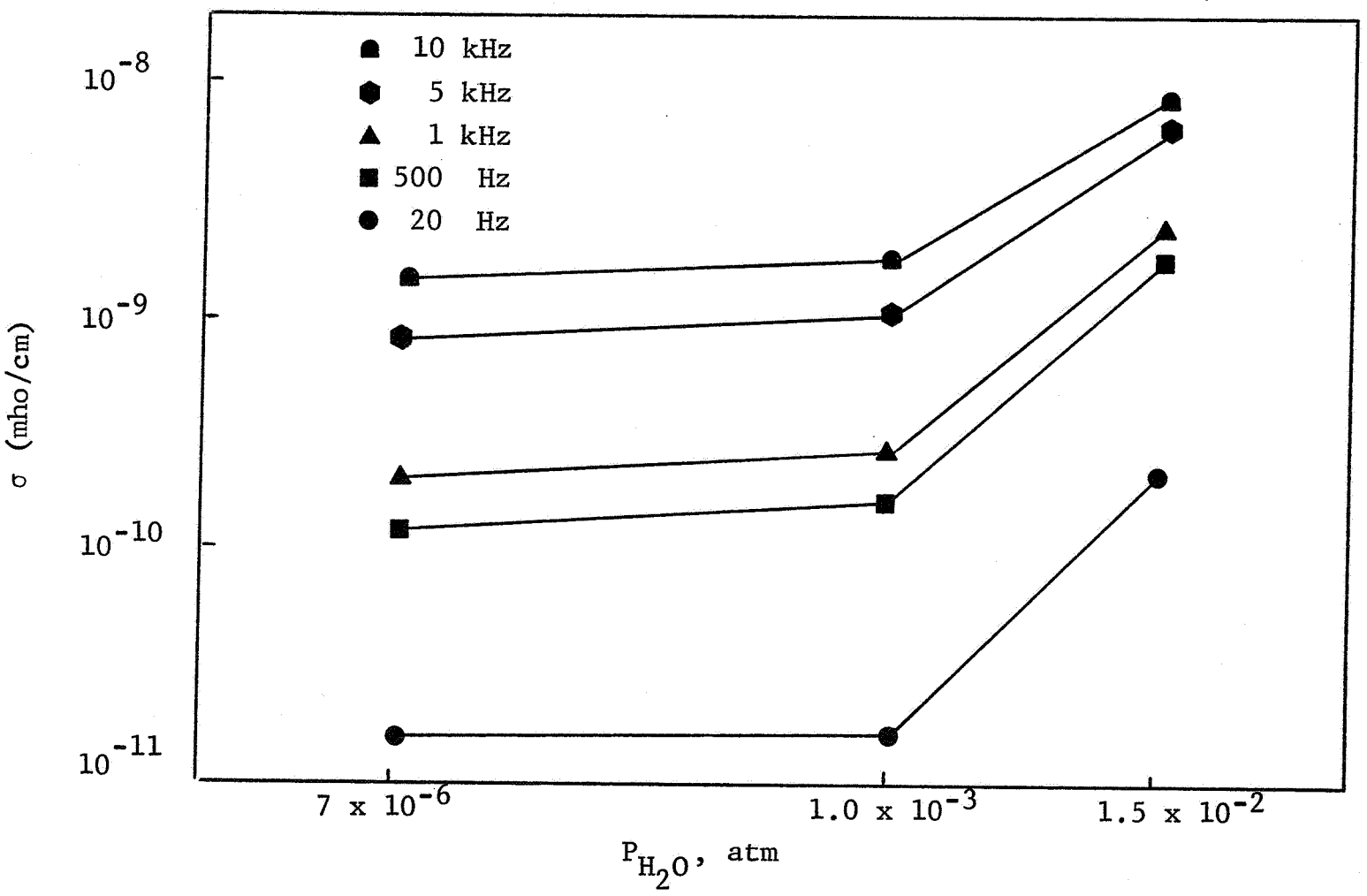

Fig. 11 - EFFECT OF P_{H_2O} ON AC CONDUCTIVITY OF SPECIMEN H-1p

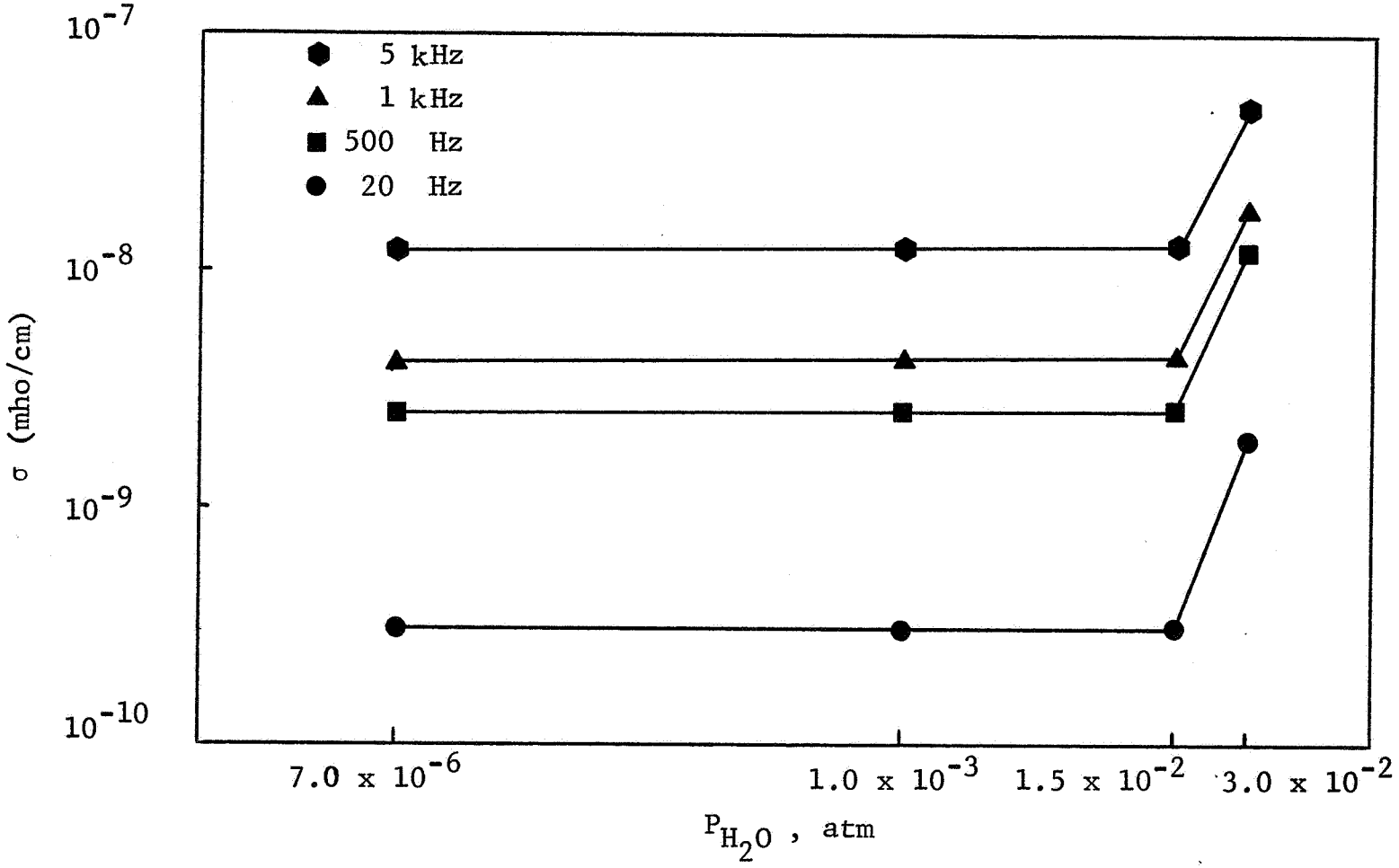

Fig.12 - EFFECT OF P_{H_2O} ON AC CONDUCTIVITY OF SPECIMEN H-2s

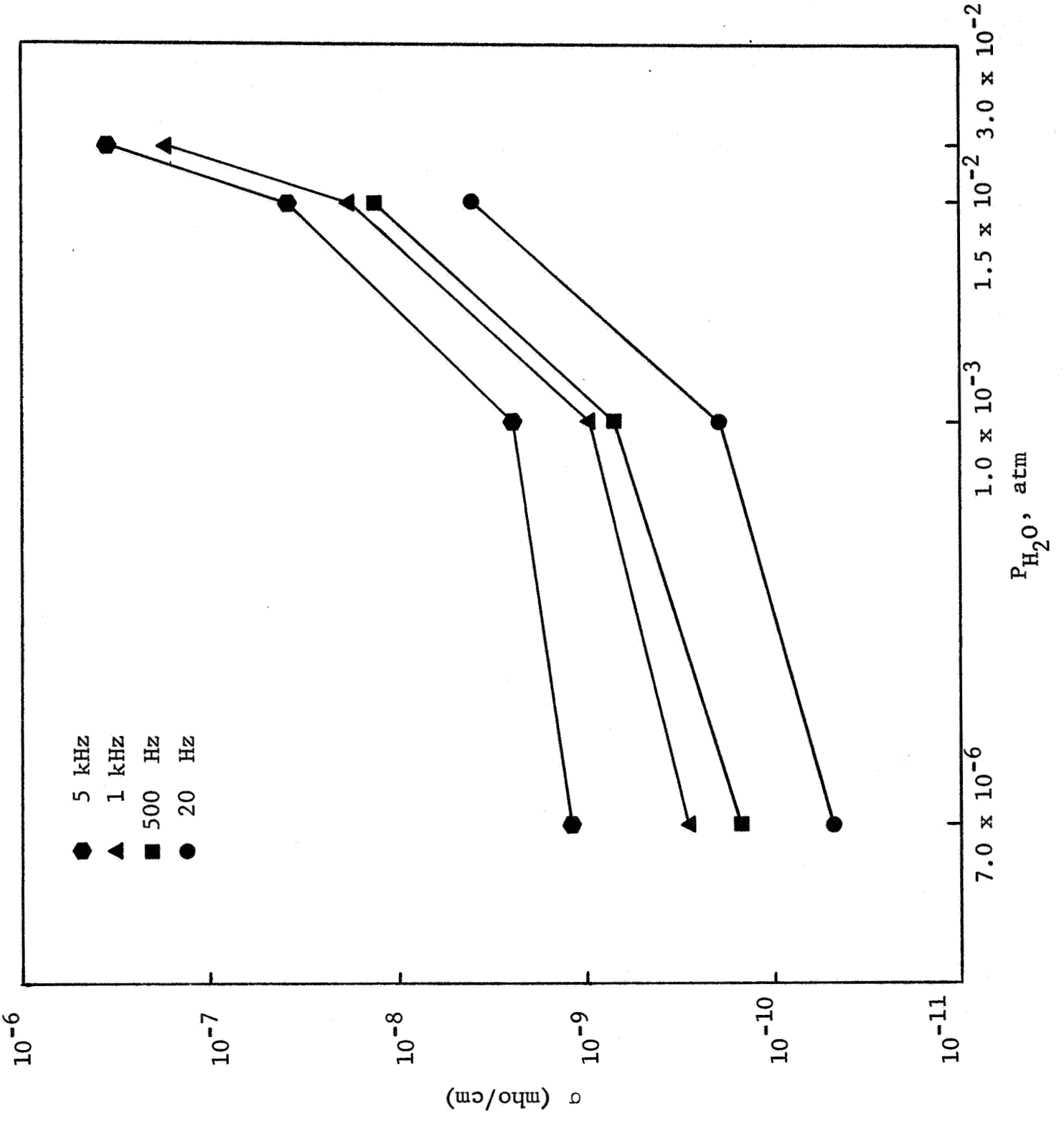

Fig. 13 - EFFECT OF P_{H_2O} ON AC CONDUCTIVITY OF SPECIMEN C-1p

material "H" in the unsintered form shows a significant change in σ_{ac} at values of $P_{H_2O} > 10^{-3}$ atm. The same material when sintered to a dense ceramic does not show any significant conductivity changes, until a value of $P_{H_2O} > 1.5 \times 10^{-2}$ atm has been reached. The data obtained on material "C" (Specimen No. C-1p) indicates that in spite of the lack of equilibration discussed below, the σ_{ac} is more sensitive to changes in P_{H_2O} values than for similar specimens prepared from material "H". The conductivity values have been obtained by exposing the test specimen for 72 hr at each successive partial pressure of water. This time period was sufficient for equilibration at the lower P_{H_2O} values for all three test specimens. At a P_{H_2O} value of 3×10^{-2} atm no changes in σ occurred for exposure times ranging from 48 to 120 hr, for the sintered specimen (H-2s). A slight change in σ was obtained for the porous, cold-compacted specimen (H-1p), while the porous, cold-compacted specimen (C-1p) prepared from material "C" did show a change in σ values for exposure times of 48 to 72 hr, indicating that equilibration had not taken place.

The frequency dispersion of the dielectric constant, K', of the cold-compacted specimens, at various P_{H_2O} values has been shown in Figs. 14 and 15. Water vapor, at partial pressures of about 1.5×10^{-3} atm and above, causes a significant increase in the dielectric constant, especially at lower frequencies (< 1 kHz).

A significant difference in starting materials "H" and "C" is that the former has a BaO/TiO_2 ratio corresponding to one indicating stoichiometry, while material "C" has a slight excess of TiO_2. The effects of stoichiometry on the change in dielectric loss due to water vapor have been summarized in Fig. 16. The experimental data indicate that even slight deviations from stoichiometry as represented by specimens H-1p and C-1p, can significantly affect the change in ac conductivity due to water vapor effects. It should be pointed out that the barium titanate powders having small differences in stoichiometry show significantly

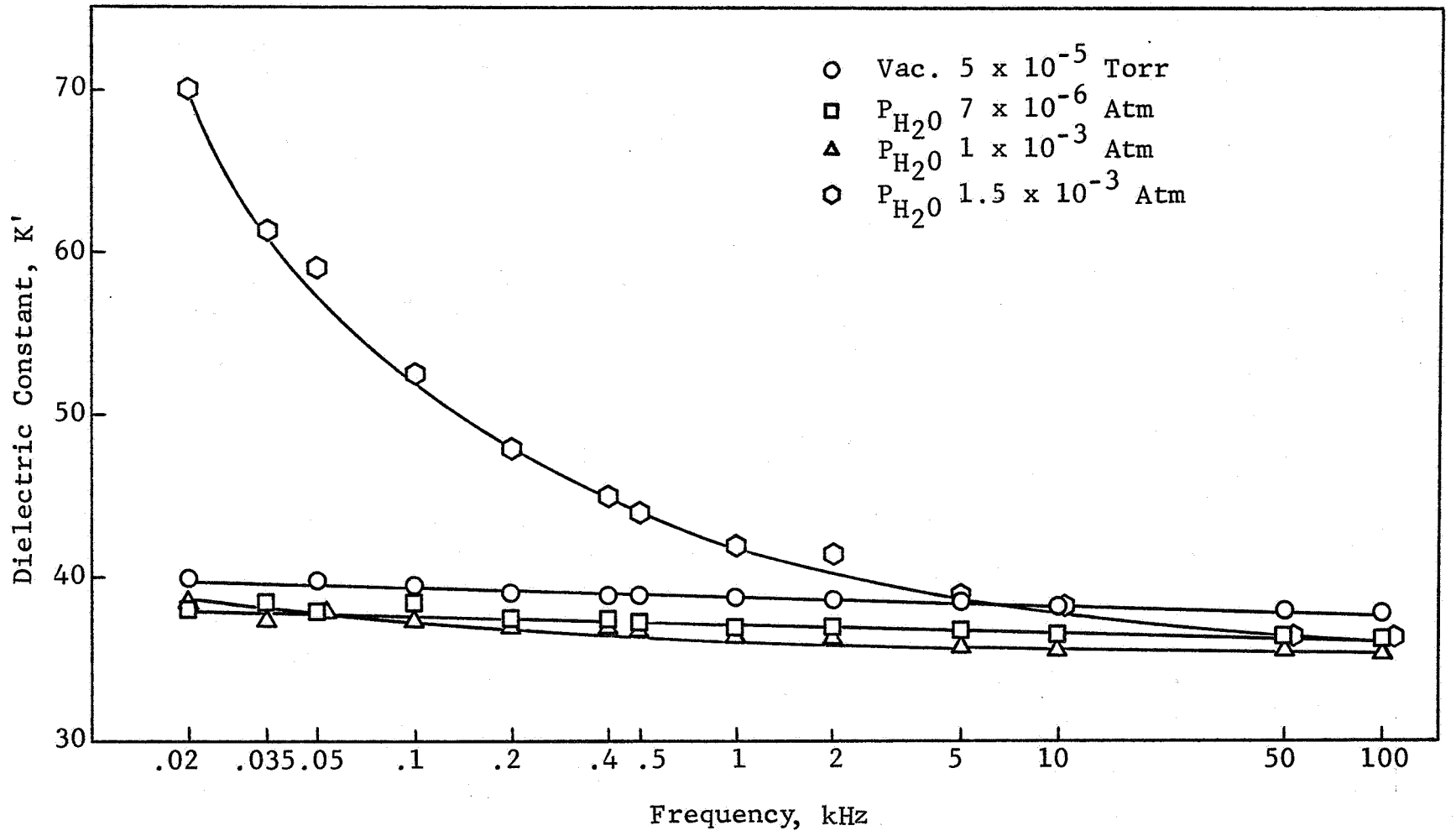

Fig. 14 - EFFECT OF P_{H_2O} ON DIELECTRIC CONSTANT K' OF SPECIMEN H-1p

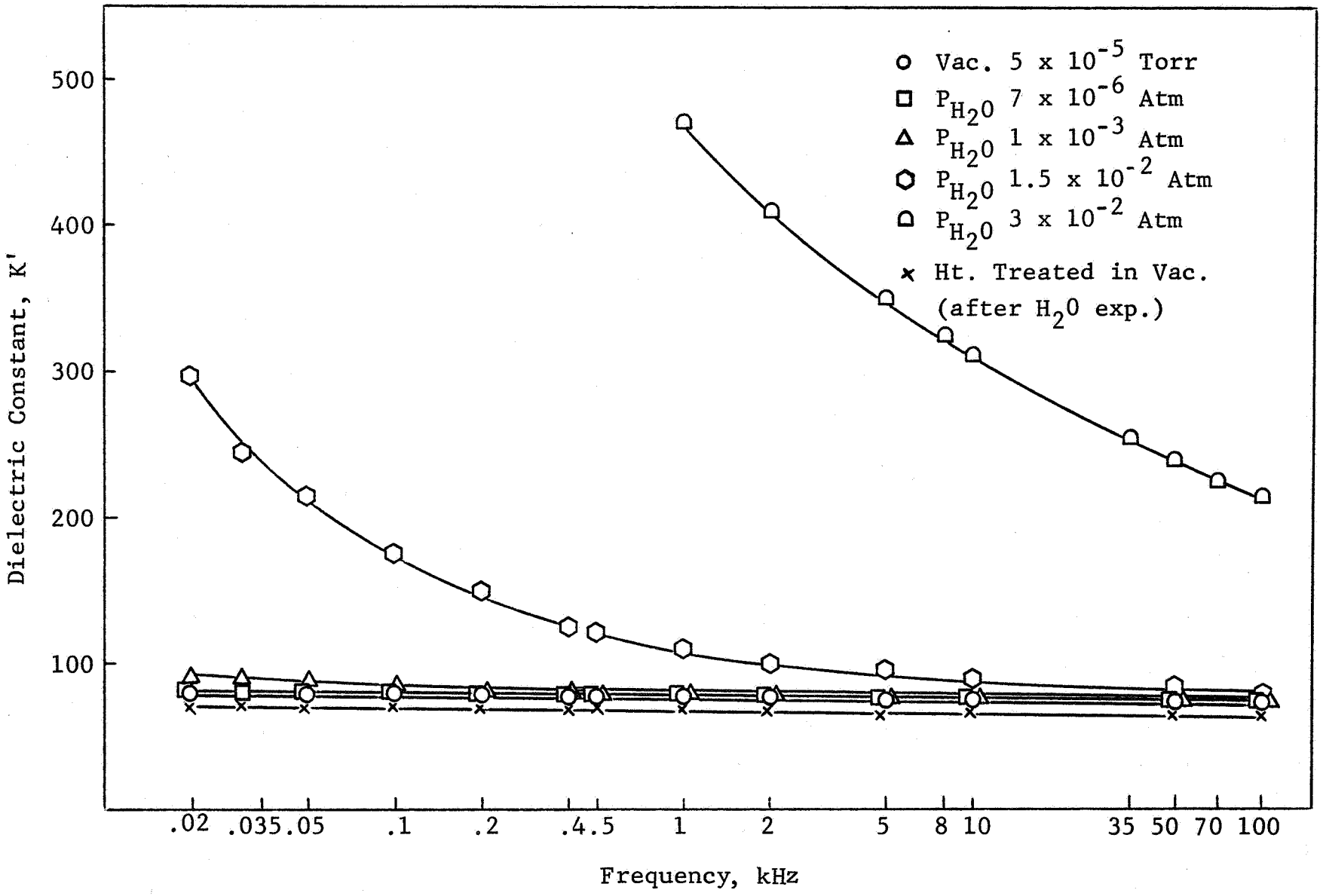

Fig. 15 - EFFECT OF P_{H_2O} ON DIELECTRIC CONSTANT K' OF SPECIMEN C-1p

different dielectric loss phenomena due to water vapor, but have nearly identical values of D and σ_{ac} at a P_{H_2O} value of 7×10^{-6} atm and in vacuum ($\sim 10^{-6}$ torr). The enhanced dielectric loss in the material with a slight excess of TiO_2 ("C-1p"), as compared to the stoichiometric material ("H-1p"), only manifests itself with increasing partial pressure of H_2O, as shown in Fig. 16.

On the basis of this experimental evidence, we have hypothesized that the differences in the dielectric loss behavior, as a function of very slight deviations from stoichiometry, are due to different manners in which water interacts with stoichiometric and off-stoichiometric "$BaTiO_3$" surfaces. It is possible that at low P_{H_2O} values, physical adsorption of water takes place with both types of $BaTiO_3$ material. With an increase in P_{H_2O}, water is more easily chemisorbed on off-stoichiometric barium titanate powders than on stoichiometric material due to the valence requirements at the surface. Whether chemisorbed water creates other surface defects more easily with the off-stoichiometric than the stoichiometric material is a possibility that needs to be confirmed. It is conceivable that in barium titanate material with excess Ti, the injected protons H^{+1} from the adsorbed water, easily reduces the Ti^{+4} to Ti^{+3}, thus causing an increase in the loss. The exact nature of the adsorbed species and the defects created therein could be verified by a combination of techniques such as infrared adsorption spectra and n.m.r.

However, these results do indicate that the surfaces of barium titanate powders can be characterized by evaluating the changes in ac conductivity due to controlled partial pressure of water. Further, it may be possible to monitor very small deviations in stoichiometry (BaO/TiO_2 ratio) from significant changes in the ac conductivity ($\Delta\sigma$) as a function of P_{H_2O}.

b. Effects of Gaseous Environments on Dielectric Properties of $BaTiO_3$

The effects of gaseous environments on the dielectric characteristics of a dense, sintered $BaTiO_3$ have also been

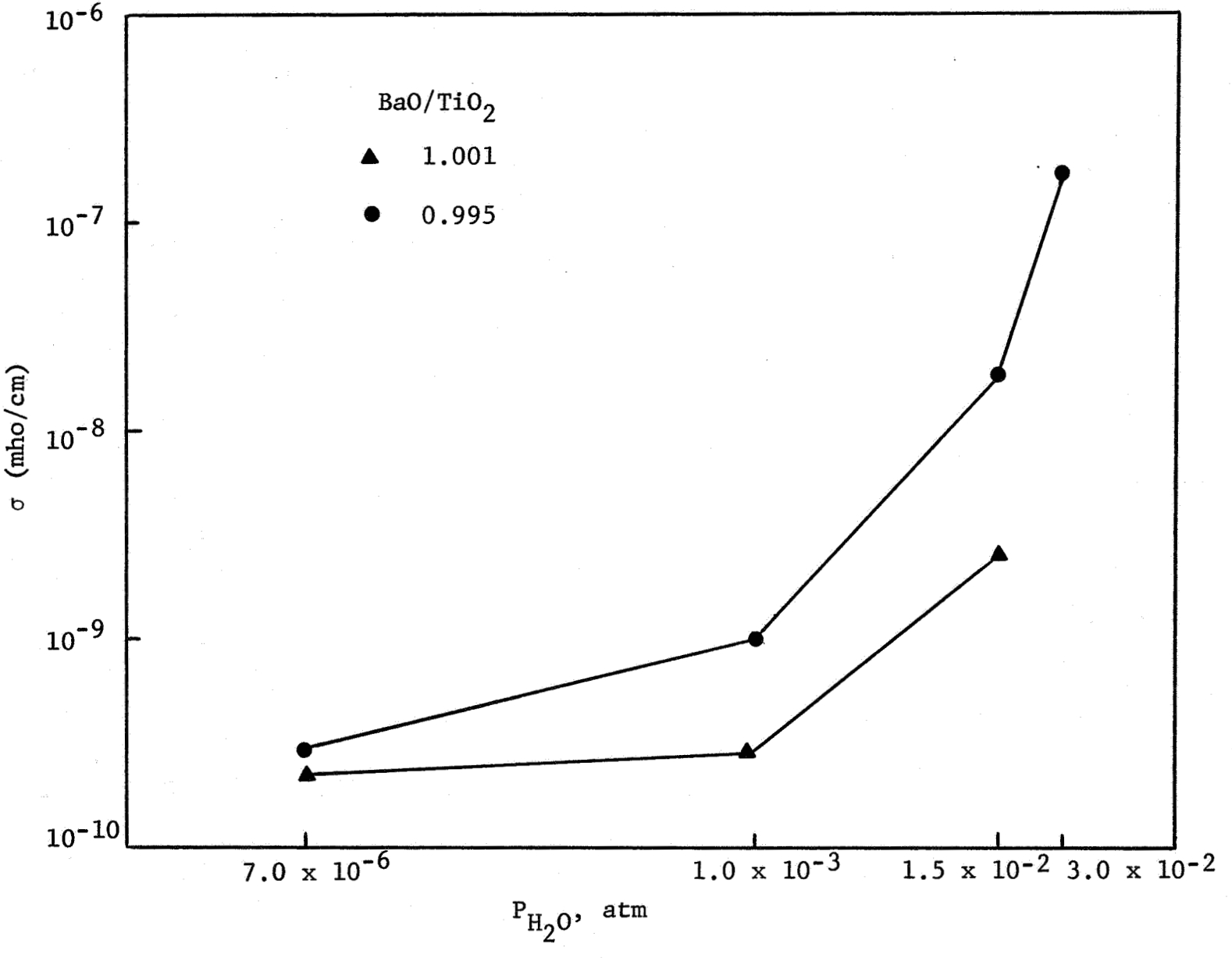

Fig. 16 - EFFECT OF STOICHIOMETRY ON DIELECTRIC LOSS DUE TO WATER VAPOR ON $BaTiO_3$ POWDERS (Measured at 1 kHz)

evaluated. A high-purity $BaTiO_3$ material designated as "F" (see Table III) was used.

The results tend to indicate that K', D, and σ_{ac} of the sintered $BaTiO_3$ specimen does not change significantly when measured either in air, oxygen, nitrogen or under a vacuum of 10^{-5} to 10^{-6} torr. Figures 17, 18, and 19 show the effect of these specific atmospheres on the dielectric behavior of sintered $BaTiO_3$. It is quite probable that, at lower pressures in the vacuum system, the effects may be different. At a vacuum of 10^{-6} torr, it takes 0.23 sec to form a monolayer of adsorbed gas, while at 10^{-9} torr, it takes 38 min to form a monolayer. Therefore, it would be interesting to study the dielectric properties of $BaTiO_3$ under a vacuum of about 10^{-9} torr, where sufficient experimental time would be available to study the intrinsic surface characteristics without the effects of possible adsorbed layers.

The dielectric characteristics of $BaTiO_3$ are significantly affected by water vapor as shown in the preceding section. Figure 17 shows the large frequency dispersion of the dielectric constant due to water vapor (P_{H_2O} at 3×10^{-2} atm). At frequencies less than 2 kHz, the values of K' due to the effect of water vapor are significantly higher than those obtained in oxygen, nitrogen, or vacuum. For instance, at 20 Hz the dielectric constant (K'), due to water vapor effects, was 2,740 as compared to about 2,050 under the other atmospheres. The loss tangent is also significantly higher when measured under a water partial pressure of 3×10^{-2} atm, as shown in Fig. 18b. Figure 19 shows the ac resistivities under the various gaseous environments.

The data indicate that the dielectric loss is virtually independent of the oxidizing nature of the atmosphere. The controlling factor seems to be the partial pressure of the water vapor.

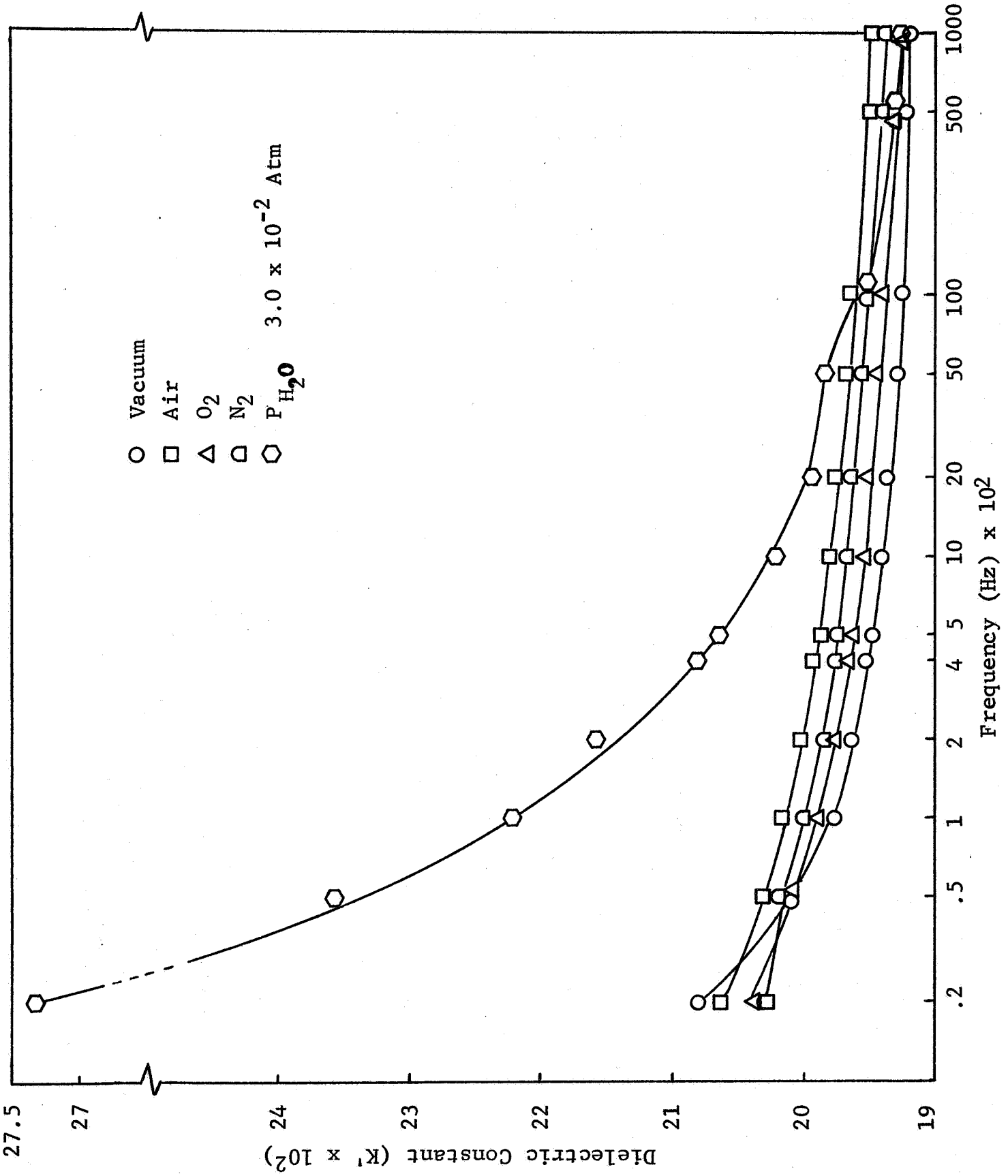

Fig. 17 - EFFECT OF GASEOUS ATMOSPHERES ON FREQUENCY DISPERSION OF DIELECTRIC CONSTANT FOR SAMPLE F3 (SINTERED 1350°C)

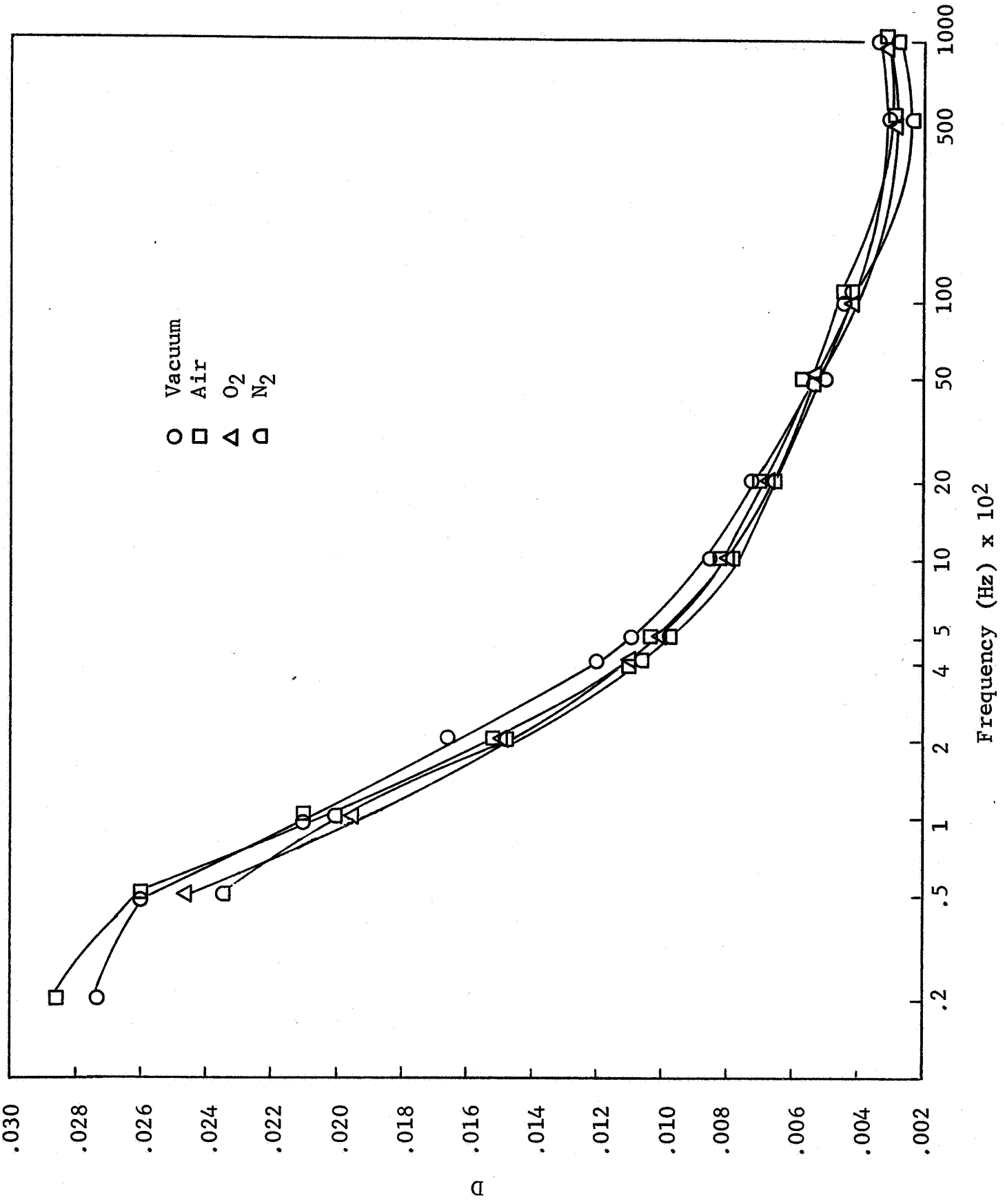

Fig. 18a - EFFECT OF GASEOUS ATMOSPHERES ON FREQUENCY DISPERSION OF D FOR SAMPLE F3 (SINTERED 1350°C)

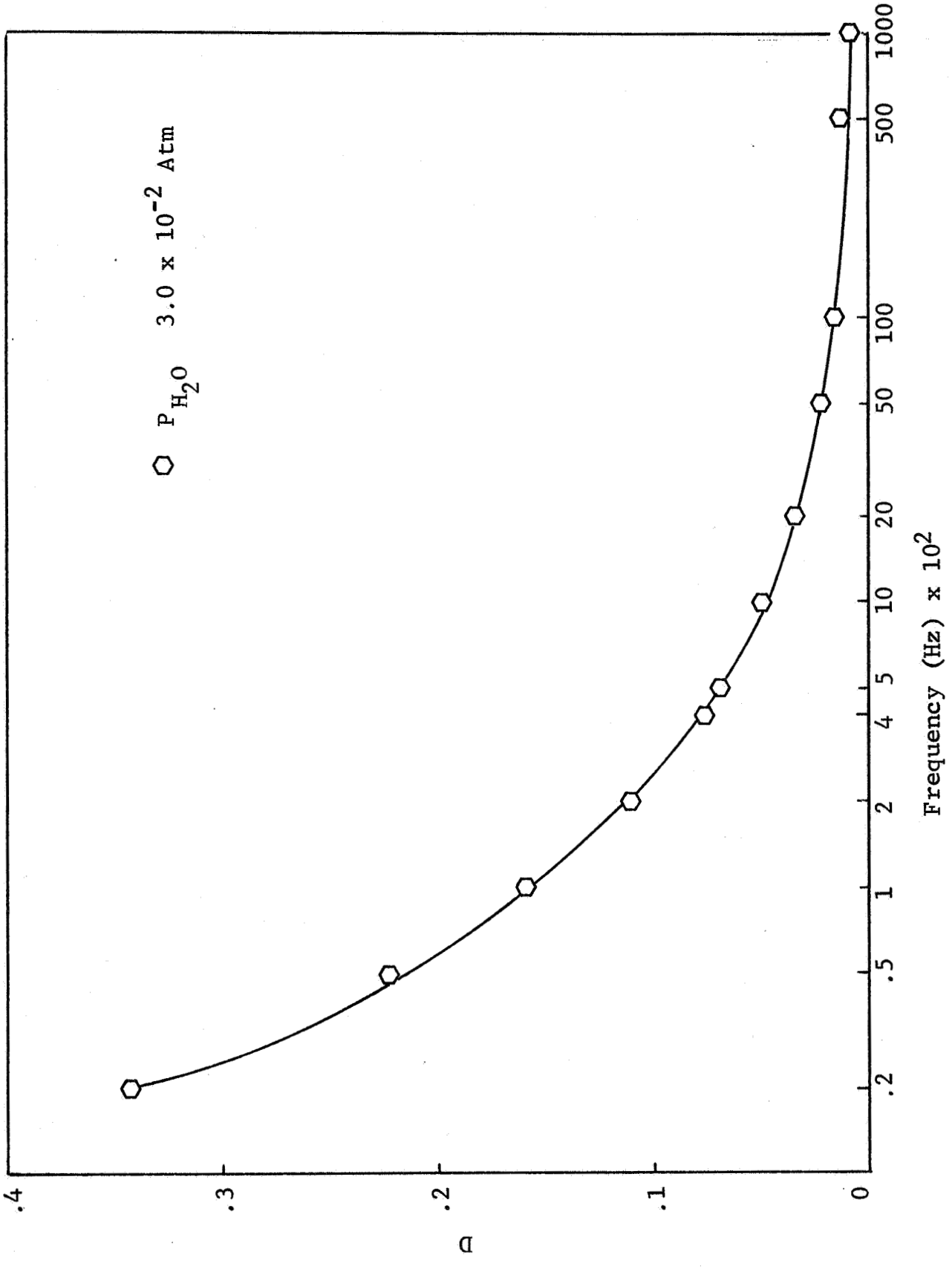

Fig. 18b - FREQUENCY DISPERSION OF D FOR SAMPLE F3 (SINTERED 1350°C)

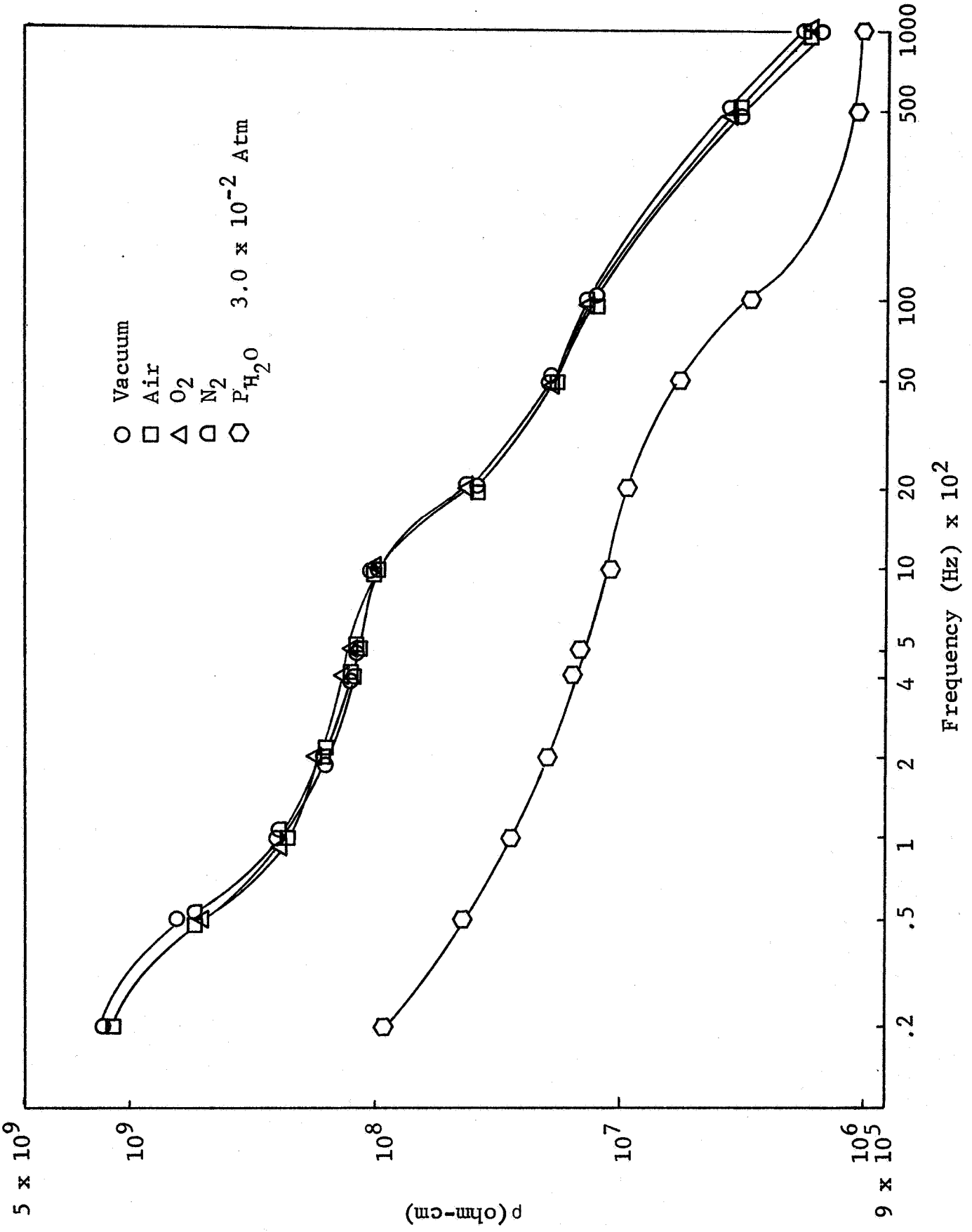

Fig. 19 - EFFECT OF GASEOUS ATMOSPHERES ON FREQUENCY DISPERSION OF RESISTIVITY FOR SAMPLE F3 (SINTERED 1350°C)

E. Dielectric Properties of $BaTiO_3$ at Infrared and Optical Frequencies

1. Introduction

In an anisotropic dielectric such as $BaTiO_3$, the dielectric constant is a tensor and, being a ferroelectric, each component is a nonlinear function of field and to each other. The real and imaginary parts of the nonlinear complex tensor component of permittivity are now no longer related through the normal relaxation processes (such as Debye or Maxwell-Wagner type), or their modified forms, or through the classical dispersion equations. When one considers ceramic $BaTiO_3$, the complexities multiply, such as orientation, second phase, grain boundary, microstress, piezoelectric stresses, and so on. In a ceramic, one may write the permittivity,

$$\epsilon = \underset{\text{electronic}}{\epsilon_e} + \underset{\text{ionic}}{\epsilon_i} + \underset{\text{domain wall}}{\epsilon_d} + \underset{\text{micro stresses}}{\epsilon_a} + \underset{\text{surface layer}}{\epsilon_s} + \underset{\text{grain boundary}}{\epsilon_b}$$

In a ferroelectric state, the domain wall motion and microstresses (arising from piezoelectric reaction, and crystal anisotropy, etc.) make a significant contribution to the permittivity, producing a nonlinear behavior under the thermal and electrical stresses and causing instabilities of the permittivity values with time.

In attempting to identify the various contributions of polarization by frequency dispersion, the domain wall motion could present some difficulty. For instance, the 90° wall is known[24] to relax slowly over a frequency range from dc to 10^9 Hz. The 180°

domain wall relaxes in a different manner. Furthermore, because of the strong piezoelectric action in ferroelectric barium titanate, each grain acts as a resonator; the resonant frequency is determined by the dimension of the grain. A range of grain size implies a range of resonance frequencies, normally in the range 10^7 to 10^{10} Hz. This frequency band is further perturbed by the microstresses arising from the crystal anisotropy. Thus the analysis of the dispersion curve is complicated owing to the presence of the ferroelectric state in the material. Therefore, to study the role of the grain boundary in the dielectric properties of $BaTiO_3$ ceramics, it is essential to eliminate some of the other polarization processes and enter into a linear nonferroelectric state where interpretation of the experimental data will be more meaningful. It is possible to go beyond the ferroelectric region by either working with $BaTiO_3$ above its Curie temperature in the cubic state, or above the microwave frequencies where $BaTiO_3$ ceases to be in the ferroelectric state.

Above the Curie point, besides the grain boundary effect, other effects such as ionic defects and surface layers will still contribute to the dielectric constant. At optical and infrared frequencies, however, such effects will not be present. Therefore, studies on the grain size dependence of the dielectric properties of barium titanate at the infrared and optical frequencies will be very valuable for delineating the grain boundary dielectric constant. At these frequencies it is mainly the electronic polarization that contributes to the dielectric constant. Thus, if the electronic polarizability of the grain boundary differs from that of the grain, a marked change will occur as a function of grain size in the reflection spectra and consequently in the dielectric spectra should be noticed. The reflection spectra of both single-crystal and polycrystalline barium titanate have been reported.[25,26] However, no study on the grain size dependence of the reflection spectra has been made.

The grain size dependence of the absorption edge of barium titanate in the optical region is also of interest, as it may be indicative of the defect structure and stoichiometric effects of the grain and grain-boundary regions.

2. Experimental Procedure

The experimental work essentially consisted of preparing barium titanate samples of varying grain size and obtaining their reflection spectra in the wavelength region from 0.325μ to 30μ.

Barium titanate specimens of varying grain sizes were prepared by sintering in an oxygen atmosphere. The general procedures and chemical analysis of the $BaTiO_3$ powders have been described in Sections V-B and V-C.

Electron micrographs of the fired samples were taken by two-stage replication techniques. Micrographs of both the as-sintered surface as well as the fracture surface have been obtained.

Carefully polished $BaTiO_3$ specimens were then analyzed for their reflectance characteristics.

Spectral reflectance data were taken near normal incidence with a Perkin-Elmer 621 grating double-beam spectrophotometer under N_2 purge. The resolution of the spectrophotometer is from 2 cm^{-1} to 5 cm^{-1} in different frequency regions. The accuracy of the reflectivity is ±3% in the range 300 to 900 cm^{-1}.

Absolute reflectance spectra of the samples were taken from 0.325 to 2.7μ with a Beckman DK-2A spectrophotometer using the Edwards-type of integrating sphere attachment. The absolute hemispherical spectral reflectance was obtained from these measurements.

The dielectric properties were computed on an IBM-7099 computer, from the experimentally obtained spectral reflectance data, by using the Kramer-Kronig relationship.

3. Theoretical Concepts

An analysis of the reflection spectra to compute the real and imaginary parts of the dielectric constant involves using the Kramer-Kronig relationship and the Fresnel equation for normal incidence.

At normal incidence the Fresnel equation for the reflection or radiation from an absorbing medium of complex index of refraction, N is given by:

$$N = n - ik$$

where n and k, the real and imaginary parts of the complex index of refraction, are related by the equation:

$$\left|r\right| \quad e^{i\theta} = r = \frac{n-ik-1}{n-ik+1} \tag{4}$$

where r^2 corresponds to the reflected intensity at the incident surface and θ is the phase angle.

Separating the real and imaginary parts of N from Eq. 4 yields:

$$n = \frac{1 - r}{1 + r^2 - 2r \cos \theta} \tag{5}$$

$$k = \frac{2r \sin \theta}{1 + r^2 - 2r \cos \theta} \tag{6}$$

From Eqs 5 and 6 it follows that if the amplitude $\left|r\right|$ and the phase angle, θ, are known, the optical constants n and k can be solved. From the optical constants, the real and imaginary parts of the dielectric constant can be obtained from the relationships:

$$\epsilon_1 = n^2 (1 - k^2) \tag{7}$$

$$\epsilon_2 = 2nk$$

where ϵ_1 and ϵ_2 are the effective dielectric constant and the dissipation factor, respectively.

The reflectance measurement determines $\left|r\right|^2$ and $\left|r\right|$. Furthermore, if $\ln \left|r\right|$ is known over the entire frequency spectrum,

θ at any single frequency ω_o can be determined from the Kramer-Kronig relationship.

The Kramer-Kronig relationship is given by:

$$\theta(\omega_o) = \frac{2\omega_o}{\pi} \int_o^\infty \frac{\ln|r(\omega)|}{(\omega^2 - \omega_o^2)} \tag{9}$$

The usefulness of this approach is due to the fact that negligible error results from a lack of knowledge of the frequency spectrum remote from the point of interest. Therefore, Eq. 9 can be further simplified and written as:

$$\theta(\omega_o) = \frac{1}{\pi} \int_o^\infty \frac{d \ln|r(\omega)|}{d\omega} \ln \frac{\omega + \omega_o}{\omega - \omega_o} \cdot d\omega \tag{10}$$

Equation 10 shows that the phase at any arbitrary point is proportional to an integral over the entire spectrum of the derivative of the product of the attenuation and a weighting function at each point. The weighting function peaks sharply at the point of interest and flattens out and becomes small at remote points. A constant percent error in the attenuation characteristic will not influence the phase determination.

4. Results and Discussion

a. Electron Micrograph Analysis

An analysis of the electron micrographs of the specimens prepared from starting material "C" have been made. Figures 20 to 26 show the electron micrographs of the samples sintered at 1240°, 1260°, 1280°, 1300°, 1320°, 1340°, and 1360°C, respectively. The micrographs were taken by two-stage replication technique. The results indicate that the samples fired at 1240° and 1260°C have a small range of grain sizes; the dark region observed in the photomicrographs is due to material scooped out during replication. Both samples are underfired and have rather low mechanical strength. Samples fired at higher temperatures have larger grain sizes, as expected. A considerable range of grain sizes was obtained in the specimens fired at 1340° and 1360°C. The average grain sizes

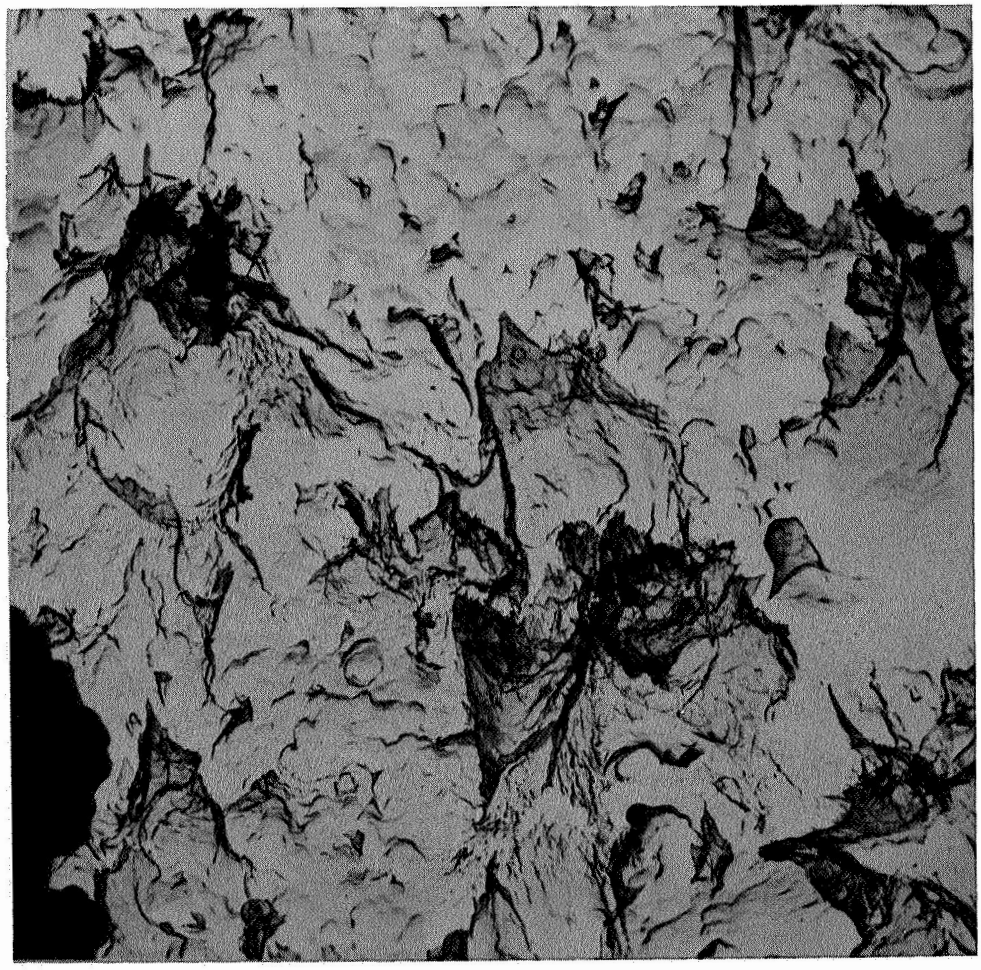

Fig. 20 - ELECTRON MICROGRAPH OF $BaTiO_3$ "C" SINTERED AT 1240°C (X15500)

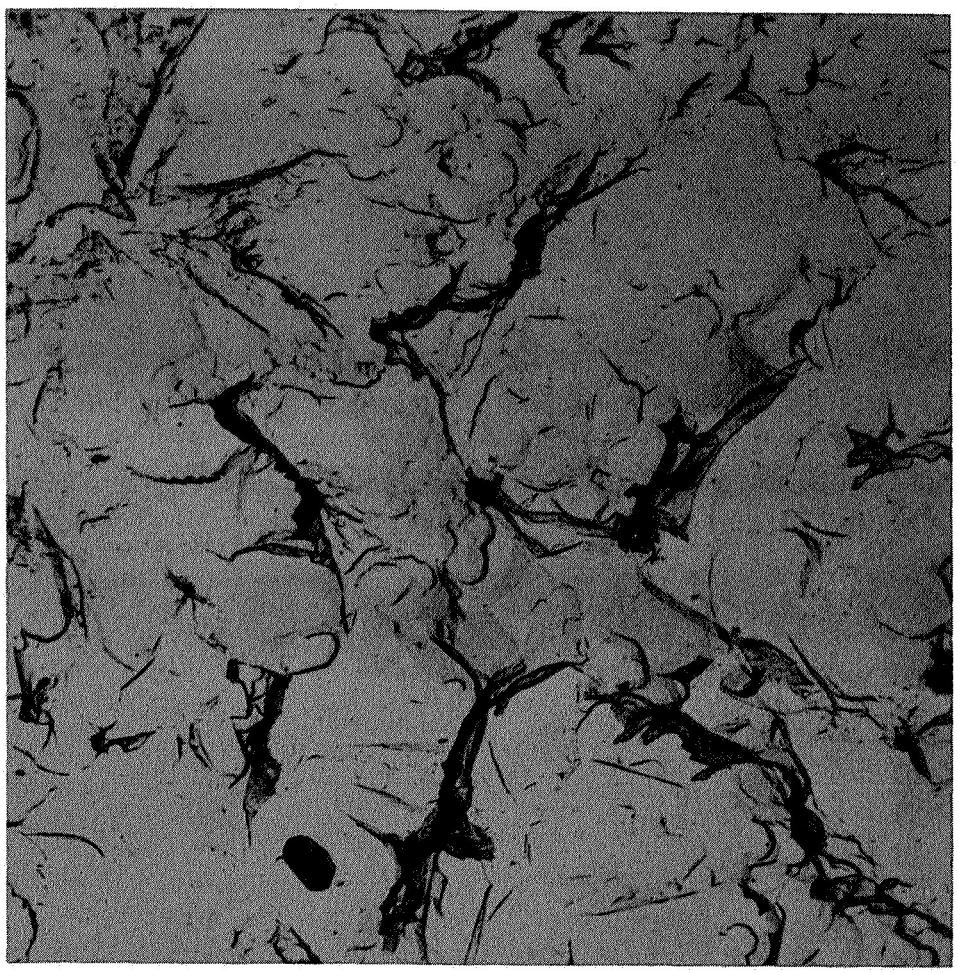

Fig. 21 - ELECTRON MICROGRAPH OF $BaTiO_3$ "C" SINTERED AT 1260°C (X15500)

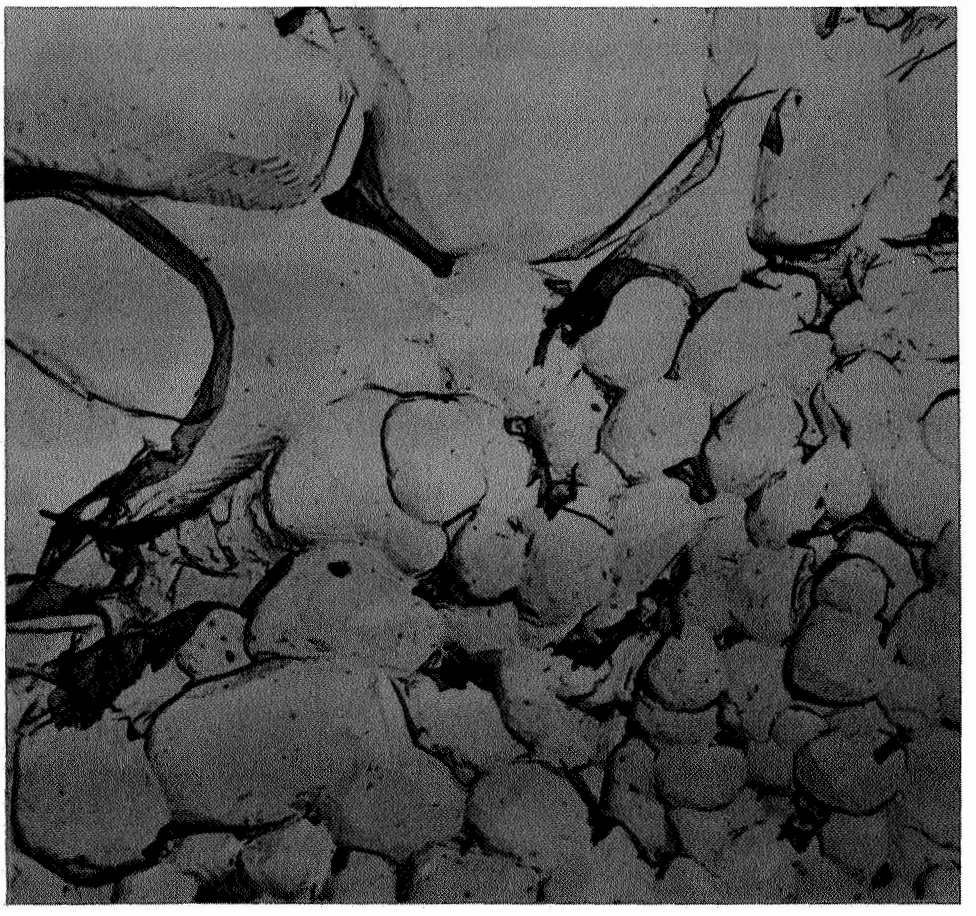

Fig. 22 - ELECTRON MICROGRAPH OF $BaTiO_3$ "C" SINTERED AT 1280°C (X15500)

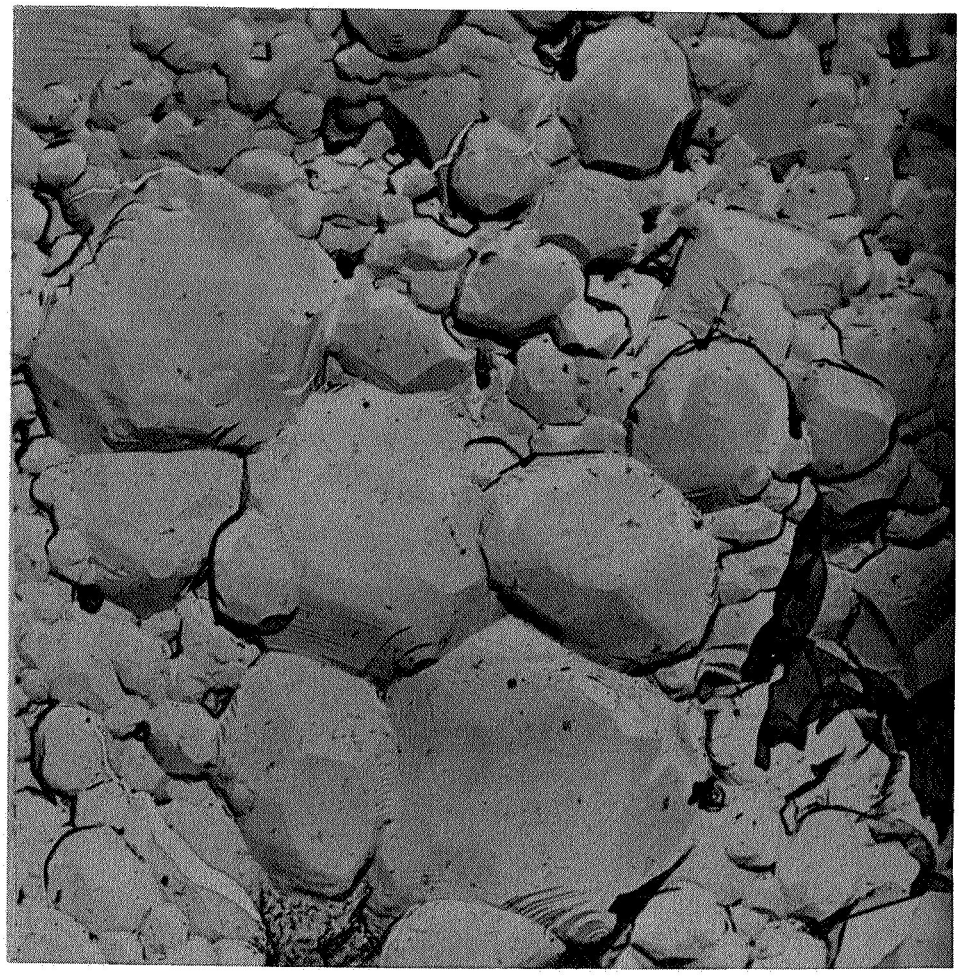

Fig. 23 - ELECTRON MICROGRAPH OF $BaTiO_3$ "C" SINTERED AT 1300°C (X15500)

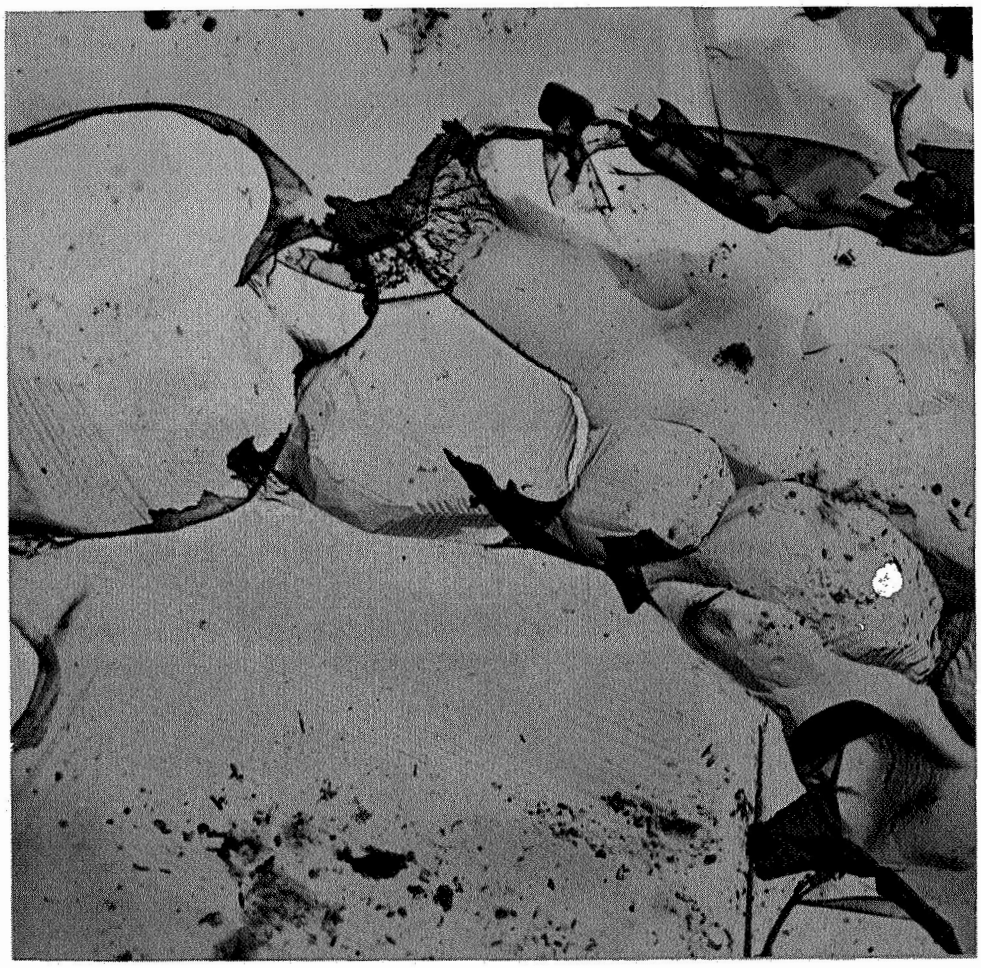

Fig. 24 - ELECTRON MICROGRAPH OF $BaTiO_3$ "C" SINTERED AT 1320°C (X15500)

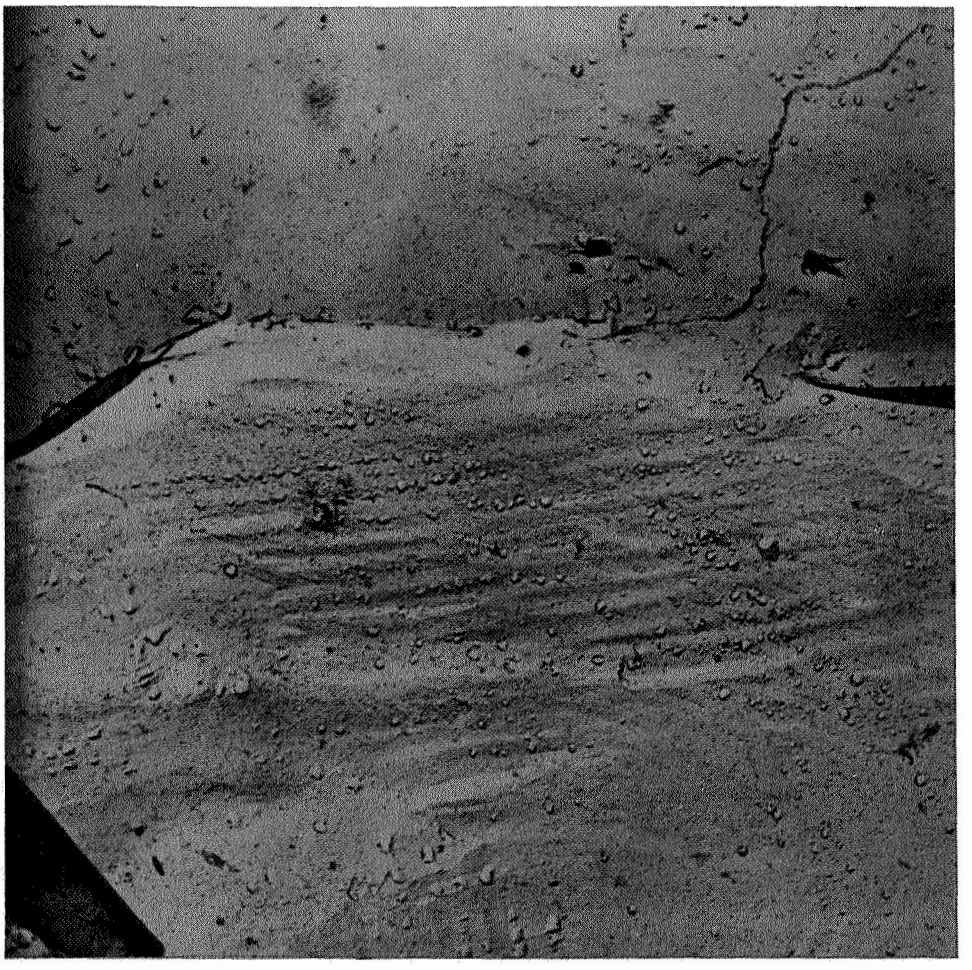

Fig. 25 - ELECTRON MICROGRAPH OF $BaTiO_3$ "C" SINTERED AT 1340°C (X1550^)

Fig. 26 - ELECTRON MICROGRAPH OF $BaTiO_3$ "C" SINTERED AT 1360°C (X15500)

for the samples were determined over the entire range of firing temperatures and are shown in Table V. The samples also have varying densities, less than desirable in some cases.

Although the electron micrographs of the second set of specimens prepared from material "G" have not been taken, an increase in grain size with increasing sintering temperatures is to be expected. The sintering temperatures and the densities of the second set of specimens prepared from material "G" are presented in Table VI.

b. Spectral Reflectance

The reflectance spectra of the polished specimens of $BaTiO_3$ material "C" in the frequency region 900 to 300 cm^{-1} is shown in Fig. 27. Minimum reflectivity occurs at frequency near 800 cm^{-1}; the restrahlen band appears in the 475 to 775 cm^{-1} region, and seems to be dependent upon sintering temperature.

The results of the dielectric spectra obtained from the reflection spectra are shown in Figs. 28 and 29. Since the test specimens have a range of densities, a porosity correction on the dielectric constant was made. Owing to the dielectric anisotropy and varying shape of the grains, it is difficult to find the correct method of averaging. A logarithmic average formula, which is known to work well, as long as the component dielectric constant does not differ from each other by more than 10, and this is true in our case, was used. The formula is given by:

$$\bar{c} \log \bar{\epsilon} = c_1 \log \epsilon_1 + c_2 \log \epsilon_2$$

where c_1 and c_2 are the two concentrations corresponding to the two dielectric constants, ϵ_1 and ϵ_2, and $\bar{c}$ = concentration of the mixture. For air, $\epsilon_2 = 1$, so that $\log \bar{\epsilon} = (c_1/\bar{c})(\log \epsilon_1) = (d_1/d) \log \epsilon_1$, where d_1 is the apparent density and d is the true density or:

Table V

MICROSTRUCTURAL CHARACTERISTICS OF SINTERED $BaTiO_3$ "C" TEST SPECIMENS

Sintering Temperature, °C	Density		Grain Size Range, u
	g/cm^3	% Theoretical	
1200	4.21	70.0	--
1240	4.81	80.0	0.4 to 0.6
1260	4.99	80.5	0.4 to 1.0
1280	5.33	88.6	0.4 to 2.5
1300	5.22	87.0	0.5 to 3.0
1320	5.21	86.6	2 to 10
1340	5.51	91.6	5 to 25
1360	5.48	91.0	10 to 25

Table VI

PHYSICAL CHARACTERISTICS OF SINTERED $BaTiO_3$ "G" TEST SPECIMENS

Sintering Temperature, °C	Density	
	g/cm^3	% Theoretical
1200	4.696	78
1220	4.756	79
1240	5.057	84
1340	5.418	90
1360	5.478	91

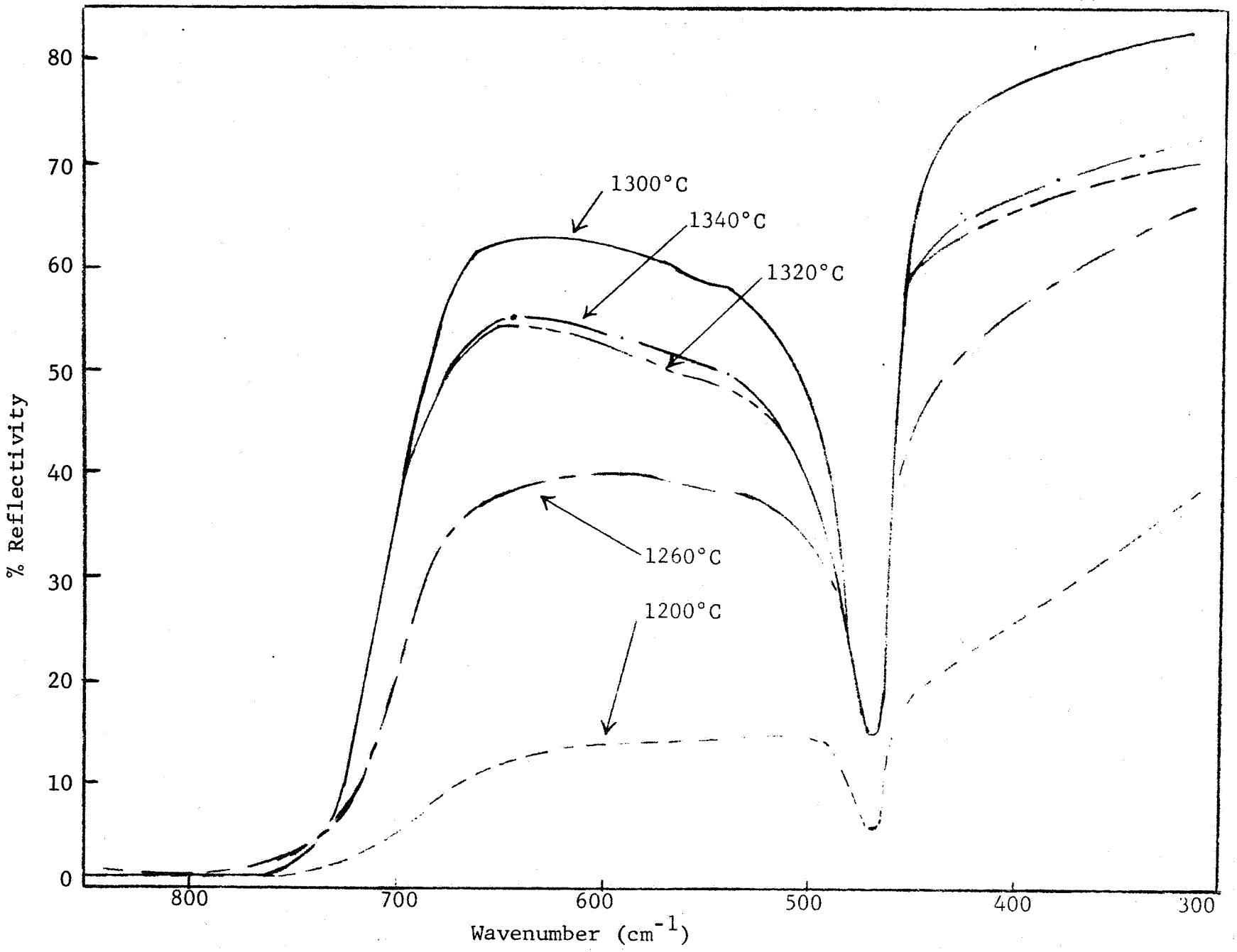

Fig. 27 - REFLECTANCE SPECTRA OF $BaTiO_3$ "C" SINTERED AT DIFFERENT TEMPERATURES

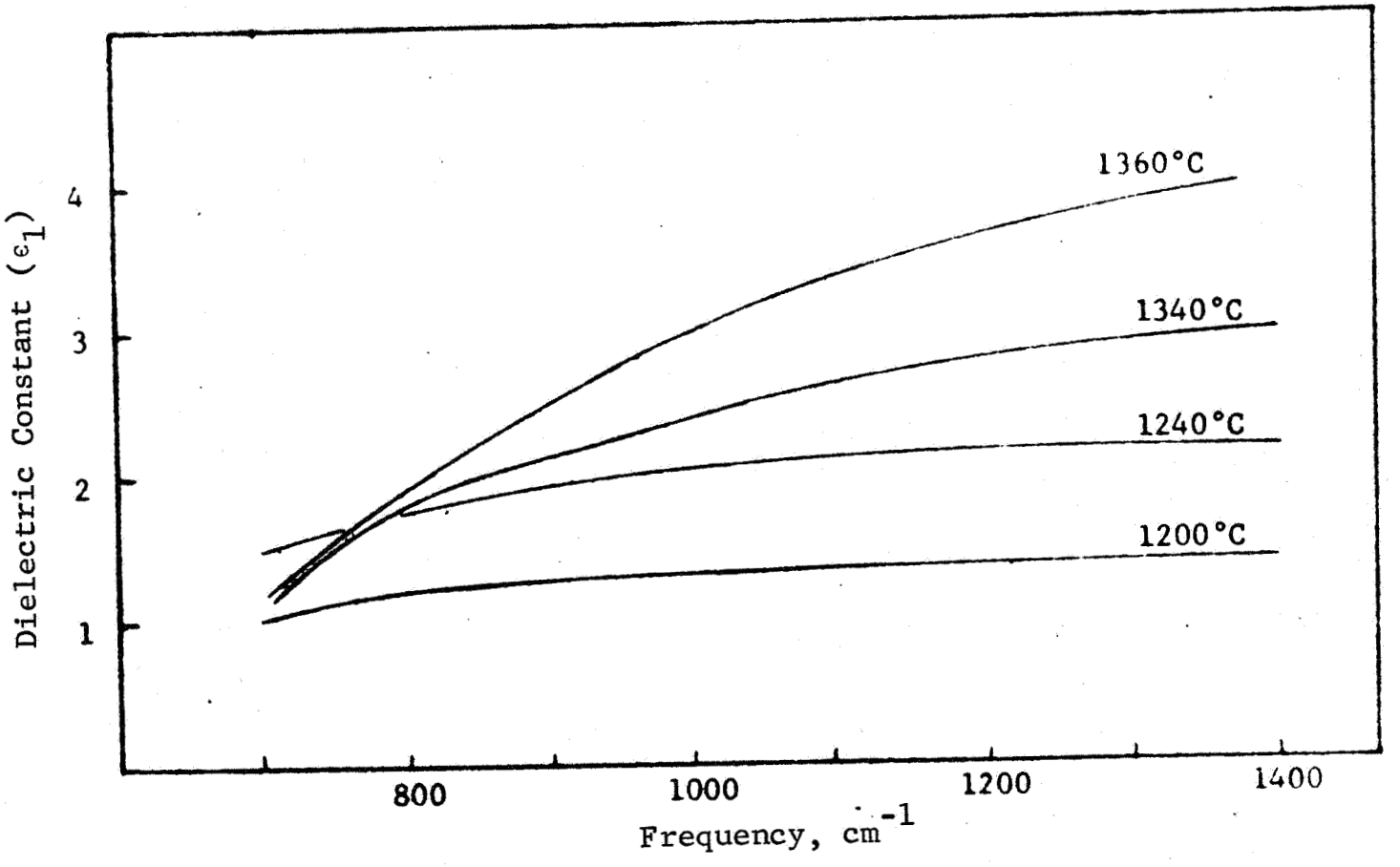

Fig. 28 - REAL PART OF DIELECTRIC CONSTANT OF $BaTiO_3$ "C" VS FREQUENCY FOR DIFFERENT SINTERING TEMPERATURES

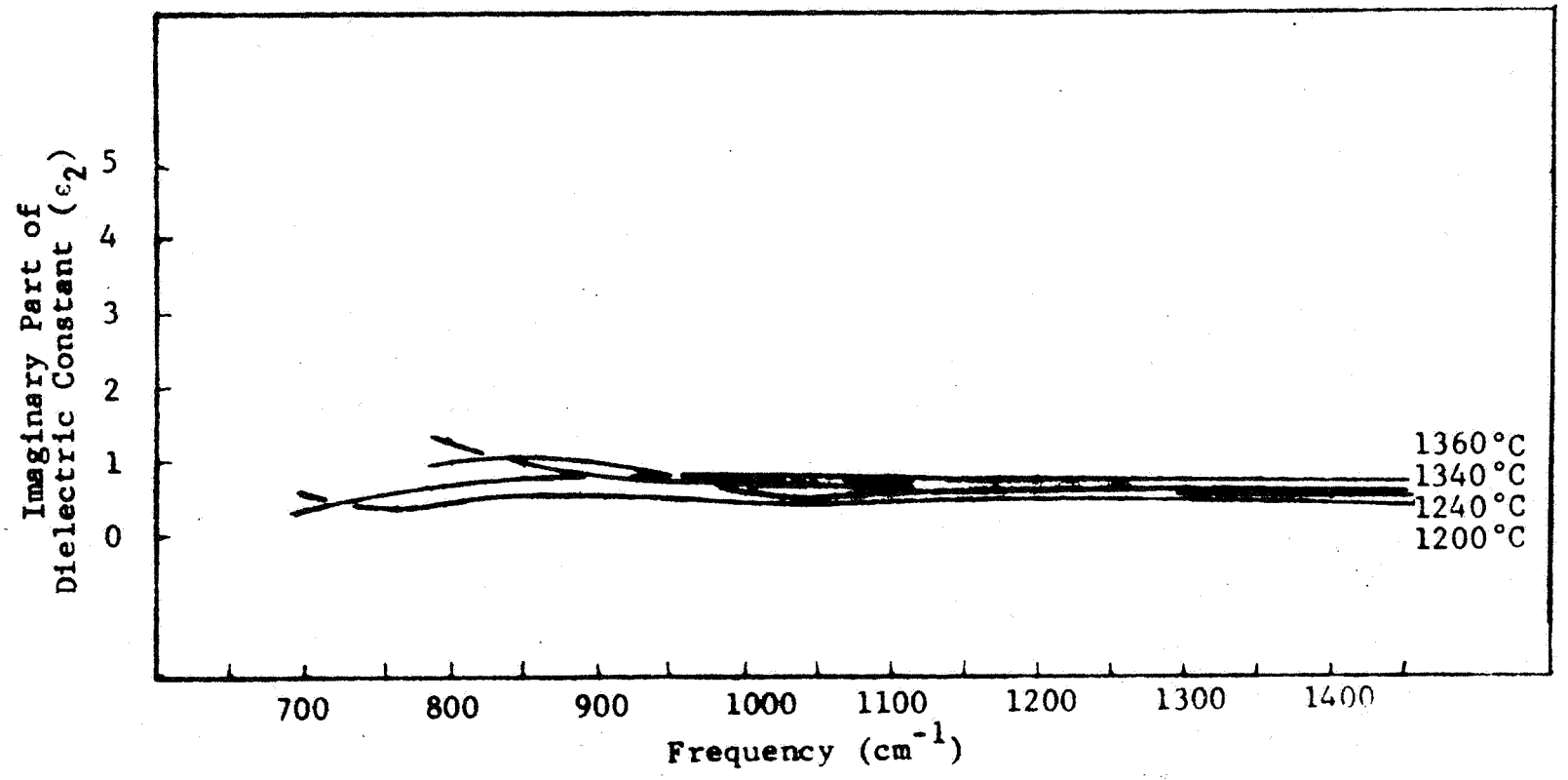

Fig. 29 - IMAGINARY PART OF DIELECTRIC CONSTANT OF $BaTiO_3$ "C" VS FREQUENCY FOR DIFFERENT SINTERING TEMPERATURES

$$\log \epsilon_1 = \frac{d}{d_1} \log \bar{\epsilon}$$

$$= \frac{6.02}{d_1} \cdot \log \bar{\epsilon}$$

The corrected dielectric constant (ϵ_1) spectra computed from these reflection spectra are shown in Fig. 30. The results indicate that the dielectric constant increases with an increase in frequency and sintering temperature. An increase in sintering temperature (1200° to 1360°C) implies larger grain size, and therefore, the dielectric constant increases with increasing grain size, as well as with increasing frequency in the range 300 cm^{-1} to 1600 cm^{-1} (i.e., from 9 x 10^{12} to 5.1 x 10^{13} Hz). In this frequency range there is little ionic contribution to the dielectric constant, since the infrared absorption bands corresponding to the ionic motion and lattice vibrations occur below this frequency range. Also, there is no ferroelectric domain wall or dipolar contribution to the dielectric constant at these frequencies. The mechanism of polarization is mainly electronic. These results, therefore, tend to indicate that the electronic part of the dielectric constant increases with increasing grain size. They also suggest that the grain size dependence of the dielectric constant in barium titanate is not merely ferroelectric, but a considerable contribution is nonferroelectric in origin.

The frequency dispersion of the imaginary part of the dielectric constant for various sintering temperatures is shown in Fig. 29. The imaginary part (ϵ_2) shows a very slight increase with grain size. However, there is no marked variation with frequency.

Reflectance spectra of the second set of samples prepared from the powder "G" are shown in Figs. 31 and 32. Reflectance spectra of these specimens prepared from capacitor grade $BaTiO_3$ was found to be similar to that of the high-purity "C" material.

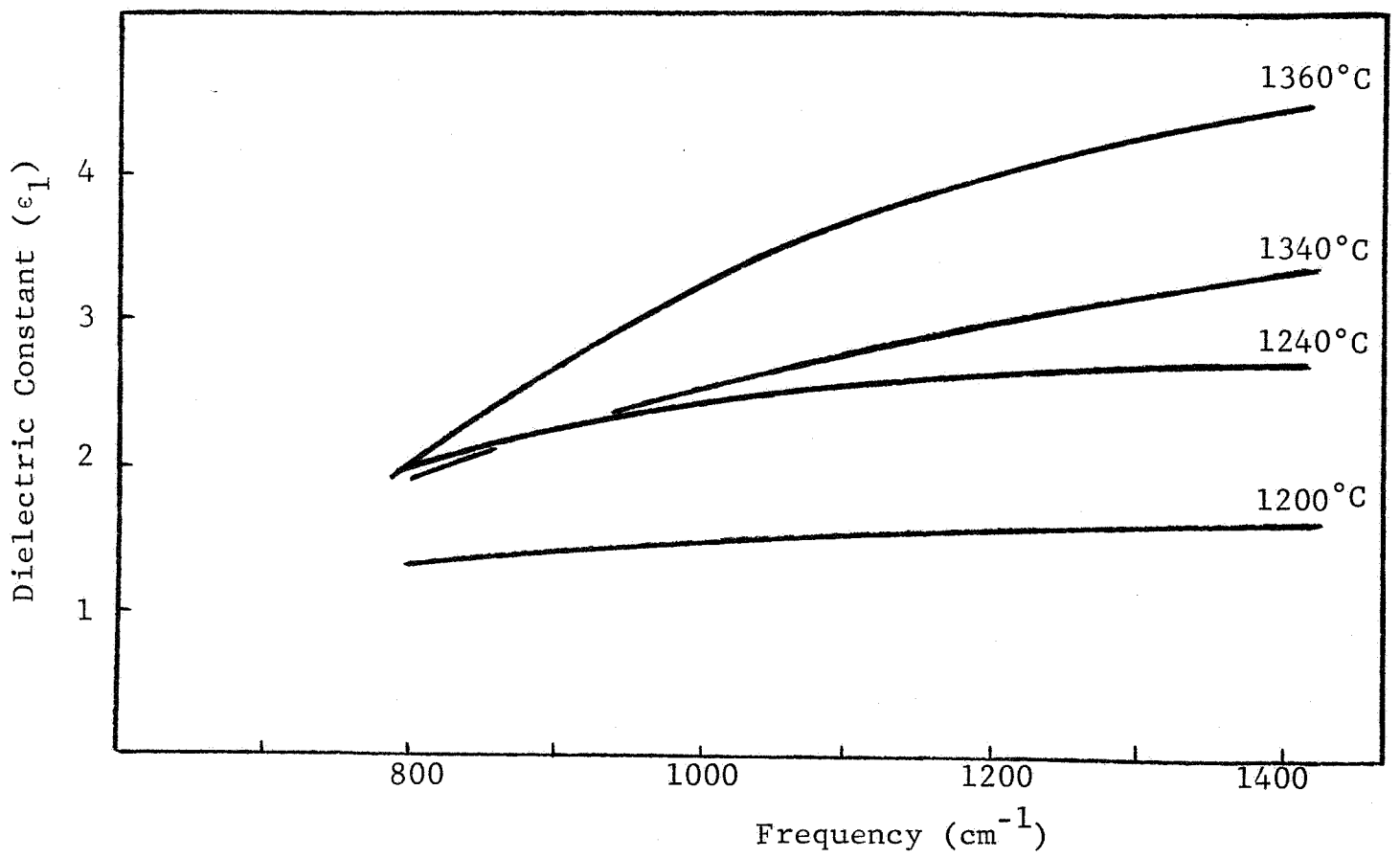

Fig. 30 - CORRECTED INFRARED DIELECTRIC CONSTANT OF $BaTiO_3$ "C" VS FREQUENCY FOR DIFFERENT SINTERING TEMPERATURES

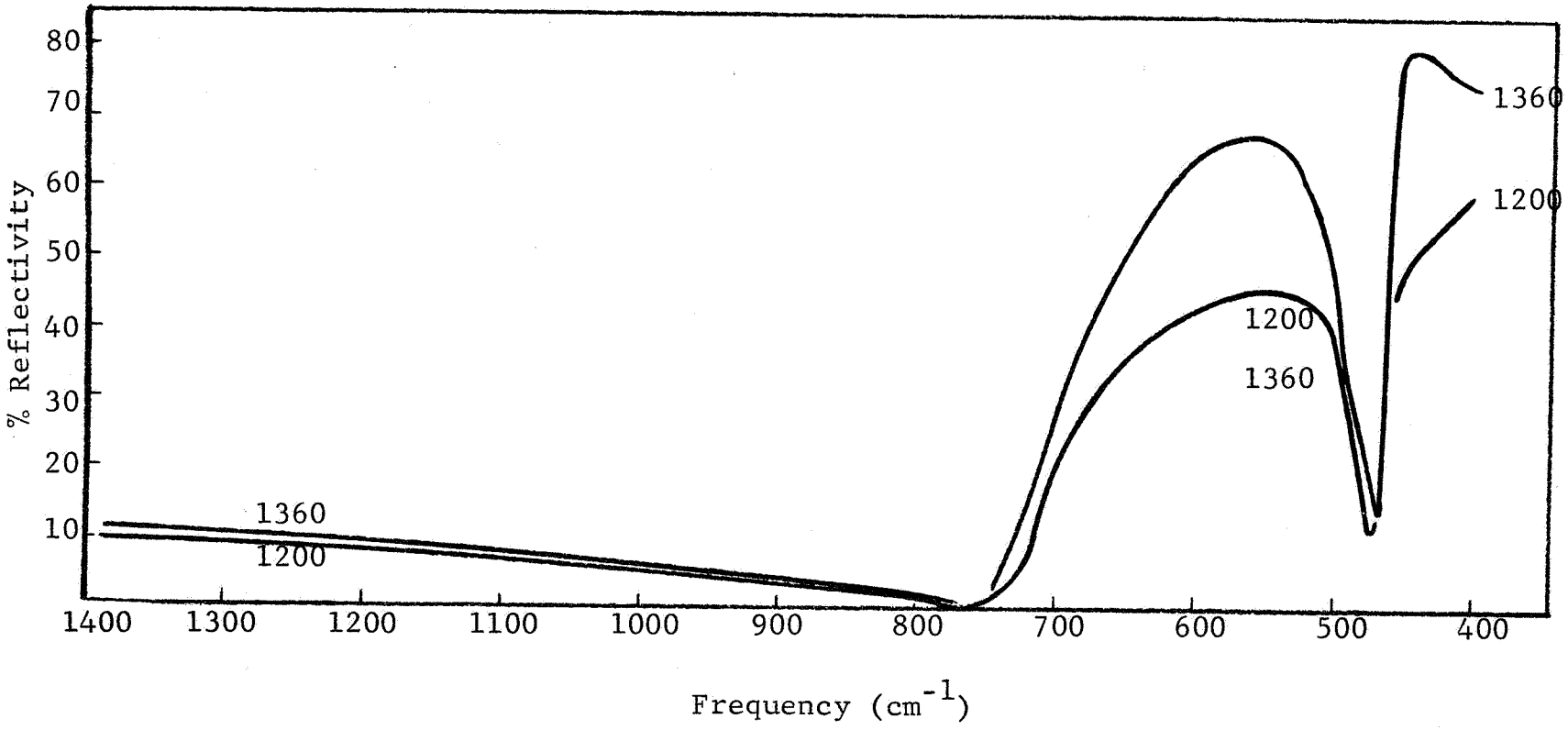

Fig. 31 - REFLECTION SPECTRA OF $BaTiO_3$ "G"
SINTERED AT DIFFERENT TEMPERATURES

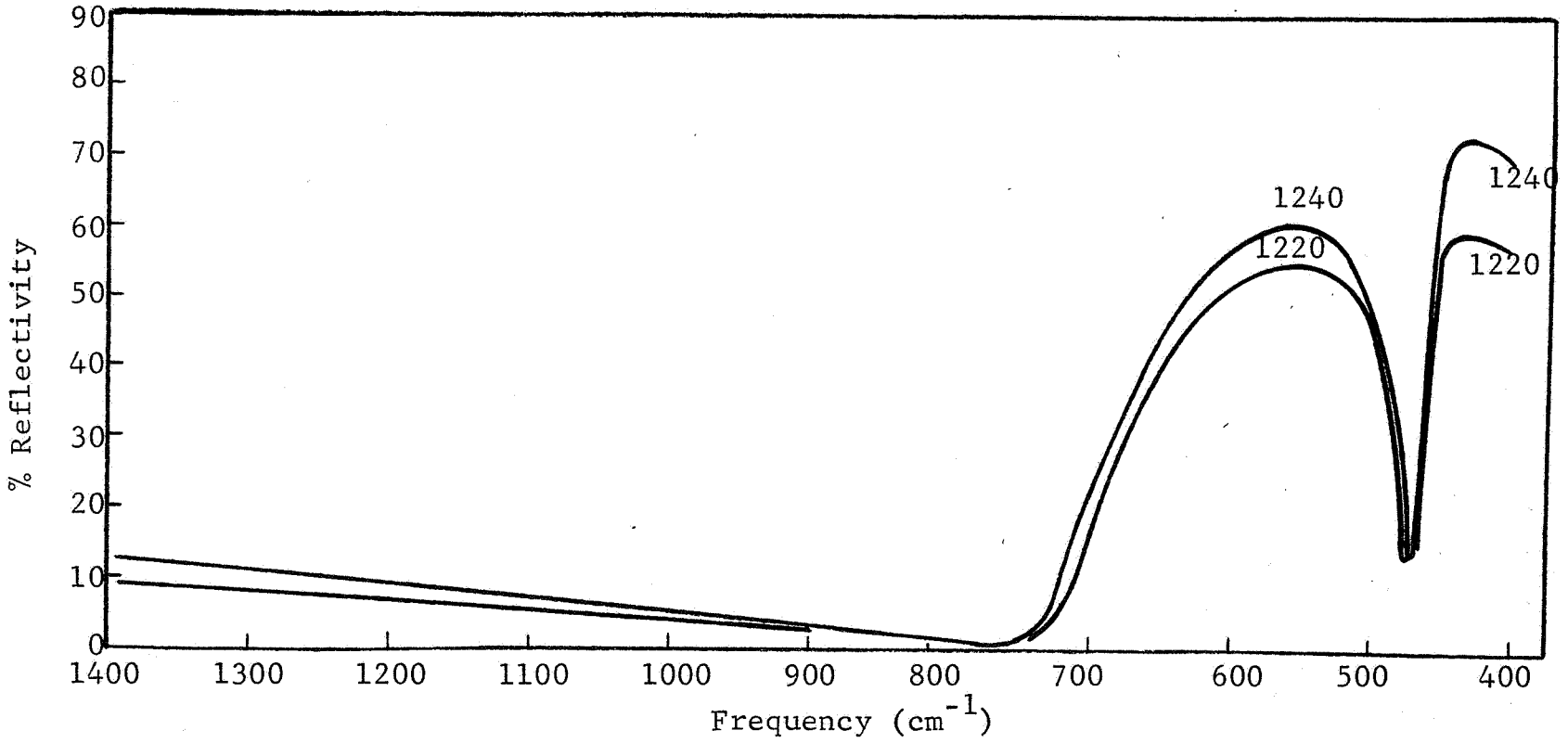

Fig. 32 - REFLECTION SPECTRA OF $BaTiO_3$ "C"
SINTERED AT DIFFERENT TEMPERATURES

The corrected dielectric constant computed from the reflectance data are shown in Fig. 33. In this case also the dielectric constant increases with increasing grain size. Thus we can conclude from these two sets of data that the dielectric constant decreases with the decrease in grain size in the infrared frequency range. Since the relative proportion of the boundary phase increases with decrease in grain size, it could be inferred that the infrared dielectric constant of the grain boundary is lower than that of the grain, in the frequency range studied.

c. Absolute Reflectance

The variation of absolute reflectance with the wavelength is shown in Fig. 34 for a range of 0.325 to 0.7μ and in Fig. 35 for a range of 2.0 to 2.7μ for the first set of $BaTiO_3$ specimens (material "C") sintered at various temperatures. Sintering temperatures are shown adjacent to the traces on these figures. It is seen from Fig. 34 that $BaTiO_3$ has an absorption band in the region of 0.325 to 0.4μ and from Fig. 35, an absorption band at 2.3μ.

It is also seen from Fig. 34 that towards the right of the absorption edge, the reflectivity decreases with an increase in the sintering temperature, and consequently, with an increase in grain size.

The band in Fig. 35 at 2.3μ is observed only in a sintered material. In an unsintered material or in a material sintered up to about 1200°C, this band does not show at all. In $BaTiO_3$ ceramics, sintering, grain growth, and the formation of grain boundaries which bond the grains begin at around 1200°C. So this band appears to be connected with the electronic processes at the grain boundary, possibly due to the absorption of photons by free carriers at the grain boundary, since the grain boundary region is known to contain many types of defects which give rise to free carriers.

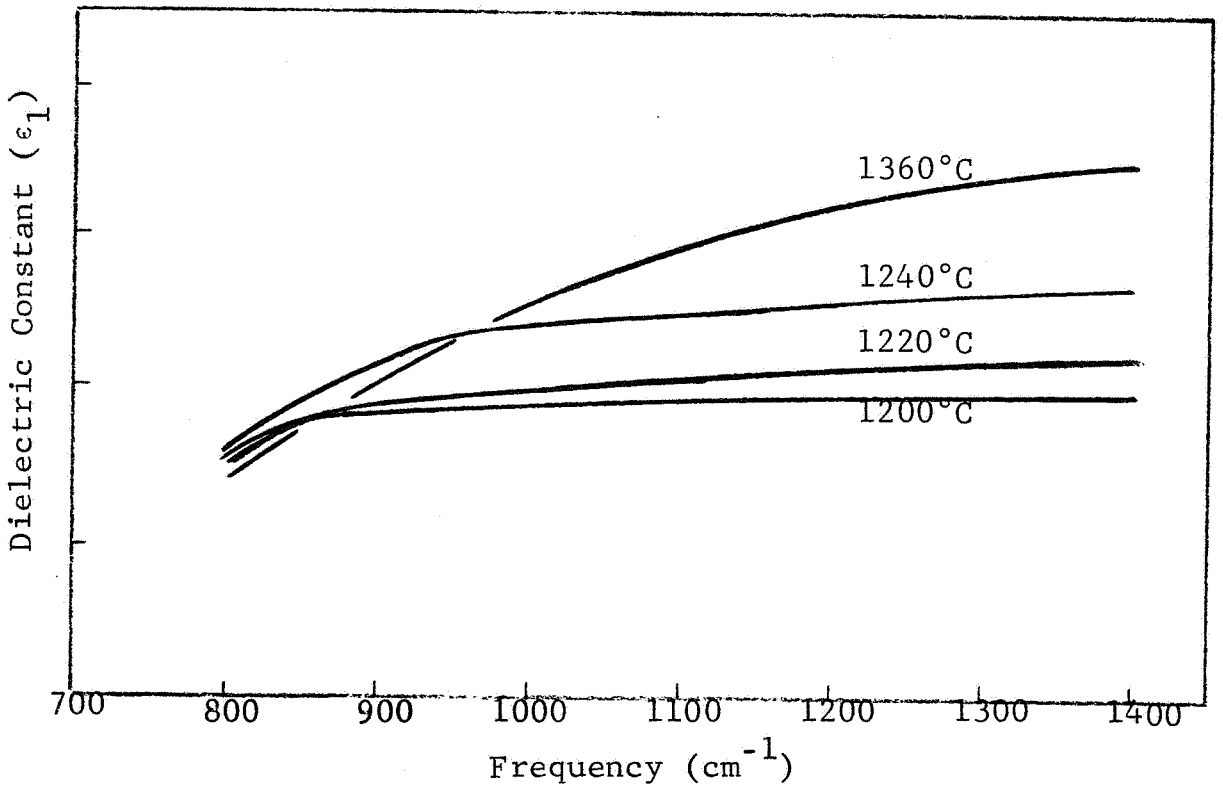

Fig. 33 - CORRECTED INFRARED DIELECTRIC CONSTANT OF $BaTiO_3$ "G" VS FREQUENCY FOR DIFFERENT SINTERING TEMPERATURES

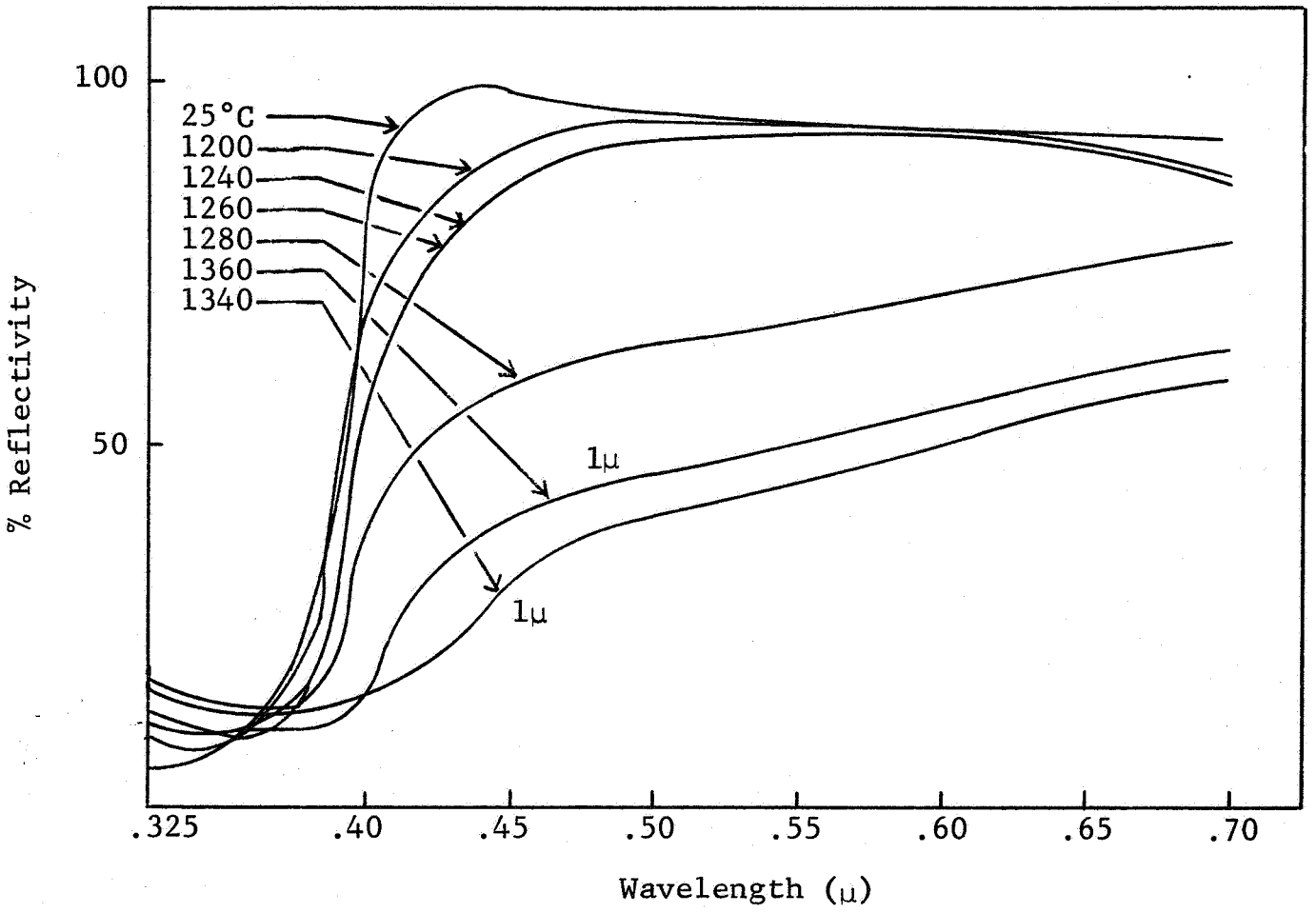

Fig. 34 - ABSOLUTE REFLECTIVITY OF $BaTiO_3$ "C" SINTERED AT DIFFERENT TEMPERATURES

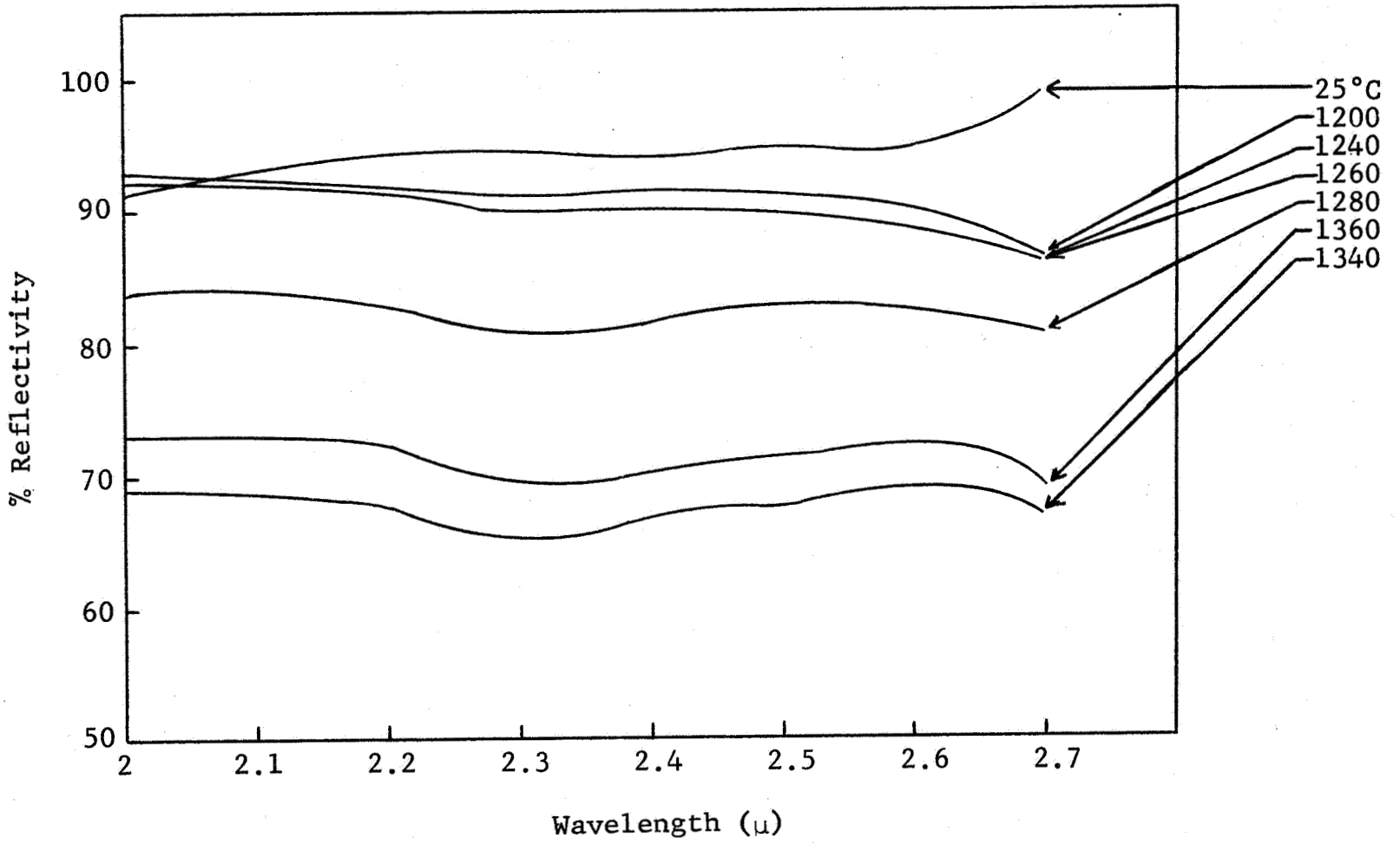

Fig. 35 - ABSOLUTE REFLECTIVITY OF $BaTiO_3$ "C" SINTERED AT DIFFERENT TEMPERATURES

The above experiments were performed with a second set of specimens having different purity levels; similar absolute reflectance spectra were obtained. Absolute reflectance spectra of the second set of samples are shown in Fig. 36 for the range 0.325 to 0.55μ and in Fig. 37 for the range 0.7 to 2.7μ.

The absorption edge centered at around 0.36μ is seen to increase toward higher wavelength with the increasing sintering temperature, but it is more gentle in slope than the corresponding less-sintered material. Possible explanations for the variation in the absorption edge with the sintering temperature or the grain size may be interpreted as follows. Firstly the barium titanate used in this case contains slightly excess TiO_2. As the sintering proceeds, $BaTiO_3$ and TiO_2 react and form the $BaTi_2O_5$ phase at the grain boundary. Thus, in an unsintered or less-sintered material, one observes the absorption edge due to $BaTiO_3$ and a slight amount of TiO_2; whereas in a sintered material, the absorption edge is due to $BaTiO_3$ and $BaTi_2O_5$. The step in the reflection spectra at 0.35μ of the unfired sample is interpreted as being due to unreacted TiO_2. A second possible explanation is that the number of oxygen vacancies increases with higher sintering temperatures and, therefore, results in change in the absorption edge.

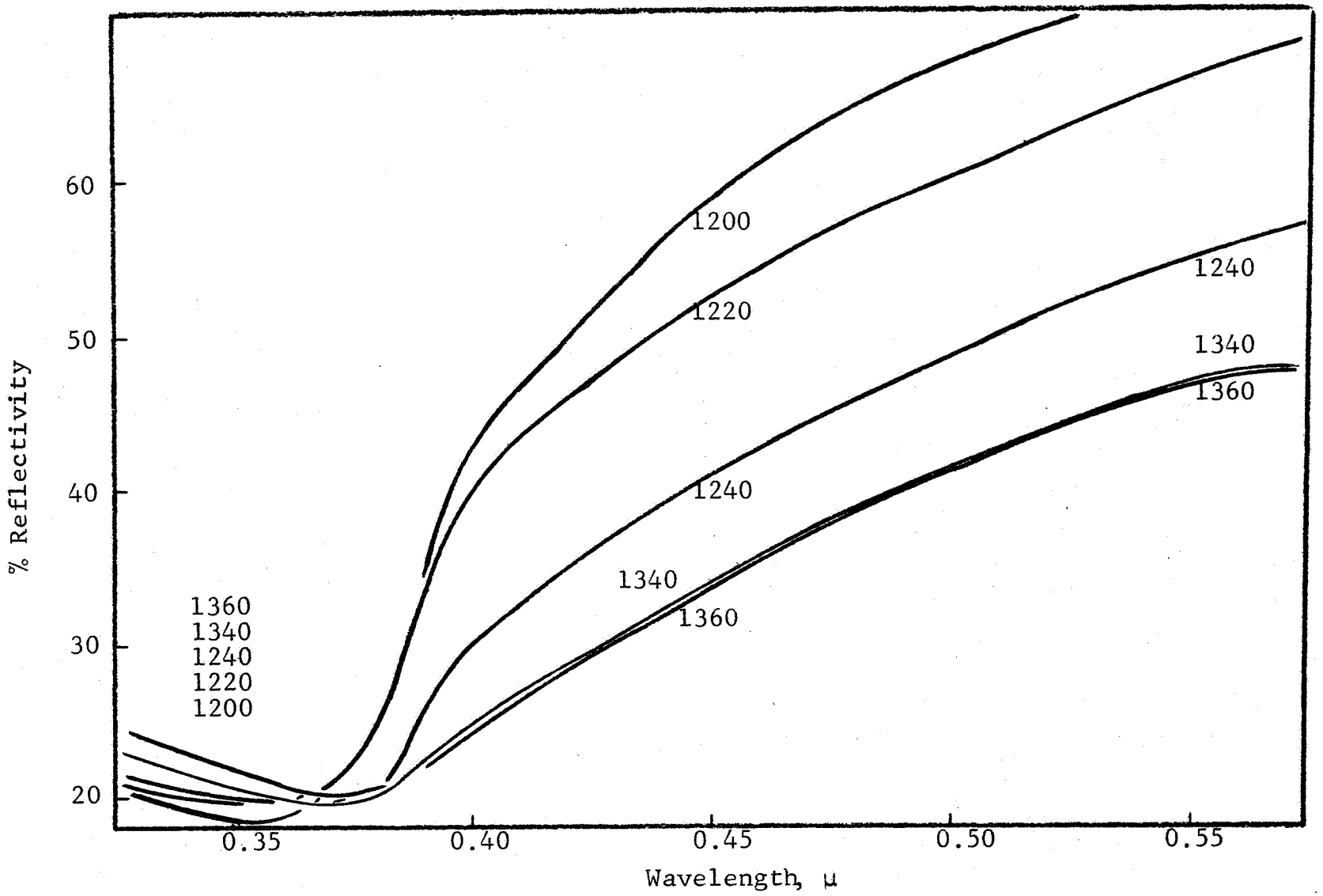

Fig. 36 - ABSOLUTE REFLECTIVITY OF $BaTiO_3$ "G" SINTERED AT DIFFERENT TEMPERATURES

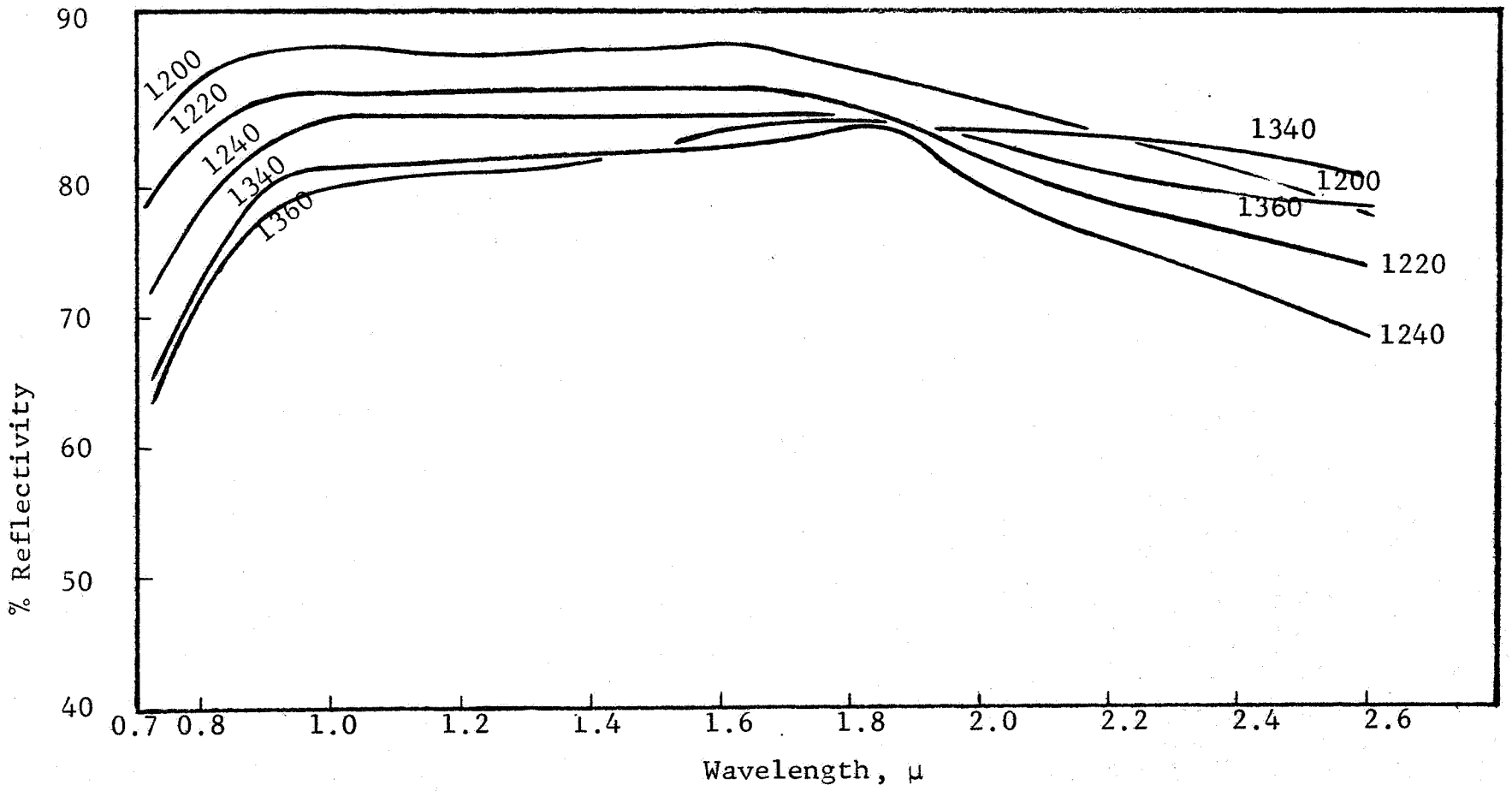

Fig. 37 - ABSOLUTE REFLECTIVITY OF $BaTiO_3$ "G" SINTERED AT DIFFERENT TEMPERATURES

F. Use of Electron Beam Scanning (EBS) Technique for Direct Measurement of Dielectric Properties of Grains and Grain Boundaries

1. Introduction

The electron beam scanning (EBS) technique is a new and powerful approach to the study of the dielectric properties of grain boundaries and interfaces.

The EBS system, developed at IITRI, was first constructed in 1965, and has been described previously.[27] In this technique one surface of the dielectric material is charged with a scanning electron beam in vacuum. The charge measurement is obtained in the form of a video signal output, which is a measure of the spatially resolved conductivity of the sample. The use of an electron beam to produce an equipotential insulator surface has several desirable features. The charging source is basically high impedance, beam currents are easily measured and controlled, and excellent guarding of the measurement area occurs automatically for most scanning patterns. For a study of grain boundaries and interfaces, its most significant feature is that the area of dielectric evaluation is of the order of the electron beam spot size, and can be made very small. This, coupled with the ability to move the area of measurement to various positions on the sample in a simple manner, makes it a unique tool for studying the dielectric properties of grain boundaries, as a function of grain size, stoichiometry, and other microstructural parameters.

A preliminary attempt has been made to adapt the existing EBS system for studying the dielectric properties of grain boundaries in $BaTiO_3$.

2. Experimental Procedure

The mechanical arrangements for dielectric measurements using this technique are straightforward. Figure 38 is a schematic diagram of the EBS system. The sample is backed on one side by a metallic electrode while the other side is irradiated by an electron

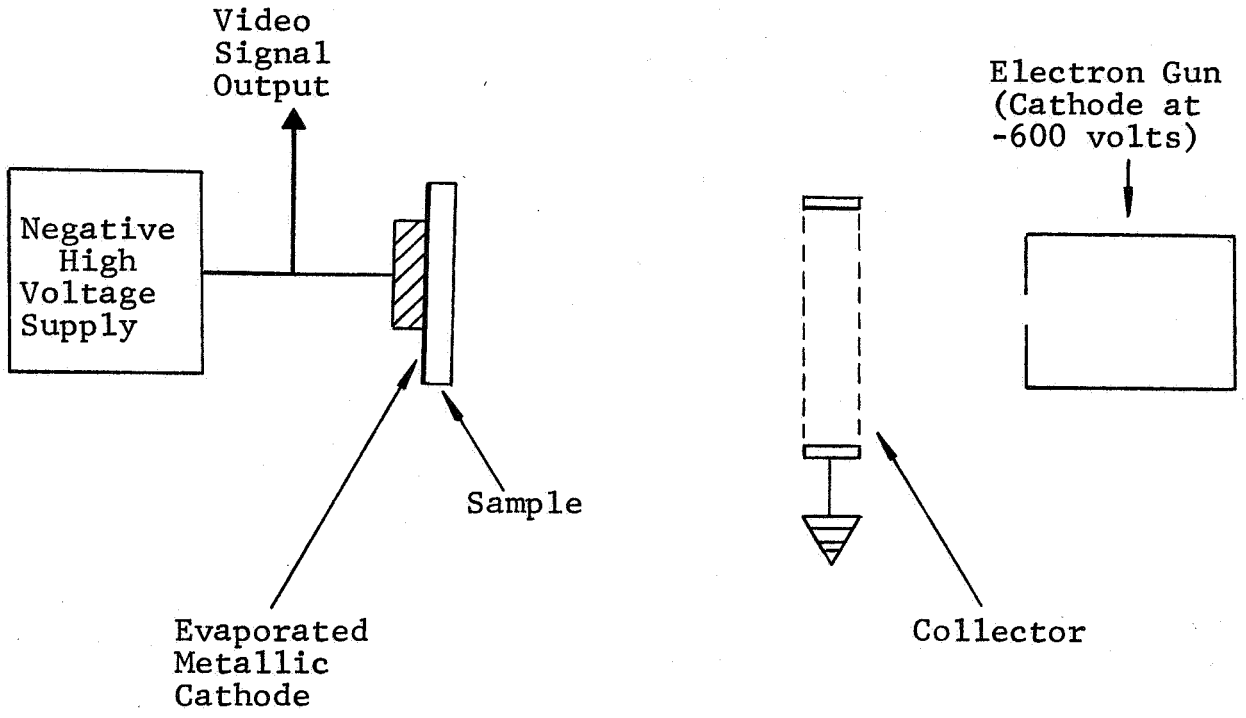

Fig. 38 - SCHEMATIC DIAGRAM OF THE ELECTRON BEAM SCANNING SYSTEM

beam produced by a conventional electron gun. A collector grid or a large-diameter collector ring is placed close to the sample. The collector electrode may be at ground potential, and the backing electrode is connected to a variable high-voltage supply, initially at ground potential. If the electron accelerating potential is of the order of several hundred volts and if the secondary electron emission coefficient (δ_{eff}) of the insulator is greater than unity at this voltage, then initially the potential of each spot on the insulator which is bombarded by the primary beam will tend to change from zero to a positive value. The sample surface potential will come to an equilibrium value a few volts above ground, when $\delta_{eff} = 1$. The sample is then no longer being charged. If the backing electrode is then slowly raised to a high potential of either polarity while the electron beam continues to scan the sample in a regular pattern, each spot on the front surface of the sample will be brought back to the same equilibrium potential whenever the beam strikes it. The charge deposited on the sample will be opposite in polarity to that of the high-voltage backing electrode and of a magnitude sufficient to charge the sample capacitance to the potential difference between its surfaces and also to compensate for the conduction which has occurred between its surfaces.

The determination of dielectric properties depends on knowing the voltage drop across the sample and the charge deposited on the sample by the electron beam.

3. Results and Discussion

Results have been obtained on a 10 mil thick multicrystalline specimen obtained from an imperfect portion of a high-purity $BaTiO_3$ single crystal boule. This multicrystalline specimen was chosen for the preliminary experiment because it has large crystals and well-defined boundaries through the entire thickness of the specimen.

On scanning the specimen, a higher intensity signal was obtained along the boundary profile. This indicated that the

dielectric constant in the region of the grain boundaries is higher than that in the grains.

However, certain further modifications in the EBS system are needed before a quantitative evaluation of the dielectric properties of the boundary and grain regions can be made. The signal-to-noise level in the present EBS system is clearly marginal for this purpose. Considerable scattering of the beam occurs with the present electron gun geometry. A cleaner beam could probably be obtained using a different type of gun structure involving magnetic deflection.

By carrying out the necessary modifications on the present EBS system, including a reduction in the size of the beam spot, it may be possible to study directly the dielectric characteristics of the grain boundary region as a function of grain size. This, of course, could be a significant breakthrough in the study of boundaries and interfaces in polycrystalline materials.

Preliminary as the present results are, they offer evidence that in the $BaTiO_3$ specimen studied, the dielectric constant of the grain boundary regions is higher than that of the grains, in the audio frequency range.

VI. CONCLUSIONS

The detailed results and the conclusions of each of the theoretical and experimental studies performed have been discussed in previous sections. These studies enabled us to characterize the bulk, surface, and grain-boundary behavior of $BaTiO_3$ ceramics.

The surface defect layer of $BaTiO_3$ particles was described by a barrier-layer model that qualitatively explains their experimental dielectric properties. The adsorption of oxygen and the trapping of intrinsic or injected electrons at acceptor states result in a higher resistivity of the surface depletion layer.

The creation and the interaction of surface defects due to water vapor on micron- and submicron-sized powders were studied. Small deviations in stoichiometry (BaO/TiO_2 ratio) result in significant changes in ac conductivity as a function of partial pressure of water vapor.

The relationship between the dielectric constants of the bulk and grain boundary as a function of grain size in sintered $BaTiO_3$ ceramics was theoretically and experimentally studied. The increase in dielectric constant with decreasing grain size (to 1μ) at audio- and radio-frequencies was explained on the basis that the dielectric constant of the grain-boundary phase is higher than that of the grain and changes from a high value for large grains to a small value for small grains; the dielectric constant of the grain remains constant. That the grain-boundary region has a higher dielectric constant than the grain at low frequencies was experimentally verified by an electron-beam scanning technique. In the infrared-frequency range, where $BaTiO_3$ is not ferroelectric, the relative dielectric constant decreases slightly with decreasing grain size. Therefore, a considerable contribution to the grain-size dependence of the dielectric constant in $BaTiO_3$ ceramics is probably nonferroelectric in origin.

On the basis of the work done, electroceramics such as $BaTiO_3$ can be effectively characterized for microelectronic applications. Furthermore, the characterization of ceramic materials in terms of bulk, surface, and grain-boundary properties, which can be translated for designing electronic devices, serves a practical purpose.

VII. PERSONNEL

Major contributors to this program include; A. J. Mountvala, project leader, concepts and theoretical analysis of electronic behavior of surfaces and grain boundaries, and characterization of surface defects in $BaTiO_3$ powders; A. G. Pincus, consultant on materials' preparation and behavior; A. K. Goswami, dielectric properties of $BaTiO_3$ at infrared frequencies; H. Seiwatz, development of electron beam scanning technique; and W. R. Logan, sample preparation and dielectric loss tests. Dr. S. L. Blum, Director, Ceramics Research, provided administrative supervision. The work reported herein was performed under the technical direction of Flight Instrumentation Division, Microelectronics Section, Langley Research Center.

Respectfully submitted,
IIT RESEARCH INSTITUTE

A. J. Mountvala
Senior Scientist
Ceramics Research

APPROVED:

S. L. Blum
Director
Ceramics Research

REFERENCES

1. Mountvala, A. J., "Characterization of Ceramic Materials for Microelectronic Applications," NASA Contract No. NAS1-4870, Summary Report No. 1, (November 1966).

2. Buessem, W. R., Cross, L. E., Goswami, A. K., "Phenomenological Theory of High Permittivity in Fine Grained Barium Titanate," J. Am. Ceram. Soc. 49(1)33-36 (1966).

3. Kriegel, W. W., Palmour, H., "The Role of Grain Boundaries and Surfaces in Ceramics," Material Science Research 3, Plenum Press (1966).

4. Mountvala, A. J., Murray, G. T., "The Role of Grain Boundary in the Elevated Temperature Fracture Behavior of Magnesia," Phil. Mag. 13(123)441-52 (1966).

5. Anliker, M., Burger, H. R., Kanzig, W., Helv. Phys. Acta 27, FASC 2, 99-124 (1954).

6. Kanzig, W., Phys. Rev. 98, 549-50 (1955).

7. Chynoweth, A. G., Phys. Rev. 102, 705 (1956).

8. Gerthsen, P., Hardtl, K., Z. Naturforsch. 18a, 423 (1963).

9. Goswami, A. K., Bull. Am. Ceram. Soc. 45(8)754 (1966).

10. Brandmayr, R., Brown, A., Dunlap, A., USAERDL Tech. Rep. 2326 (Jan. 1963).

11. Herzog, A., J. Am. Ceram. Soc. 47(3)107-15 (1964).

12. "Properties of Ultrafine Grained $BaTiO_3$ Super-Pressed at Low Temperatures," Tech. Rep. U.S. Army Electronics Command, ECOM 2719 (August 1966).

13. Gallagher, C. S., Phys. Rev. 88, 721 (1952).

14. Pearson, G. L., Read, W. T., Morin, F. J., Phys. Rev. 93, 666 (1954).

15. Chang, R., J. Appl. Phys. 34, 1564 (1963).

16. Mountvala, A. J., unpublished work.

17. Brandmayr, R. J., Brown, A. E., Dunlap, A. M., Tech. Rep. ECOM 2614, U. S. Army Electronics Command (May 1965).

18. Rupprecht, G., Winter, W., Waugh, J. S., Tech. Rep. S-452, Raytheon Co. (July 1962).

19. Heywang, W., J. Am. Ceram. Soc. 47, 484 (1964).

20. Van Daal, H. J., Bosman, J., Conference on Electronic Processes in Low-Mobility Solids, Sheffield, U.K. (April 1966).

21. Anderson, P. J., Horlock, R. F., Oliver, J. F., Trans. Faraday Soc. 61(516)2754-62 (1965).

22. Stuart, W. I., Whateley, T. L., Trans. Faraday Soc. 61(516) 2763-71 (1965).

23. Weyl, W. A., Terhune, N., Ceram. Age (August 1953).

24. Fousek, J., Brezina, B., J. Phys. Soc. Japan 19(6)830-38 (1964).

25. Ballantyne, J. M., Phys. Rev. 136(2A)A429-36 (1964).

26. Murzin, V. N., Demeshina, A. I., Sov. Phys. Solid State 6(1)144-52 (1964).

27. Seiwatz, H., "Proceedings of the Fifty-First Meeting of the Juniper Committee," Sanida Corporation (May 1966).